

DISS. ETH NO. 28002

Autonomous Parameter Selection of Manufacturing Processes with Applications in Grinding and Turning

A thesis submitted to attain the degree of

DOCTOR OF SCIENCES of ETH ZURICH

(Dr. sc. ETH Zurich)

presented by

MARKUS TOBIAS MAIER

MSc ETH ME

born on 1.4.1989

citizen of Germany

accepted on the recommendation of

Prof. Dr.-Ing. Dr. h.c. Konrad Wegener, examiner

Prof. Dr.-Ing. Hans-Christian Möhring, co-examiner

Prof. Peter Krajnik, PhD, co-examiner

2022

Acknowledgements

This work was performed during my employment at inspire AG and would not have been possible without the help of many people. First, I would like to thank Prof. Konrad Wegener, head of the institute for machine tools and manufacturing at ETH Zurich, for the possibility to work on this exciting research topic and his continuous support during the thesis. Furthermore, I would like to thank Prof. Hans-Christian Möhring, chair and director institute for machine tools management at the University of Stuttgart, and Prof. Peter Krajnik, head of the manufacturing research group at Chalmers University of Technology, for being co-examiners of this thesis. I am thankful to Lukas Weiss, head of machines and machine concepts at inspire AG, for continuously acquiring new projects and supporting the collaboration with industrial partners. I would like to thank Dr. Alisa Rupenyan, head of advanced control and IoT at inspire AG, for supporting the publication process of various research articles.

I am thankful to my colleagues Mansur Akbari and Ruben Zwicker for the collaboration to apply autonomous parameter selection to turning processes. I would like to thank my colleagues Thomas Gittler and Christopher König for their good collaboration while jointly working on industrial projects.

Furthermore, I would like to thank my colleagues Mohamadreza Afrasiabi, Bircan Bugdayci, Marcel Gerstgrasser, Martin Postel, Eduard Relea, and Nico Zimmermann for discussions on various topics and making inspire AG a fun place to work. This thesis was supported by several highly motivated and dedicated students namely Mario Breu, Christopher König, Hannes Kunstmann, Yves Locher, Monica Pasqualotto, Sven Schmid, Tobias Spiegelburg, Gian-Leza Spinas, Patrick Vettiger, Vinzenz Widmer, and Ruben Zwicker.

I would like to thank Dr. Stephan Scholze, Christian Bobst, Frank Egger and Christian Zenger from Agathon AG for the long-lasting collaboration and support to optimize grinding processes.

I am thankful to my parents for the continuous support during my life. Furthermore, I would like to thank my beloved partner Kerstin and my young daughter Selina for the patience and support during this work.

Table of Contents

Symbols and abbreviations.....	vi
Abstract	xiii
Zusammenfassung	xv
1 Introduction.....	1
2 Fundamentals of manufacturing processes	3
2.1 Turning	3
2.2 Grinding.....	8
2.3 Manufacturing costs	12
3 State of the art in parameter selection of manufacturing processes.....	14
3.1 Expert systems	16
3.2 Optimization	20
3.2.1 Process modeling.....	20
3.2.2 Selection of experiments	26
3.2.3 Determination of optimal parameters.....	27
3.3 Performance measurement in grinding.....	28
3.3.1 Cost quantity measurement	31
3.3.2 Workpiece quality measurement	32
3.3.3 Process quantity measurement	33
3.4 Performance measurement in turning.....	35
3.5 Research gap.....	35
3.5.1 Data-driven optimization for knowledge acquisition.....	35
3.5.2 Quantification of process performance by sensor setup	36
3.5.3 Prior knowledge and transfer of knowledge	37
3.6 Objectives	37
3.7 Outline of thesis.....	38
4 Gaussian process models and Bayesian optimization.....	39
4.1 Gaussian process regression	39
4.2 Gaussian processes for multi-task learning	44
4.3 Gaussian process classification	47

4.4	Bayesian optimization	48
5	Optimization of simulated turning process	54
5.1	Methodology.....	54
5.1.1	Simulation environment	54
5.1.2	Convergence of optimization	55
5.1.3	Unconstrained Bayesian optimization.....	56
5.1.4	Constrained Bayesian optimization.....	57
5.2	Simulation results	59
5.3	Conclusion	61
6	Optimization of longitudinal turning.....	62
6.1	Methodology.....	62
6.1.1	Optimization task and cost calculation.....	62
6.1.2	Experimental set-up.....	63
6.1.3	Optimization implementation.....	64
6.1.4	Convergence criterion	65
6.2	Experimental results	66
7	Performance measurement for grinding of tungsten carbide inserts ...	70
7.1	Experimental set-up.....	70
7.1.1	Grinding operation	70
7.1.2	Grinding burn	72
7.1.3	Temperature measurement	73
7.1.4	Gas measurement	74
7.1.5	Surface roughness measurement	74
7.2	Results of performance measurement	74
7.2.1	In-process detection of grinding burn	74
7.2.2	Grinding burn and surface roughness constraint.....	76
7.2.3	Maximum dressing interval.....	78
7.3	Conclusions	79
8	Optimization of plunge face grinding of tungsten carbide	80
8.1	Methodology.....	80

8.1.1	Experimental setup	80
8.1.2	Cost calculation	81
8.1.3	Optimization Implementation	83
8.2	Results	85
9	Optimization of plunge face grinding of PCBN	90
9.1	Methodology.....	90
9.1.1	Grinding setup and machine.....	90
9.1.2	Measurement fiber.....	91
9.1.3	Microscopic reference measurement.....	93
9.1.4	Optimization objective and cost calculation	94
9.1.5	Optimization implementation.....	95
9.2	Results	96
9.2.1	Validation of wear sensor.....	96
9.2.2	Wear and grinding costs	97
9.2.3	Grinding optimization	98
9.2.4	Wear of grinding and conditioning	99
9.3	Discussion and conclusion	100
10	Prior knowledge and transfer of knowledge	102
10.1	Methodology.....	102
10.1.1	Experimental setup.....	102
10.1.2	Optimization task and cost calculation	103
10.1.3	Modelling	104
10.1.4	Optimization procedure.....	107
10.2	Experimental results	109
11	Conclusion and Outlook	114
Bibliography.....		117
Appendix A	Equations for multi-task learning	135
Appendix B	Expectation propagation algorithm	136
List of publications relevant to thesis		138

Symbols and abbreviations

Latin characters

A	number of orders
a_{co}	conditioning distance
$a_{d,dw}$	wear of dressing wheel during dressing
$a_{d,gw}$	wear of the grinding wheel during dressing
$a_{d,q}^i$	coefficients of LMC model
a_{dw}	thickness of dressing wheel
a_{EI}	expected improvement acquisition function
a_{EIC}	constrained expected improvement acquisition function
a_{gw}	abrasive layer thickness of grinding wheel
a_p	depth of cut
a_{pg}	infeed per side
b	width of the undeformed chip thickness
$\underline{\underline{B}}_q$	coregionalization matrix
C	grain concentration
$c(\underline{x})$	constraint function
C_{AW}	order repetition costs
C_{dw}	cost of dressing wheel
C_{FE}	individual production costs
C_{FO}	follow-up costs
C_{gw}	cost of grinding wheel
C_I	cost per cutting edge
C_{LH}	labor costs

c_{max}	maximum allowed value for constraint
$c_{max,i}$	maximum allowed value for constraint i
C_{min}	lowest measured cost
C_{MH}	machine hour rate
C_o	operator cost per hour
C_T	total manufacturing costs per part
$C_{t,min}$	true minimal costs
C_v	model coefficient Taylor equation
C_{vo}	preparatory costs
C_w	tool wear costs
C_{WH}	tool wear costs per time
D	diameter of workpiece, number of tasks
d_G	abrasive grain size
D_i	diameter of workpiece at cut i
E	earnings from workpiece sale
f	feed per revolution
\underline{f}	vector-valued function
$f(\underline{x})$	objective function
$F(Z)$	cumulative standard normal distribution
F_c	cutting force
$\underline{f}_*(\underline{x}_*)$	posterior mean vector for multi-task learning
f_d	output function d
$f_l(\underline{x})$	latent function
f_{osc}	oscillation frequency

h	undeformed chip thickness
$\underline{\underline{I}}$	identity matrix
$\underline{\underline{I}}_N$	identity matrix with dimension $N \times N$
k	model coefficient Taylor equation
$\underline{\underline{K}}, \underline{\underline{K}}_\theta$	covariance matrix
$\underline{\underline{K}}_*(\underline{x}_*, \underline{x}_*)$	posterior covariance matrix for multi-task learning
$\underline{\underline{K}}(\underline{X}, \underline{X})$	matrix for multi-task learning, as calculated in Appendix A
$\underline{k}(\underline{x}_*)$	covariance vector between \underline{x}_* and \underline{x}_1 to \underline{x}_t
$k(\underline{x}, \underline{x}')$	covariance function
$k_{c1,1}$	model coefficient Kienzle equation
$\underline{\underline{K}}_{x*}$	matrix for multi-task learning, as calculated in Appendix A
$k_q(\underline{x}, \underline{x}')$	covariance function q
K_v	modified Bessel function
L	lot size
l	length of workpiece
l_i^2	length scale parameters of dimension i
$m(\underline{x})$	mean function
$\underline{m}(\underline{x})$	vector of mean functions
m_c	model coefficient Kienzle equation
n	number of constraints
N	number of data points per output
$N(\mu, \sigma^2)$	normal distribution with mean μ and variance σ^2
n_{cuts}	number of cuts
$\underline{\underline{P}}$	diagonal matrix containing characteristic length scale parameters l_i^2

$p(\underline{y}_t \underline{\theta})$	marginal likelihood
$p_{f,i}(\underline{x})$	probability that constraint i is fulfilled
$p_{f,Ra}(\underline{x})$	probability that surface roughness constraint is fulfilled
$p_{f,g}(\underline{x})$	probability that temperature constraint is fulfilled
$p_{Ra,\min}(\underline{x})$	minimal probability that surface roughness constraint is fulfilled
$p_{g,\min}(\underline{x})$	minimal probability that temperature constraint is fulfilled
Q	number of kernels
r	distance between input parameters
R	ratio between grinding wheel wear and conditioning distance
R_a	surface roughness
$R_{a,\max}$	maximum allowed surface roughness
R_q	number of latent functions in each group with same kernel
R_t	kinematic surface roughness
r_ε	corner radius of cutting tool
S	total similarity
s	number of ground sides
s_i	similarity of feature i
T	tool life
t	number of measurements
t_c	cutting time
t_d	dressing time
t_e	job time
t_g	grinding time
t_i	time to change worn out insert

U	utility
$u_q^i(\underline{x})$	latent functions
$VB_{B,\max}$	maximum width of flank wear land
VB_B	average width of the flank wear land
v_c	cutting speed
v_{co}	average conditioning feed rate
$v_{c,\min}$	optimal cutting speed for minimization
$v_{c,opt}$	predicted optimal cutting speed
v_{fa}	axial feed rate
$v_{fa,opt}$	predicted optimal axial feed rate
V_g	removed material per workpiece
V_w	removed workpiece material until wheel is dull
w_i	weigh of feature i
$\underline{x}, \underline{x}', \underline{x}_*$	process parameters
\underline{X}	input values for all measured outputs of all tasks
$\underline{x}_{\leq t}$	vector of t process parameter measurement locations
\underline{x}_{\max}	optimal process parameters for maximization
\underline{x}_{\min}	optimal process parameters for minimization
\underline{x}_{next}	next process parameters determined by Bayesian optimization
\underline{x}_{opt}	predicted optimal process parameters
y	true cost function
\underline{y}	output vector of N measurements and D tasks
$\bar{\underline{y}}$	true cost function with noise

$$\underline{y}_t \quad t \text{ measurements at process parameters } \underline{x}_{1:t}$$

Greek characters

Γ	gamma function
ε	measurement noise
ε_R	relative error of optimization result
ε_{stop}	threshold value of stopping criterion
ε_t	error of optimization result
ϑ	grinding temperature
ϑ_{\max}	maximum allowed grinding temperature
$\underline{\theta}$	hyperparameter vector of Gaussian process
$\underline{\theta}^*$	hyperparameters maximizing the marginal log likelihood
$\underline{\theta}_{co}^*$	hyperparameters for estimating cost
$\underline{\theta}_{Ra}^*$	hyperparameters for estimating roughness
$\underline{\theta}_U^*$	hyperparameters for estimating utility
$\underline{\theta}_{\vartheta}^*$	hyperparameters for estimating temperature
κ	tool cutting edge angle
$\mu_d(\underline{x})$	posterior mean of output d
$\mu_t(\underline{x})$	posterior mean
$\mu_{t,c_i}(\underline{x})$	posterior mean of constraint i
$\mu_{t,co}(\underline{x})$	posterior mean cost
$\mu_{t,Ra}(\underline{x})$	posterior mean surface roughness
$\mu_{t,U}(\underline{x})$	posterior mean utility
$\mu_{t,\vartheta}(\underline{x})$	posterior mean temperature
ν	smoothness parameter of Matern kernel

$\sigma_d^2(\underline{x})$	posterior variance of output d
σ_f^2	signal variance
σ_N^2	signal noise
$\underline{\sigma}_N^2$	signal noise vector for multi-task learning
$\sigma_t^2(\underline{x})$	posterior variance
$\sigma_{t,c_i}^2(\underline{x})$	posterior variance of constraint i
$\sigma_{t,co}^2(\underline{x})$	posterior variance of cost
$\sigma_{t,Ra}^2(\underline{x})$	posterior variance of roughness
$\sigma_{t,U}^2(\underline{x})$	posterior variance of utility
$\sigma_{t,g}^2(\underline{x})$	posterior variance of temperature
$\phi(Z)$	probability density function of a standard normal distribution

Abbreviations

BO	Bayesian optimization
CBN	cubic boron nitride
CBO	constrained Bayesian optimization
DM	data models
GP	Gaussian process
KRM	knowledge representation models
PCBN	polycrystalline cubic boron nitride
RSM	response surface methodology

Abstract

The process parameter selection of manufacturing processes heavily influences production costs and the quality of produced parts. Optimal process parameters depend on the individual specification of the manufacturing process such as machine, tool, workpiece, and cooling lubricant. For most manufacturing processes an enormous variety of combinations exist, new combinations are added continuously, and some properties are unknown due to trade secrets, making the selection of process parameters demanding. In industrial environments, the selection of process parameters is mainly performed by experienced operators, using a combination of experience and trial and error. Hence, the performance of today's manufacturing processes is heavily influenced by operator experience and operator availability.

In this work, procedures for autonomous parameter selection based on Gaussian process models and Bayesian optimization are developed and tested exemplarily for turning and grinding. Using a few experiments, autonomous parameter selection is successfully applied to the selection of feed per revolution and cutting speed for longitudinal turning of 1.4125 steel bars. The objective of the turning optimization is to minimize the production costs, while fulfilling the maximum allowed surface roughness of the final workpiece.

Afterwards, autonomous parameter selection is extended to plunge face grinding of tungsten carbide and polycrystalline cubic boron nitride (PCBN) cutting inserts. For plunge face grinding, the grinding wheel wear and the grinding temperature is measured by utilizing optical fibers embedded perpendicular to the grinding wheel surface in the abrasive layer. The fibers are used by a pyrometer to measure temperature at the contact zone of grinding wheel and workpiece, and an interferometer is used to measure grinding wheel wear. For grinding of tungsten carbide, the axial grinding feed rate and cutting speed are optimized to minimize the individual production costs, while fulfilling constraints of temperature and surface roughness. For grinding of PCBN, axial grinding feed rate and average conditioning feed rate are optimized to minimize individual production costs, while considering grinding process stability. Gaussian process classification is used for modeling of the grinding process stability, extending the previous Gaussian process regression approach.

Finally, the use of prior knowledge and transfer of knowledge is demonstrated for the optimization of cutting speed in longitudinal turning. All approaches utilizing prior knowledge or transfer of knowledge reduce the number of experiments by at least 40% compared to a standard approach without prior knowledge.

Zusammenfassung

Die Prozessparameterauswahl von Fertigungsprozessen beeinflusst die Produktionskosten und die Qualität der gefertigten Teile stark. Optimale Prozessparameter hängen von der individuellen Spezifikation des Fertigungsprozesses wie der Maschine, dem Werkzeug, dem Werkstück und dem Kühlschmiermittel ab. Für die meisten Fertigungsprozesse existiert eine enorme Vielfalt von Kombinationen, neue Kombinationen werden kontinuierlich hinzugefügt und einige Eigenschaften sind aufgrund von Betriebsgeheimnissen unbekannt, was die Auswahl der Prozessparameter anspruchsvoll macht. In industriellen Umgebungen wird die Auswahl der Prozessparameter hauptsächlich von erfahrenen Bedienern durchgeführt, welche eine Kombination aus Erfahrung und Versuch und Irrtum nutzen. Daher wird die Leistung heutiger Fertigungsprozesse stark von der Bedienererfahrung und Bedienerverfügbarkeit beeinflusst.

In dieser Arbeit werden Vorgehensweisen zur autonomen Parameterauswahl basierend auf Gauss Prozessmodellen und Bayesscher Optimierung entwickelt und exemplarisch für das Drehen und Schleifen getestet. Unter Verwendung von wenigen Experimenten wird die autonome Parameterauswahl erfolgreich für die Auswahl des Vorschubs pro Umdrehung und der Schnittgeschwindigkeit beim Längsdrehen von 1.4125 Stahlstangen angewendet. Das Ziel der Drehoptimierung ist die Minimierung der Produktionskosten bei gleichzeitiger Einhaltung der maximal zulässigen Oberflächenrauheit des fertigen Werkstücks.

Danach wird die autonome Parameterauswahl auf das Querseiten-Planschleifen von Wendeschneidplatten aus Hartmetall und polykristallinem kubischem Bornitride (PKB) erweitert. Beim Querseiten-Planschleifen werden der Schleifscheibenverschleiss und die Schleiftemperatur unter Ausnutzung optischer Fasern gemessen, die senkrecht zur Schleifscheibenoberfläche in die Schleifschicht eingebettet sind. Die Fasern werden von einem Pyrometer verwendet, um die Temperatur an der Kontaktzone von Schleifscheibe und Werkstück zu messen und ein Interferometer wird verwendet, um den Schleifscheibenverschleiss zu messen. Beim Schleifen von Hartmetall werden die axiale Vorschubgeschwindigkeit und die Schnittgeschwindigkeit optimiert, um die individuellen Produktionskosten zu minimieren und gleichzeitig die Temperatur- und Oberflächenrauheitsrandbedingungen zu erfüllen. Für das Schleifen von PKB werden die axiale Vorschubgeschwindigkeit und die

durchschnittliche Konditioniergeschwindigkeit optimiert, um die individuellen Produktionskosten zu minimieren und gleichzeitig wird die Schleifprozessstabilität berücksichtigt. Die Gauss Prozess Klassifizierung wird zur Modellierung der Schleifprozessstabilität verwendet, was den vorangegangenen Gauss Prozess Regressions Ansatz erweitert.

Schliesslich wird die Nutzung von Vorwissen und Übertragung von Wissen zur Optimierung der Schnittgeschwindigkeit beim Längsdrehen demonstriert. Alle Ansätze, welche Vorwissen oder Übertragung von Wissen nutzen, reduzieren die Anzahl der Experimente um mindestens 40% im Vergleich zu einem Standardansatz ohne Vorwissen.

1 Introduction

In general, the aim of manufacturing is to produce high quality products at low cost. Figure 1.1 shows the cost structure of typical automotive parts, where manufacturing costs account for 72 - 82% of the total cost and are much larger compared to material costs. Within the manufacturing costs the biggest share is attributed to mechanical processing with a contribution of 42 - 67% to the total cost. Therefore, mechanical processing costs have a substantial impact on final cost, which requires careful selection of process parameters to keep the processing costs minimal.

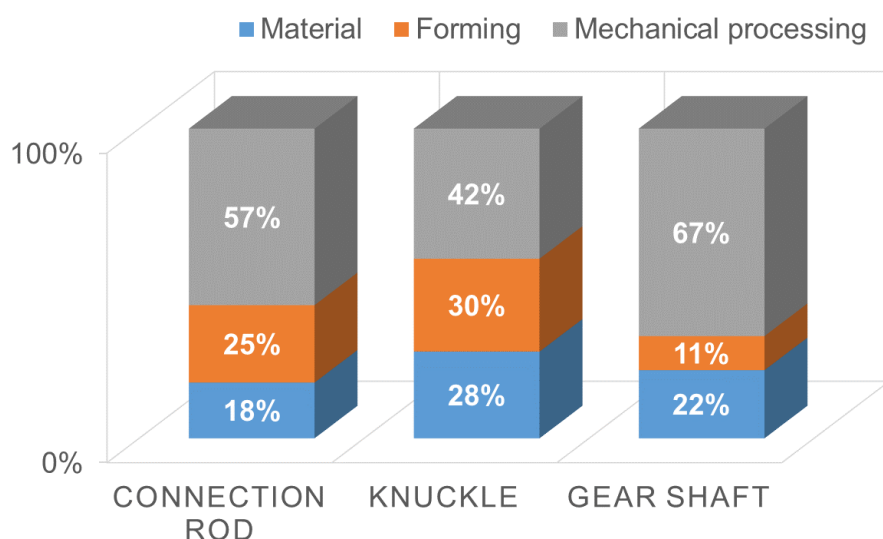


Figure 1.1: Cost structure of different automotive parts according to [168]

Producing high quality products typically reduces the process window in manufacturing, which makes finding acceptable machine settings challenging and often leads to solutions where the cost-efficient parameters are close to the boundary of the process window. For example, producing parts with a high surface quality can only be achieved with a small subset of machine settings, whereas a larger subset of machining settings is feasible to produce parts with a low surface quality. Consequently, producing high quality products typically increase the need for elaborate parameter selection.

An important and continuing trend is the shift from mass production with high product volume per variant and low product variety to customized products with increased product variety, to better meet the demand, as described in [87]. The

trend towards an increased product variety leads to smaller batch sizes, which requires frequent adjustment of the process set-up.

Today the process set-up is mainly performed by machine operators, as in previous decades. Typically, the machine settings, such as feed rate and cutting speed, are determined based on trial and error tests and operator experience. Very often, the tuning is performed in a non-standardized way due to the different operator experience levels and different operator approaches. Typically, expert operators find optimal solutions with only a few experiments, whereas novice and less skilled operators require many costly experiments to find optimal solutions, propose suboptimal solutions or in worst case are unable to find process parameters which fulfill the product requirements.

The selection of machining parameters is therefore a bottleneck for cost efficient production. Due to the demand for high quality products and smaller batch sizes, this situation will likely escalate. To allow a frequent process set-up with increased requirements on product quality, methods supporting the less skilled and novice operators are needed.

Expert systems have been proposed to support the parameter selection of manufacturing processes. According to [72], expert systems represent human knowledge and make use of it to simulate human reasoning. The underlying motivation to apply expert systems is to support less skilled or novice users by using collected knowledge of domain experts. However, the main difficulty of expert systems is knowledge acquisition because knowledge must be transferred painstakingly from human experts to a format suitable for computers, as reported in [42]. Therefore, the scope of this thesis is to autonomously acquire knowledge for parameter selection of manufacturing processes by interaction with the manufacturing system. The autonomous parameter selection of the frequently used turning and grinding process are investigated exemplarily.

2 Fundamentals of manufacturing processes

First, a brief introduction to manufacturing processes is provided, which serves as a foundation for autonomous parameter selection. Manufacturing processes can be categorized according to DIN 8580 [34], defining primary shaping, forming, dividing, joining, coating, and modifying material properties as the main groups. In [34] the main groups are further subdivided up to the level of a single process. For example, within the main category dividing, turning is categorized as cutting with defined cutting edge and grinding is categorized as cutting with undefined cutting edge. As illustrated in [34], there exist a vast variety of manufacturing processes. Many of them requiring the selection of parameters for cost efficient and high-quality production. In this thesis the fundamentals are focused on grinding and turning because autonomous parameter selection is demonstrated exemplarily for these two processes. Covering all manufacturing processes is out of scope of this thesis and the interested readers are referred to [80-84] for introductions to various manufacturing processes. Nevertheless, the optimization methods used are not limited to turning and grinding and might be adapted to other manufacturing processes.

2.1 Turning

According to DIN 8589-1 [35], within the class of turning operations there are different processes, such as facing, straight turning, and threading. Figure 2.1 shows a schematic of the longitudinal straight turning process. The velocity at the interaction of the cutting insert and workpiece is called cutting speed v_c . The cutting insert removes material from the workpiece with a fixed depth of cut a_p and moves along the cylinder with a feed per revolution f . The depth of cut, cutting speed, and feed per revolution are input parameters for the cutting operation and must be selected.

An important measure to characterize the turning process is the cross section of the undeformed chip, which is schematically shown in Figure 2.2. The undeformed chip is a theoretical measure to characterize the process and should not be confused with the actual chip of the cutting process. As reported in [167], the undeformed chip thickness can be calculated as

$$h = f \sin \kappa \quad (2.1)$$

and the width of the undeformed chip is,

$$b = \frac{a_p}{\sin \kappa} \quad (2.2)$$

where κ is the tool cutting edge angle.

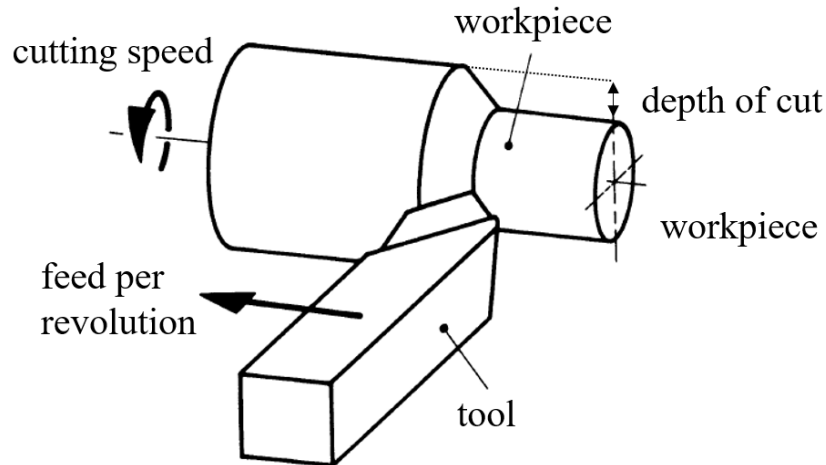


Figure 2.1: Longitudinal straight turning adapted from DIN 8589-1 [35]

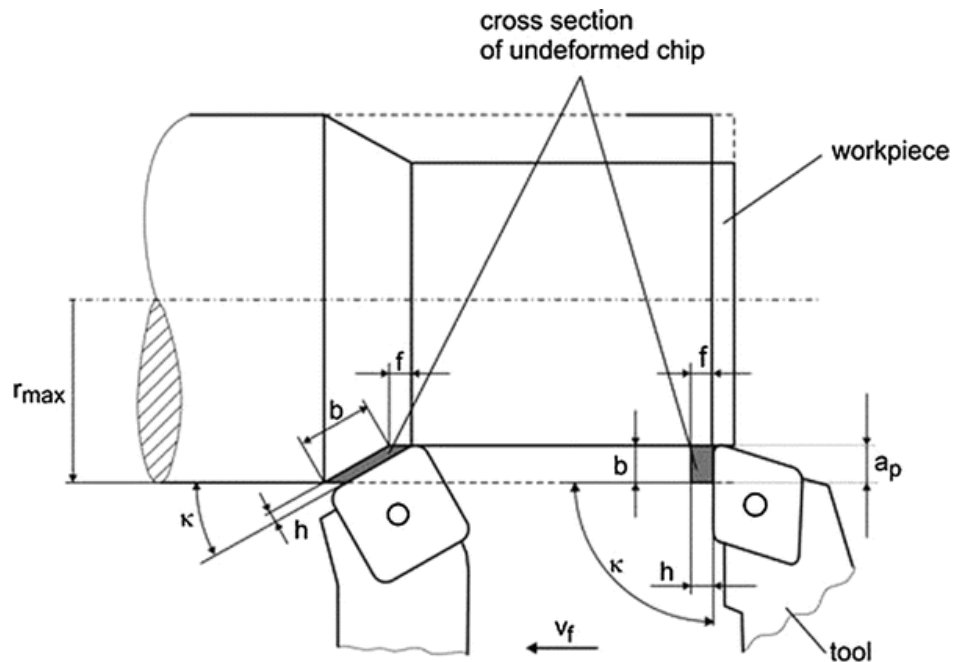


Figure 2.2: Undeformed chip thickness in turning according to [167]

The undeformed chip thickness is often used to empirically relate process inputs with process outputs. For example, based on the undeformed chip thickness h and the width of the undeformed chip thickness b , the cutting force F_c can be estimated according to the Kienzle equation, as described in [81],

$$F_c = k_{c1,1} h^{(1-m_c)} b \quad (2.3)$$

where $k_{c1,1}$ and m_c are model coefficients.

Based on the process kinematics one can also estimate the surface roughness of the final workpiece. The final surface roughness is often predicted by the kinematic surface roughness R_t , which according to [81] can be calculated as follows,

$$R_t = \frac{f^2}{8 \cdot r_\varepsilon} \quad (2.4)$$

where f is the feed per revolution and r_ε is the corner radius of the tool. As explained in [81], the underlying principle for the surface roughness generation is that the tool moves with a specific feed per revolution f along the workpiece, creating a distinct groove pattern on the workpiece surface. Figure 2.3 shows a surface roughness fit based on experimental data. The roughness model can accurately model the general roughness trend but is unable to predict the experiments precisely. Overall, a high feed per revolution leads to a deterioration of the surface roughness but also to a reduction of the cycle time. Hence, surface roughness requirements must be balanced with process cycle time.

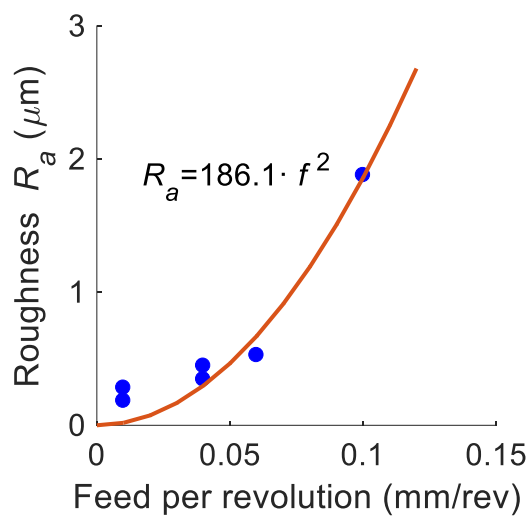


Figure 2.3: Surface roughness for turning of 1.4125 steel bars using a coated cemented carbide cutting tool with a corner radius of 0.2 mm and a constant depth of cut of 0.3 mm

Another important aspect of turning is cutting insert wear. Figure 2.4 top schematically shows different wear measures of the cutting insert. According to

ISO 3685 [70] different criteria, such as maximum width of the flank wear land $VB_{B,\max}$ or average width of the flank wear land VB_B are used as wear measures. Figure 2.4 bottom shows the determination of the tool life by continuously measuring the average width of the flank wear land until the maximum allowed average width of the flank wear land is reached, which serves as the tool life criterion.

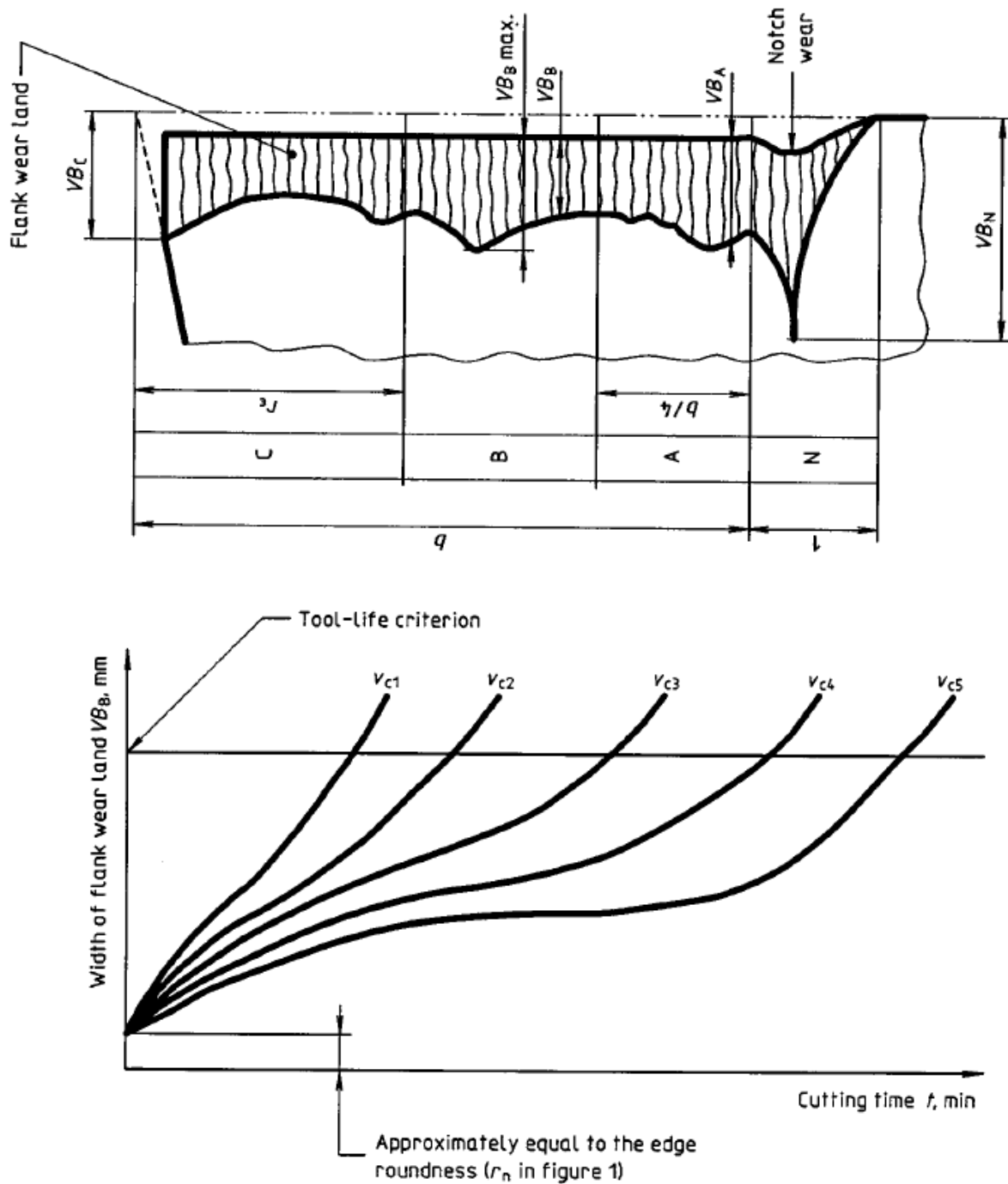


Figure 2.4: Measurement of tool life according to ISO 3685 [70]

Afterwards the tool life T can be correlated with the cutting speed v_c according to the Taylor equation, as described in [81],

$$T = C_v \cdot v_c^k \quad (2.5)$$

where C_v and k are model coefficients. Figure 2.5 shows exemplarily the tool life and a Taylor equation fit for cutting of 1.4125 steel bars using a coated cemented carbide cutting tool. Similar to the previous surface roughness model, the general trend of the tool life model is captured accurately but the tool life model does not match experiments precisely. For high cutting speeds the tool life is shorter and accordingly the insert must be replaced more frequently for high cutting speeds. However, higher cutting speeds lead to shorter cycle times due to a faster operation. To optimize the turning process, it is necessary to balance cost of cycle time and cost of tool wear.

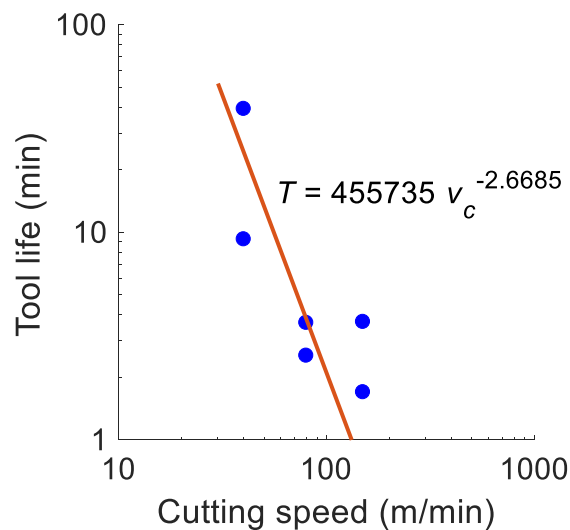


Figure 2.5: Tool life for manufacturing of 1.4125 steel bars using a coated cemented carbide cutting tool with a corner radius of 0.2 mm and a constant depth of cut of 0.3 mm

The measured turning quantities such as surface roughness and tool life do not only depend on the selected process parameters but also on the properties of cooling lubrication, turning machine, workpiece and cutting tool. Table 2.1 summarizes the main groups and the corresponding properties, which influence the turning process. According to [81], typical cutting materials are tool steels, cemented carbides, ceramics, boron-nitride and diamond, sometimes coated in order to enhance the cutting properties. Besides the different tool materials also different tool geometries exist, which are specified in DIN ISO 1832 [39]. As listed in DIN ISO 513 [37], typical workpiece materials are steel, stainless steel,

cast iron, non-ferrous metals, superalloys, titanium, and hard materials. Both, workpiece and tool materials can be further subdivided by their individual material composition leading to an enormous variety of workpiece and tool combinations.

Table 2.1: Summary of main groups and properties influencing the turning process

Group	Properties
Process parameters	Feed per revolution Cutting speed Depth of cut
Turning machine	Machine stiffness Maximum power of drives Maximum rotational speed of spindle Accuracy of machine tool
Cutting tool	Cutting material and coating type Tool geometry
Workpiece	Workpiece material Workpiece geometry
Cooling lubrication	Cooling lubricant specification Cooling nozzle type Cooling flow rate, velocity, and orientation

2.2 Grinding

Figure 2.6 shows the interdependency of the grinding process. Special to grinding is the coupling of the grinding process with the conditioning process. A review on conditioning of grinding wheels is presented in [178]. According to [145], the conditioning process can be subdivided in profiling, sharpening, and cleaning of the grinding wheel.

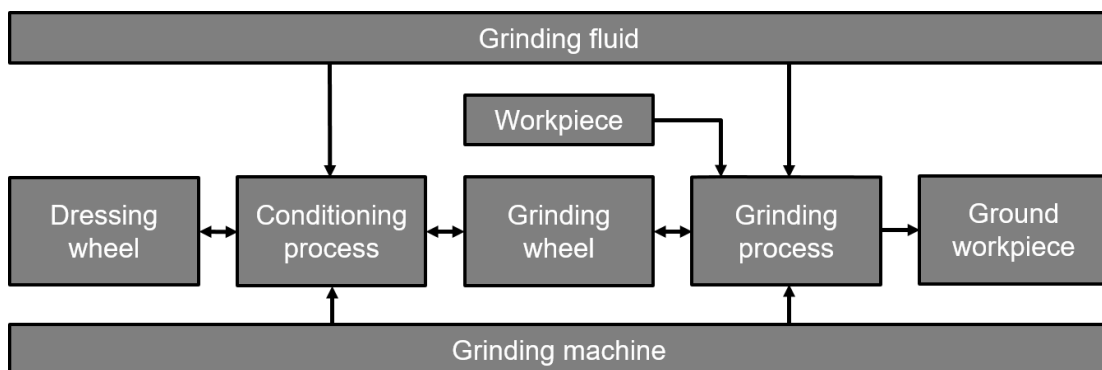


Figure 2.6: Causalities of the grinding process adapted from [68]

As listed in DIN 8589-11 [36], there are various grinding processes such as surface grinding, cylindrical grinding, and profile grinding. A special surface grinding operation is plunge face grinding, often used for grinding of cutting inserts and investigated in this thesis. The plunge face grinding operation is schematically shown in Figure 2.7. Special to plunge face grinding is that there is a surface contact between grinding wheel and workpiece and not only a line contact as for many other grinding operations. In plunge face grinding, the grinding wheel moves with an axial feed rate v_{fa} towards the workpiece, while it is rotating with a constant cutting speed v_c and oscillates with a frequency f_{osc} . The grinding wheel is oscillated with a fixed frequency to ensure uniform wear of the grinding wheel. At the end of the grinding process, the programmed workpiece position is kept constant for a predefined spark-out period to allow a reduction of residual grinding forces. The reduction of residual grinding forces is important to allow a minimization of geometry errors of the final workpiece.

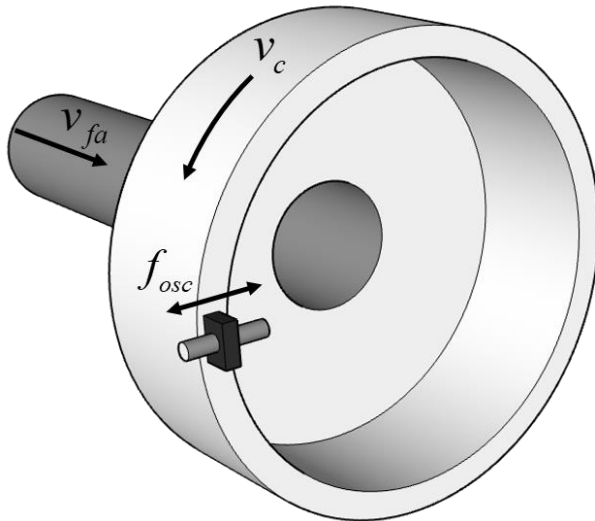


Figure 2.7: Schematic of plunge face grinding

Similar to turning, the undeformed chip thickness is often used to empirically relate input parameters with process outputs. Friemuth [45] developed a relation for the undeformed chip thickness for plunge face grinding, assuming circular abrasive grains,

$$h \approx 0.89d_G \left(\frac{v_{fa}}{C \cdot v_c} \right)^{0.4} \quad (2.6)$$

where d_g is the abrasive grain size and C is the grain concentration. The dependency developed by Friemuth is in line with previous work from Wobker [183] and Fritsch [46], who qualitatively obtained the same results as Friemuth, with slightly different numerical values due to different model assumptions. As an application example of the undeformed chip thickness, Friemuth [45] showed that a high undeformed chip thickness is correlated with higher residual compressive stress of the final workpiece.

Another important aspect of grinding is grinding wheel wear. According to [189], grinding wheel wear can be classified into attritious wear of grains, grain fracture, and bond fracture. Attritious wear corresponds to flattening of the grains and leads to a dulling of the wheel, which finally results in high grinding forces, as reported in [110]. Grain and bond fracture cause a self-sharpening effect of the grinding wheel [189]. Grinding wheel wear heavily depends on the process parameters, workpiece and grinding wheel. Furthermore, grinding wheel wear can be classified according to the resulting wear pattern in radial and edge wear, as described in [82].

The workpiece materials in plunge face grinding of cutting inserts are cutting materials as previously introduced in section 2.1. Various grinding wheels with different properties are used as tools. Figure 2.8 shows grinding wheel specification details. For plunge face grinding of inserts mainly diamond abrasives are used. One can choose the grain size and the concentration, which specifies the grain volume in carat per unit abrasive layer. Furthermore, one is free to choose the bond material. Vitrified bonds are the hardest bonds, resin bonds show the lowest hardness and metallic bonds are in between, as listed in [112]. In plunge face grinding of inserts the conventional ceramic grinding materials are used for dressing of the grinding wheel, mostly the abrasive materials of the dressing wheel are either aluminum oxide or silicon carbide, depending on the bond type of the grinding wheel. Furthermore, the grinding and dressing wheels can be specified according to hardness and structure, which must be selected depending on the grinding process.

B 126 C50 B 54

			Bond designation	Internal code, which defines bond type
			Bond	
		B	Resin bonded	
		M	Metal bonded	
		Concentration	The grain concentration shows the grain volume in carat per unit volume of the grinding layer	
		Grit size description	Grit size indication in μm (average grit diameter according to FEPA)	
		35 – 181 μm		
		Abrasive description		
	B		CBN	
	D		Diamond	

89A 60 M 5 V 217

			Bond designation	Internal code, which defines bond type
			Bond	
		V	vitrified bonded	
		B	resin bonded	
		E	elastic bonded	
		G	galvanic bonded	
		Structure	The higher the number, the more open the wheel	
		Hardness	Hardness ascends alphabetically e.g.	
	G		Soft	
	R		Hard	
	Grit size description		Grit size indication in mesh (sieve size per inch)	
	14 – 36		COARSE	
	46 – 60		MEDIUM	
	80 – 220		FINE	
	800 – 1 200		VERY FINE	
	Abrasive description			
	10A		Regular aluminium oxide	
	50A		Mixture of 89A and 10A	

Figure 2.8: Specification of grinding wheel abrasive: CBN and diamond (top) and conventional ceramic (bottom) by Tyrolit [172]. The specification of the conventional ceramic grinding material of Tyrolit is in line with the DIN ISO 525 [38].

Similar to turning, many different machine, workpiece, tool, cooling lubrication and dressing setup combinations exist in grinding, which influence the selection of optimal process parameters. Table 2.2 summarizes the main groups and corresponding properties, which influence the plunge face grinding process. As can be seen in Table 2.1 and Table 2.2, the coupling of the grinding and conditioning process leads to a higher complexity and more properties to select compared to turning, where a worn out tool is replaced with a new one instead of resharpening the tool on the machine.

Table 2.2: Summary of main groups and properties influencing the plunge face grinding process

Group	Properties
Process parameters grinding	Cutting speed Axial feed rate Oscillation frequency of grinding wheel Spark-out time
Process parameters conditioning	Axial feed rate of dressing wheel Duration of conditioning operation Rational speed of grinding wheel and dressing wheel Spark-out time
Grinding machine	Machine stiffness Maximum power of drives Maximum rotational speed of grinding wheel Accuracy of machine tool
Grinding wheel	Abrasive material Abrasive grain size Grain concentration Bond specification
Dressing wheel	Abrasive material Abrasive grain size Bond type
Workpiece	Workpiece material Workpiece geometry
Cooling lubrication	Cooling lubricant specification Cooling nozzle type Cooling flow rate, velocity, and orientation

2.3 Manufacturing costs

The main goal of autonomous parameter selection is to propose parameters which are optimal or close to optimal with respect to one or multiple objectives. In this thesis the focus is on minimization of manufacturing costs because this is most demanded by industry. However, other objectives such as minimization of environmental impact or maximization of energy efficiency are also possible alternatives. According to [169], the total manufacturing costs per part C_T can be calculated as follows,

$$C_T = \frac{C_{VO}}{A \cdot L} + \frac{C_{AW}}{L} + C_{FE} + C_{FO} \quad (2.7)$$

where C_{VO} are the preparatory costs containing for example the procurement costs of measuring instruments, C_{AW} are the order repetition costs containing for example the machine set-up time, C_{FE} are the individual production costs, C_{FO} are the follow-up costs such as quality assessment and storage costs, A are the number of orders, and L is the lot size. As explained in [169], the individual production costs C_{FE} are the combination of job time t_e , machine hour rate C_{MH} , labor costs C_{LH} , and tool wear costs per time C_{WH} .

$$C_{FE} = t_e (C_{MH} + C_{LH} + C_{WH}) \quad (2.8)$$

The follow-up costs C_{FO} depend on the performance of the high-level production planning and control system and not on the specific machine parameters. The order repetition costs C_{AW} depend on automatic tool changers, robots, and intralogistics and not on machine parameters. Therefore, follow-up costs and order repetition costs were not considered in this study. From equation (2.7) it follows that for a large lot size the contributions of the preparatory costs C_{VO} and the order repetition costs C_{AW} to the manufacturing costs per part are small. In this case the manufacturing costs per part are primarily determined by the individual production costs C_{FE} and the follow up costs C_{FO} . Consequently, for very large lot sizes performing many initial experiments to find optimal machine parameters and thereby reducing the individual production cost C_{FE} is beneficial because the contribution of the preparatory costs to the total manufacturing costs per part is minimal. However, when switching to medium and small lot sizes the cost of initial experiments significantly influences the total manufacturing costs per part. Hence, for medium and small batch sizes it is crucial to reduce the cost of initial experiments as much as possible. Throughout this thesis the cost unit is Swiss franc but for the sake of universality it is denoted as U .

3 State of the art in parameter selection of manufacturing processes

Over the past many different approaches have been proposed for parameter selection in manufacturing. Parameter selection in manufacturing builds on various areas such as artificial intelligence, optimization, process modelling, and sensorial process feedback. Rowe et al. [139] listed various approaches for artificial intelligence systems in grinding such as knowledge-based systems, expert systems, fuzzy logic systems, neural net systems, and adaptive control optimization techniques. A comprehensive overview on optimization and modelling techniques for machine tools and applications to grinding and turning is given in [131], listing the following techniques: statistical regression technique, fuzzy set theory, artificial neural networks, gray relational analysis, Taguchi robust design method, Taguchi fuzzy-based approach, factorial design method, response surface methodology (RSM), knowledge-based expert systems, principal component analysis, mathematical iterative search methods and meta-heuristics. Another review focusing on modeling and simulation in grinding is conducted by Brinksmeier et al. [15]. They categorized regression analysis, artificial neural networks, and rule-based approaches as applicable for process control, whereas other models such as molecular dynamic models, kinematic models, finite element models, and models based on first principle are not categorized as applicable for process control.

Based on the previous publications a rich set of methods for parameter selection in manufacturing exist. Figure 3.1 shows on a high level components for parameter selection of manufacturing processes. Human operators typically follow this schema for parameter selection of manufacturing process. The operators combine domain knowledge and knowledge of similar tasks with process state information such as temperature or force readings and process performance measures such as tool wear, process time and final surface roughness of the workpiece. A method for autonomous parameter selection is the use of expert systems, which are heavily based on integration of domain knowledge and only a few of these systems utilize state or performance feedback of the process. A different approach for autonomous parameter selection is to optimize the process parameters by considering domain knowledge, state measurements and performance measures. Systems based on optimization typically consist of a

model of the process, a method for the selection of parameters to improve the model by using state and performance measures, and an optimization procedure to find the best parameters according to the model. The influence of domain knowledge in optimization depends on the model choice and can vary greatly. Physical models based on first principles are heavily based on domain knowledge while neural network models are mainly based on state and performance measurements. Optimization approaches heavily based on state and performance measurements are often referred to data-driven optimization. An effective autonomous system for parameter selection should combine domain knowledge with state and performance measurements, similar to human operators. Therefore, expert systems and systems based on optimization are introduced in the following sections.

In this work the parameters are selected in the beginning of the manufacturing process and are not affected by the current state of the process such as the current tool wear state. A simple example for state based parameter adaption is force-controlled grinding, as shown in [171]. However, such systems are not applicable to autonomous parameter selection for general cases because they are too simplistic and do not consider performance measures. A more sophisticated method, using state and performance measurements for continues adaption of process parameters is reinforcement learning. [144] demonstrates reinforcement learning for cylindrical plunge grinding in simulation by selecting the infeed rate while considering the remaining grinding stock and the decrement rate of the workpiece radius as state parameters, and size and decrement rate of the workpiece radius in the end as performance measures. In total they conducted 5000 iterations for learning of optimal parameters, the first 70 iterations failed and afterwards the performance improved. Such methods work in a simulation environment. In real grinding applications their use is limited due to the high experimental costs. Therefore, expert systems and self-optimizing systems which select the parameters initially are currently closest to industrial applicability due to reasonable experimental costs.

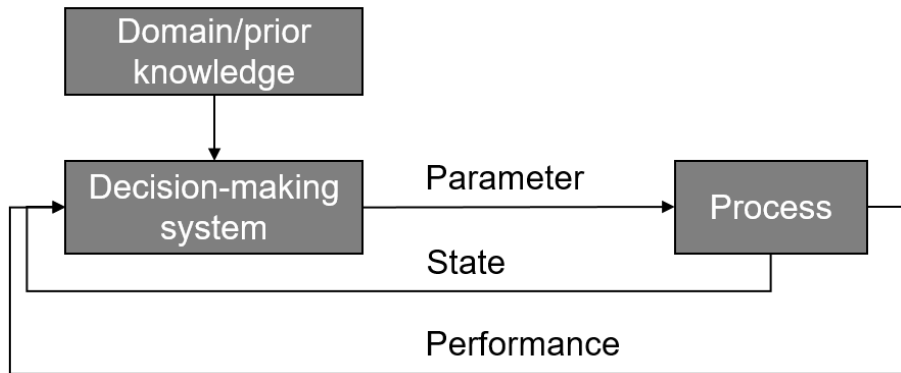


Figure 3.1: Overview of parameter selection for manufacturing processes

3.1 Expert systems

Figure 3.2 shows a typical structure of expert systems. The core of each expert system is the knowledge base where domain specific knowledge is stored. Specific domain knowledge is typically translated to a suitable expert system format by a knowledge engineer, after collection through interviewing human domain experts. Expert systems also have a user interface, where an inference engine is used to provide recommendations based on the knowledge base. Sometimes, expert systems are also equipped with an explanation module to provide reasons for the proposed recommendations.

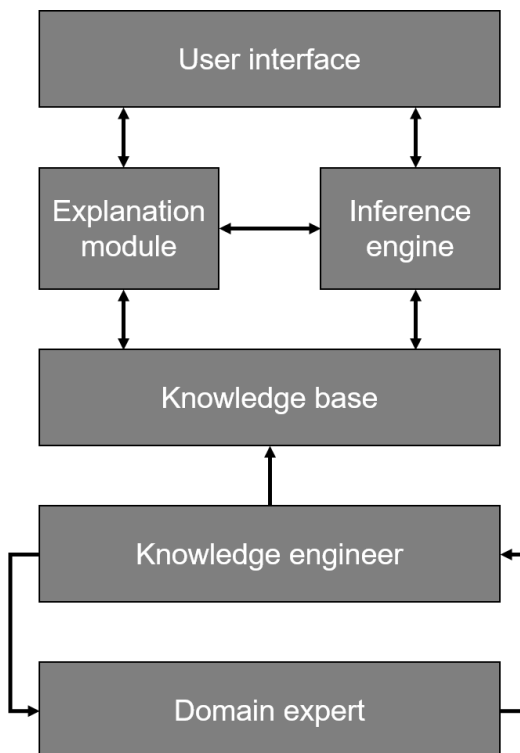


Figure 3.2: Structure of expert systems adapted from [44] and [177]

Different methods to represent the knowledge of the expert systems exist, as illustrated in Figure 3.3. For example, [118] recommends cutting tools for milling and turning by using a database for knowledge representation. Another example is given by [114], utilizing a rule-based system for selection of grinding parameters. Instead of using exact rules it is also possible to apply fuzzy logic, such as shown in [59] for recommending cutting speeds in turning, based on depth of cut and workpiece material hardness. As explained in detail in [136], fuzzy logic allows to represent imprecise information by fuzzy sets, where elements are members of a set with varying degrees – this is in contrast to classical Boolean logic, where an element can or cannot belong to a set. In [101] an ontology is used for a manufacturing control system. The simplified manufacturing system in [101] consists of two grinding machines, two milling machines, two lathes, three robot arms, and two automated guided vehicles for the production of three different products.

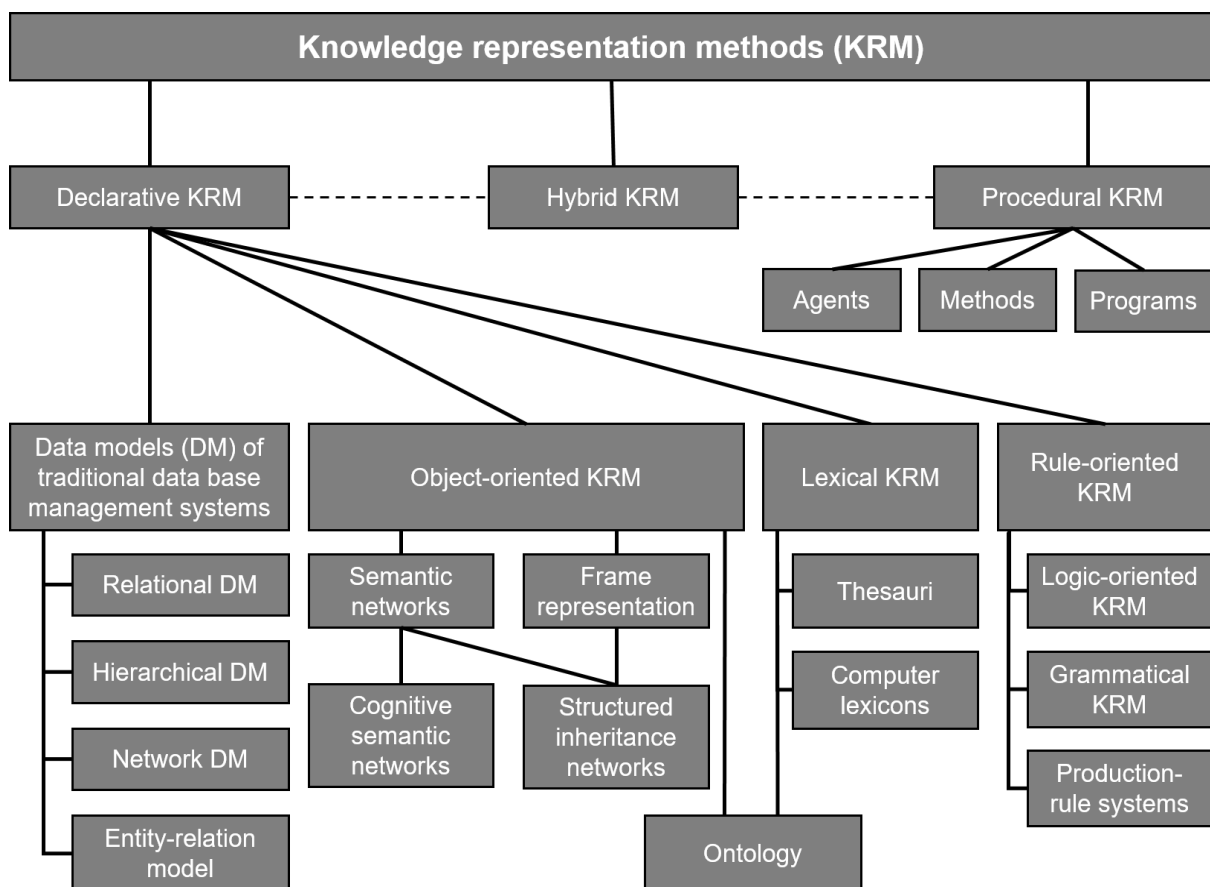


Figure 3.3: Knowledge representation methods adapted from [60, 61]

Figure 3.4 shows a performance comparison of human operators and an industrial expert system. The performance and the degree of task fulfillment varies heavily between the 75 operators, clearly showing improvement potential. The expert system shows a good performance and a degree of fulfillment of 100%. The comparison also shows the limitation of the expert system used in this case, because some operators outperform the expert system. This is obvious because the expert system cannot surpass the performance of the domain expert and knowledge engineer designing the expert system. This disadvantage becomes even more dominant for the setup of new machine, workpiece, and tool combinations where precise knowledge is missing.

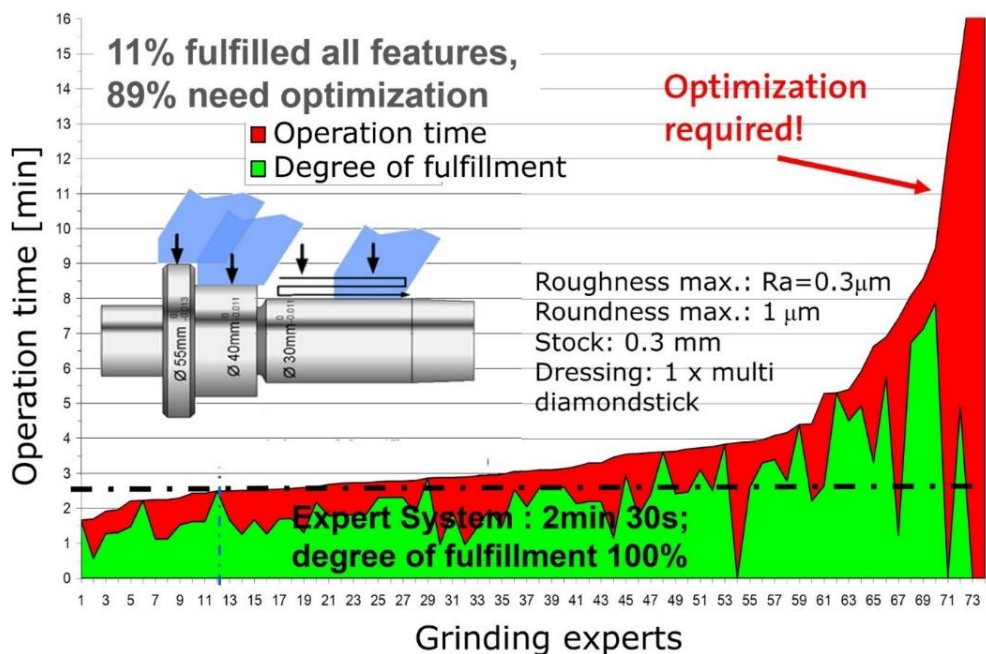


Figure 3.4: Performance comparison between human experts and an industrial expert system (F. Gaegauf, personal communication, 2011)

As described in Feigenbaum and McCorduck [42], the main shortcoming of expert systems is the acquisition of knowledge, which requires to transform human knowledge in a format suitable for computers. For example, they identified flexibility of expert system updating and the motivation for experts to share their knowledge as barriers. In order to overcome the knowledge acquisition bottleneck systems including self-learning capabilities have been developed. [143] presents an expert system with a learning module, which uses data from a grinding database to automatically generate fuzzy production rules. However, a shortcoming of the proposed system is that no data-efficient method is provided to collect the data. Instead, the expert system performance in [143] is demonstrated for one grinding case using 500 randomly simulated data points.

Another system considering learning is presented in [120] combining a database for knowledge representation with different methods for grinding parameter selection. The system in [120] uses a burn algorithm, a time constant algorithm, and a wheel dressing algorithm for parameter adjustment and gains knowledge by saving the adjusted parameters in the database for later use. The disadvantage of this learning method is that the adjusted parameters are not necessarily optimal according to a certain objective such as minimal costs because the parameter adjustment is a result of combining procedures and rules and not by optimization. As shown in [120], starting parameters for new grinding tasks can be obtained by transferring knowledge from stored tasks to new tasks by defining a total similarity S ,

$$S = \frac{\sum_{i=1}^b w_i s_i}{\sum_{i=1}^b w_i} \quad (3.1)$$

where w_i are weights, and s_i is the similarity for feature i . Following [120], for binary features the similarity for feature i can take values of one (feature is the same) or zero (feature not the same). For continuous features they calculated the similarity by a distance measure which is normalized by the feature range. In [120] the weights are specified based on the importance of each feature and the complexity of the modification. However, they do not explain how importance or the complexity of modification is quantified – in the spirit of expert systems the weights need to be defined by domain experts.

Besides the drawbacks of the current systems, the idea of acquiring knowledge by interaction with the machine is promising to overcome the knowledge acquisition bottleneck. Therefore, the next chapter investigates different optimization approaches as a method for autonomous acquisition of knowledge.

3.2 Optimization

Typically, the goal of optimization approaches is to find the process parameters \underline{x} , which minimize or maximize an objective function $f(\underline{x})$ subject to (s.t.) constraints. For a minimization problem this can be written as follows,

$$\underline{x}_{min} = \arg \min f(\underline{x}), \text{s.t. } c(\underline{x}) \leq c_{max} \quad (3.2)$$

where $c(\underline{x})$ is a constraint quantity and c_{max} is the maximum allowed value of the constraint.

Table 3.1 and Table 3.2 list various optimization approaches for grinding and turning with their optimization objectives and constraints. The optimization approach can be subdivided in methods for experiment selection, process modelling, and determine optimal parameters. Different quantities are considered as an objective such as production costs, geometry error, and cycle time. For simplified optimizations, the objective might be the machining time only. It is also possible to define multiple objectives, where different objectives such as surface roughness, grinding time and production costs are optimized simultaneously, as for example shown in [49]. The constraints are mainly introduced by the process and the final workpiece requirements such as a desired surface roughness.

3.2.1 Process modeling

Empirical models, such as the Kienzle equation (2.3), kinematic surface roughness equation (2.4), and the Taylor equation (2.5), are often used for optimization purposes, as shown in Table 3.1. The advantage of empirical models is the extensive literature and the simplicity of use. The simplicity of the models is also their main disadvantage. They might be able to show general trends but are inaccurate to match reality. For example, according to the kinematic surface roughness equation the surface roughness is only a function of feed per revolution (see equation (2.4)). As described in [81], for real turning experiments the surface roughness is not only influenced by the feed per revolution but also by built-up edge, which is not considered by the kinematic surface roughness model. A straightforward way would be to include these additional factors in the models. In practice this approach is difficult because an enormous variety of process configurations exist. Furthermore, these additional factors of the models depend on the individual process set up specification, such as workpiece, tool, cooling lubricant, and machine properties. Unfortunately, workpiece, tool, cooling

lubricant and machine properties are only known partially due to trade secrets of the respective manufacturers, quantities that are difficult to measure, and lack of documentation. Consequently, including additional factors in the empirical models is difficult for parameter selection in an industrial environment.

Polynomial fits are another class of models, which are commonly used. Most often polynomial fits are used up to the second order, as shown in Table 3.1. The advantage of these models is their flexibility of use because they are not restricted to specific tool, workpiece, cooling lubricant and machine combinations. The main disadvantage of polynomial fits in the context of autonomous parameter selection is the restriction of the function form to a second order polynomial, which can lead to inaccurate predictions of the real machining process. For example, the tool life is typically predicted according to the Taylor equation (2.5), which is a power function with a real valued exponent. A second order polynomial fit is only able to provide a rough approximation of this function and therefore leads to model errors.

To overcome the limitations of the second order polynomial, one can fit higher order polynomials. This is seldom done in the process optimization literature. Instead, as shown in Table 3.1 and Table 3.2, neural network models are chosen, offering a great model flexibility. The great model flexibility allows for data-driven optimization. Recently, systems using neural networks have made great progress in modelling complex dependencies in various fields, where large amounts of training samples are available, such as image recognition [91], speech recognition [55], and handwriting recognition [56]. In contrast to these big data applications, in manufacturing often only a few training samples are available. Due to the high flexibility of neural networks, it is necessary to fit many model parameters such as weights and biases for each layer. The combination of few training samples and many model parameters often results in overfitting, where the main shortcoming of neural networks is that they typically do not provide any uncertainty estimations of the prediction. For example, when making predictions for input parameters far away from measurements, the neural network predicts a result with the same confidence as for input parameters close to data points. This property is in clear contrast to human intuition. As shown in [47], model uncertainty information can be obtained by combining Bayesian methods with neural networks. However, to avoid the added complexity in modeling, most neural network approaches are used without model uncertainty estimations.

Gaussian process (GP) models are a class of probabilistic models, which provide uncertainty estimations. According to [134], a Gaussian process is a non-parametric model, which can be used to describe a distribution over functions. Therefore, Gaussian process models have a greater flexibility compared to a single function fit, such as a second order polynomial fit. Given the Gaussian process model and available data, a mean value and a variance can be calculated for arbitrary input combinations, as described in [134]. Typically, Gaussian process models predict lower variances close to measured points and higher variances for unexplored parameter values. The in-build uncertainty prediction makes Gaussian process models very suitable for modelling processes with only a few data points, especially in comparison to traditional neural networks. The use of Gaussian process models accelerated in recent years e.g. for wind power forecasts [21], data-efficient learning in robotics [27], control of a gas-liquid separation plant [100] and sensor placement [57]. For machining operations only a few studies using Gaussian process models exist. Focusing only on modelling, in [86] Gaussian process models are successfully used for tool wear prediction based on force measurement features in turning. The use of Gaussian process models for turning process optimization is demonstrated in [1, 5]. A detailed introduction on the underlying equations of Gaussian process models follows in chapter 4.

Table 3.1: State of the art optimization methods and objectives in grinding

Source	Method for selection of experiments	Modelling techniques for grinding process	Method to determine optimal parameters	Objective & Constraints on output
[97]	Not stated	1) Parametric regression of empirical models 2) fuzzy basis function network	Evolution strategy (described in [98])	Objectives: 1) Minimization of grinding costs 2) Minimization of cycle time 3) Weighted sum minimization of difference between roughness, grinding power, and G-ratio to desired values Constraints: Maximum grinding power, minimum G-ratio, maximum surface roughness, maximum residual stress
[49]	Taguchi method (orthogonal array)	Parametric regression of empirical models	Genetic algorithm	Multi-objective optimization of surface roughness, grinding time, and production costs constrained to workpiece removal parameters and wheel wear parameters
[147]	Full factorial design	Neural networks	Combination of weighting method (described in [190]), branch and bound method, and generalized reduced gradient method	Multi-objective optimization of power, normal force, surface roughness, and material removal rate
[99]	Fractional factorial design	Neural networks	Back propagation algorithm with Boltzmann factor	Weighted multi-objective optimization of material removal rate, surface roughness, grinding force per width, and grinding power per width constrained to a maximum grinding power per width and a maximum surface roughness

Table 3.1: State of the art optimization methods and objectives in grinding (continued)

Source	Method for selection of experiments	Modelling techniques for grinding process	Method to determine optimal parameters	Objective & Constraints on output
[94]	Taguchi method (orthogonal array)	Second order polynomial fit (RSM)	1) Taguchi (signal to noise ratio) 2) Graphically	1) Minimize geometric error 2) Minimize geometrical error with surface roughness and material removal constraint
[89]	Central composite design	Second-order polynomial fit (RSM)	1) Non-linear programming 2) Genetic algorithm	Minimization of surface roughness
[128, 132, 179]	No experiments for modelling	Empirical models from literature	[179]: Quadratic programming [128]: Particle swarm optimization [132]: 1) Artificial bee colony algorithm 2) Harmony search algorithm 3) Simulated annealing algorithm	1) Rough grinding: weighted multi-objective optimization of production costs and production rate constrained to thermal damage, wheel wear, machine tool stiffness, and surface roughness 2) Finish grinding: weighted multi-objective optimization of production costs and surface roughness constrained to thermal damage, wheel wear, machine tool stiffness, and production rate
[111]	Taguchi method (orthogonal array)	None	Grey relational analysis	Optimization of material removal rate, surface roughness, and grinding force
[152]	Taguchi method (orthogonal array)	None	Principal component analysis combined with grey relational analysis	Optimization of surface roughness, out of cylindricity, and diametral tolerance
[140]	Box-Behnken design	Second-order polynomial fit (RSM)	Multi-objective genetic algorithm	Optimization of vibration and surface roughness

Table 3.2: State of the art optimization methods and objectives in turning

Source	Method for selection of experiments	Modelling techniques for turning process	Method to determine optimal parameters	Objective & Constraints on output
[186]	Taguchi method (orthogonal array)	None	Taguchi (signal to noise ratio)	Optimization of tool life and surface roughness individually
[123]	Taguchi method (orthogonal array)	None	Taguchi (signal to noise ratio)	Multi objective optimization of tool life, cutting force and surface finish
[65]	Full factorial design	Neural networks	Genetic algorithm	Optimization of flank wear constrained to surface roughness
[5]	Full factorial design	Gaussian process regression	Strength Pareto Evolutionary Algorithm	Multi objective optimization of surface roughness, tool wear, and productivity
[1] with details provided in [142]	1) Full factorial design 2) m-EGO (adaptive sampling)	Gaussian process regression	Construct Pareto frontier from available measurements	Multi-objective optimization of surface quality and material removal rate

3.2.2 Selection of experiments

As displayed in Figure 3.5, design of experiments (DoE) methods can be grouped in sequential DoE and one-shot DoE. As can be seen in Table 3.1 and Table 3.2, experiment selection in process optimization is mostly performed using one-shot DoE. As described in [160], one-shot DoE typically requires specifying levels, for each factor where the experiments are conducted, based on experience and theoretical knowledge. Factors typically represent different process parameters such as cutting speed and feed rate. Using a full factorial design, one performs experiments for each level and factor, which leads to l^k experiments, where l are the levels and k are the factors, as described in [141]. Hence, this approach requires many experimental trials, especially for cases with several factors. Alternatively, to reduce the number of trials, fractional factorial designs are used, where for a two-level design 2^{k-p} experiments are performed, as described in [141]. For this case, the experiments of the full factorial approach 2^k are reduced by 2^{-p} . For example, setting $p = 2$ reduces the number of experiments by 1/4. Various methods exist to create factorial design schemas. Similar to fractional factorial design, the Taguchi method [162] uses orthogonal array test plans. As pointed out by [141], orthogonal arrays are not always fractional factorial designs, but fractional factorial designs are always orthogonal arrays. A disadvantage of one-shot DoE is that one needs to design the experiments in the beginning where the least is known of the process, as explained by [14]. They concluded that this favors the use of sequential designs because it allows to incorporate knowledge gained during testing. The initial specification of experiments has a second disadvantage. It is not possible to end the experimental run early as more data become available – all experiments must be finished before conclusions can be made.

Sequential experimental designs are investigated next, which according to Figure 3.5 can be categorized in space-filling and adaptive designs. As described in [146], space filling algorithms are used for parameter optimization of computer simulations, sampling the whole design space evenly. Examples for space filling methods are Latin Hypercube sampling [113] and Sobol sequence [158]. As reviewed in [102], another sequential DoE strategy is adaptive sampling. As shown in Figure 3.5, the idea of adaptive sampling is that more sample points are performed close to the optimum, whereas points far away from the optimum are sampled less often. As reported in [48] for several test cases, adaptive sampling

finds points significantly closer to the optimum than space filling approaches while keeping the number of experiments the same. Therefore, adaptive sampling is suitable for optimization problems with costly experiments or costly computer simulations. In computer science, Bayesian optimization (BO) is frequently used for adaptive sampling combined with Gaussian process models for parameter optimization of machine learning algorithms, such as shown in [156], but was also successfully applied to photovoltaic power plants [2] and robotics [103]. As described in [150], to select the next experimental point, an algorithm must balance exploration versus exploitation. For optimization problems this implies that the algorithm must make sure to not only search near the local optimum, but also investigate potential other optimal regions. [1] uses the m-EGO algorithm, an early implementation of BO for selecting the next experiment in turn. They reported 36% fewer samples compared to a full factorial design approach.

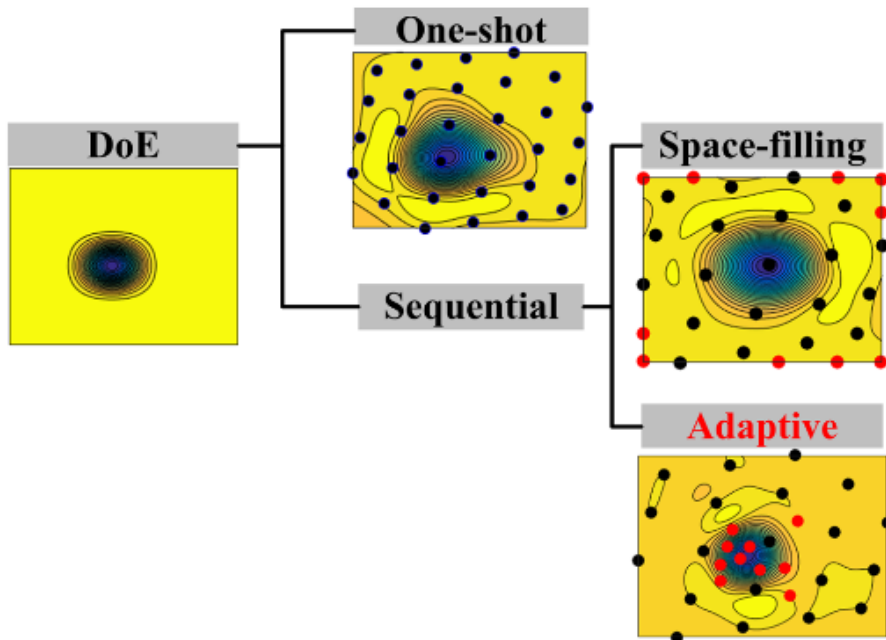


Figure 3.5: Categories of DoE methods according to [102]. For one-shot DoE, 30 experiments are used. For sequential DoE, 20 experiments are used for initialization (black dots) and 10 experiments are selected based on the corresponding sequential experimental design (red dots).

3.2.3 Determination of optimal parameters

Determination of optimal parameters by using model optimization techniques heavily depends on computing power. In the last decades there has been a massive surge in computing power following Moore's law, first described in [119]. The higher computing power also shifted the applied algorithms from computational

inexpensive methods such as gradient methods, which are prone to get stuck in local optima, to computationally more demanding methods such as meta-heuristics for global search. There exist many different algorithms for model optimization (see Table 3.1 and Table 3.2). The model complexity of typical process optimization models is moderate. Accordingly, algorithms for model optimization are not considered as the main hindrance for autonomous parameter selection of manufacturing processes.

3.3 Performance measurement in grinding

As explained in the previous section, process feedback is required to interact with the machining process. For general grinding applications many different sensors exist, as shown in an extensive review in [170]. Another review by [178] investigates monitoring of grinding wheels related to conditioning of grinding wheels. Measuring performance in the context of autonomous parameter selection is challenging for plunge face grinding because the process is mainly investigated to improve the process understanding and not for process parameter optimization. While for plunge face grinding consensus is missing about performance measurement and corresponding sensors for autonomous parameter selection, the studies focusing on an improved process understanding can shed some light on important measured quantities. Table 3.3 summarizes some studies for plunge face grinding of cemented tungsten carbide, ceramic, cermet, and polycrystalline cubic boron nitride (PCBN) insert material. The influence of many different grinding settings on various quantities has been investigated.

Table 3.3: Studies on plunge face grinding of inserts

Source	Workpiece material	Varied input/property	Measured quantity
[26]	cemented tungsten carbide	<ul style="list-style-type: none"> • cutting speed • axial feed rate • wheel binder material 	<ul style="list-style-type: none"> • insert quality • specific energy • grinding wheel topography
[45]	ceramic	<ul style="list-style-type: none"> • removed material • cutting speed • axial feed rate • radius speed • grinding wheel grain size • grinding wheel bond type • dressing type • dressing parameter • lubrication type • ceramic type 	<ul style="list-style-type: none"> • cutting edge quality • surface quality • forces • grinding wheel topography • grinding wheel wear • residual stress in the final workpiece surface • tool wear in a subsequent hard turning test of the ground inserts
[183]	ceramic	<ul style="list-style-type: none"> • conditioning parameters • removed material • ceramic type • grinding parameters • bond type • grain type • diamond concentration • lubrication type 	<ul style="list-style-type: none"> • forces • surface roughness • wear • workpiece surface zone analysis • temperature • flexural strength of final workpiece • wear of the ground insert in a subsequent turning operation
[46]	cermet	<ul style="list-style-type: none"> • removed material • grinding parameters • grain size • diamond concentration • bond type • lubrication type • wedge angle of insert • cermet type 	<ul style="list-style-type: none"> • forces • grinding wheel wear • surface roughness • cutting edge roughness • structure and crack analysis of workpiece • residual stress in the final workpiece surface
[29]	PCBN	<ul style="list-style-type: none"> • grinding parameters 	<ul style="list-style-type: none"> • grinding wheel wear
[32]	PCBN	<ul style="list-style-type: none"> • grinding parameters • grain size • bond type • dressing feed rate 	<ul style="list-style-type: none"> • wheel topography • maximum edge chipping • surface roughness • grinding forces

Table 3.3: Studies on plunge face grinding of inserts (continued)

[31]	PCBN	<ul style="list-style-type: none"> • different PCBN types 	<ul style="list-style-type: none"> • wheel topography • insert quality • grinding forces • material removal mechanism
[7]	PCBN	<ul style="list-style-type: none"> • grinding parameters 	<ul style="list-style-type: none"> • normal and tangential forces • surface roughness • wheel loading
[28]	PCBN	<ul style="list-style-type: none"> • grinding parameters • PCBN type • grinding wheel type 	<ul style="list-style-type: none"> • grinding wheel wear • insert quality
[30]	PCBN	<ul style="list-style-type: none"> • feed rate • cutting speed • oscillation frequency • process time 	<ul style="list-style-type: none"> • cutting forces • cutting energy • wheel wear • insert quality

For process optimization it is necessary to optimize individual production costs while fulfilling constraints, as exemplarily shown in Figure 3.6 for plunge face grinding of cutting inserts. For simplicity only the grinding process parameters are shown as inputs. A full list of properties influencing the grinding process is given in Table 2.2. Cost quantities, such as dressing time, maximum dressing interval and grinding time, as well as cost parameters, such as machine hourly costs and cost of the grinding wheel influence the individual production costs of the grinding operation. The cost parameters are not measured during grinding - these parameters depend on the cost structure of the factory. They depend on the location of the production site, purchasing contracts and/or actual workload of machines. The plunge face grinding process is bound by workpiece quality constraints such as surface roughness, cutting edge roughness, and grinding burn. Furthermore, the process can be constrained by process quantities. For example, high grinding temperatures can cause an ignition of grinding oil, which must be avoided to ensure a safe process. Often it is difficult to directly measure cost and quality quantities, hence process quantities such as force measurements are used to infer on cost and quality quantities. The considered cost quantities and constrained quantities are mainly determined by the grinding application.

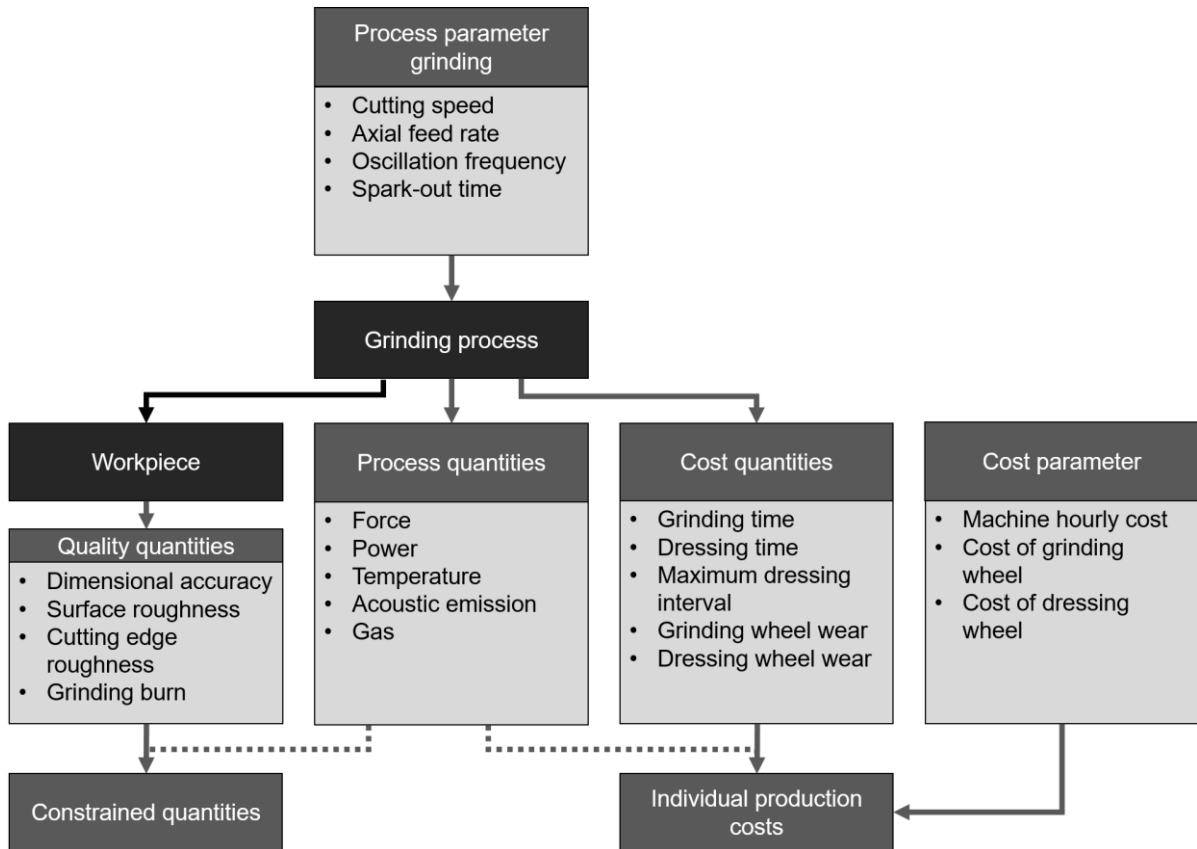


Figure 3.6: Process parameter, cost quantities, cost parameter, process quantities, and workpiece quality quantities of plunge face grinding of inserts for calculation of individual production costs and constrained quantities

3.3.1 Cost quantity measurement

Some cost quantities such as the grinding time and dressing time can be determined in a straightforward manner for a specific grinding setup. Both quantities depend on the programmed path and programmed velocity of the machine axes. Grinding wheel wear is another important cost quantity and several methods to measure or estimate grinding wear and related quantities have been proposed. For example, in [28] a microscope is used to directly measure macroscopic grinding wheel wear. Instead of directly measuring the grinding wheel wear, in [182] an imprint of the grinding wheel is used, which is later evaluated using a tactile measurement device. A similar procedure is used in [3] to measure corner wear optically by using an imprint and microscope measurements. The disadvantage of the proposed measurement procedures is that they often involve a lengthy measurement process and require a qualified operator. In [17] an external measurement system based on an optical triangulation sensor is integrated in the grinding machine for online measurement of micro and macro wear. The disadvantage of optical measurement systems is

that they get heavily disturbed by cooling lubricant and are mainly applicable to dry grinding. Another option for wear measurement is to measure the change of the workpiece size during batch grinding and to infer on the macro wear, often utilized in an industrial environment and applied in [8, 9]. While this method allows continuous correction of geometrical errors of workpieces, it does not provide a separation of grinding wheel wear and thermal deviation of the machine.

3.3.2 Workpiece quality measurement

Workpiece surface roughness can be measured by tactile or optical measurement devices. For example, in [7] a microscope is used to measure the final surface roughness after plunge face grinding of inserts. Cutting edge quality, often referred to cutting edge roughness or chipping, is another important property when grinding inserts, which describes the form deviation of the insert edge directly after grinding. In industry the quality of the cutting edge is often judged qualitatively by an operator using a magnifier or a microscope. In contrast to the qualitative industrial procedure, in [45] a tactile line measurement is used to quantify the cutting edge quality.

Grinding burn is another challenge in grinding of inserts, which causes severe damage of the workpiece. Several methods for grinding burn detection of the final workpiece exist, such as optical inspection, nital etching [71], Barkhausen noise analysis [76], Hall probe [165], or by using X-ray diffractometry [155]. Optical inspection means inspection of the workpiece surface for color changes after the grinding operation. Similar to optical inspection, nital etching is based on a final optical inspection but the workpiece is pretreated chemically by acids to improve the visibility of tempering and rehardening of the workpiece, as standardized in [71] for investigation of gears. As described in [76], Barkhausen noise analysis generates a varying magnetic field and measures the magnetization change of the workpiece which is influenced by the workpiece microstructure. Another method to measure the magnetization of the workpiece is to use a Hall probe, as shown in [165]. X-ray diffractometry on the other hand allows for chemical characterization of the workpiece by sending X-rays to the workpiece and measuring diffracted X-rays, as described in [155]. Hence many different measurement techniques based on different physical principles are available for grinding burn detection.

3.3.3 Process quantity measurement

Instead of measuring cost and quality quantities directly, process quantities such as force, power, and temperature can be used to estimate them. Often the estimation is supported by models, relating the process quantities with the cost and quality quantities. In an industrial environment, operators also detect grinding burn during operation indirectly by burn of grinding lubricant, which can be detected olfactorily. Table 3.4 summarizes industrial and lab sensors for process quantities in grinding and their applications. [73] shows grinding burn detection of cylindrical grinding using grinding temperature measurements at the contact zone. Using temperature measurements of the grinding zone directly is very promising for grinding burn detection as it allows to directly measure the cause of the grinding burn. It is also possible to combine different sensor signals. For example, the ratio between normal force and tangential force has been used in [90] as a wheel sharpness indicator. Another example is given in [148], utilizing acoustic emission, spindle electric current, and power signals for classification of grinding burn. Figure 3.7 and Figure 3.8 show different sensor types and sensor locations in grinding. For process quantities a great variety of sensors and sensor locations exist.

Table 3.4: Sensors for process monitoring and their applications in grinding

Reference	Measured quantity	Application
[171]	Normal force	Grinding contact detection and force-controlled grinding
[53]	Normal force	Chatter detection
[90]	Normal force Tangential force	Wheel sharpness indicator
[120]	Power	Spark-out time reduction
[67]	Power	Burn detection and grinding wheel life detection
[73]	Temperature	Prediction of workpiece surface layer properties
[77]	Acoustic emission	Conditioning monitoring
[96]	Acoustic emission	Detection of run-out error
[187]	Acoustic emission	Classification of sharp and dull grinding wheel
[188]	Acoustic emission	Grinding burn detection
[148]	Acoustic emission Electric current Power	Classification of grinding burn

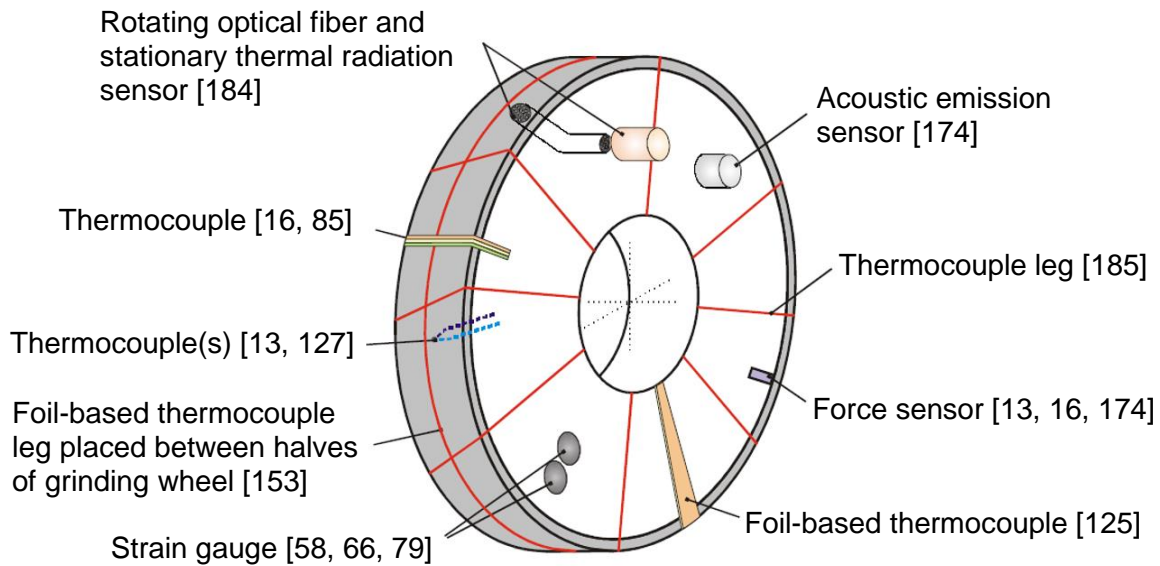


Figure 3.7: Grinding wheel-based sensors for measuring process quantities adapted from [13]

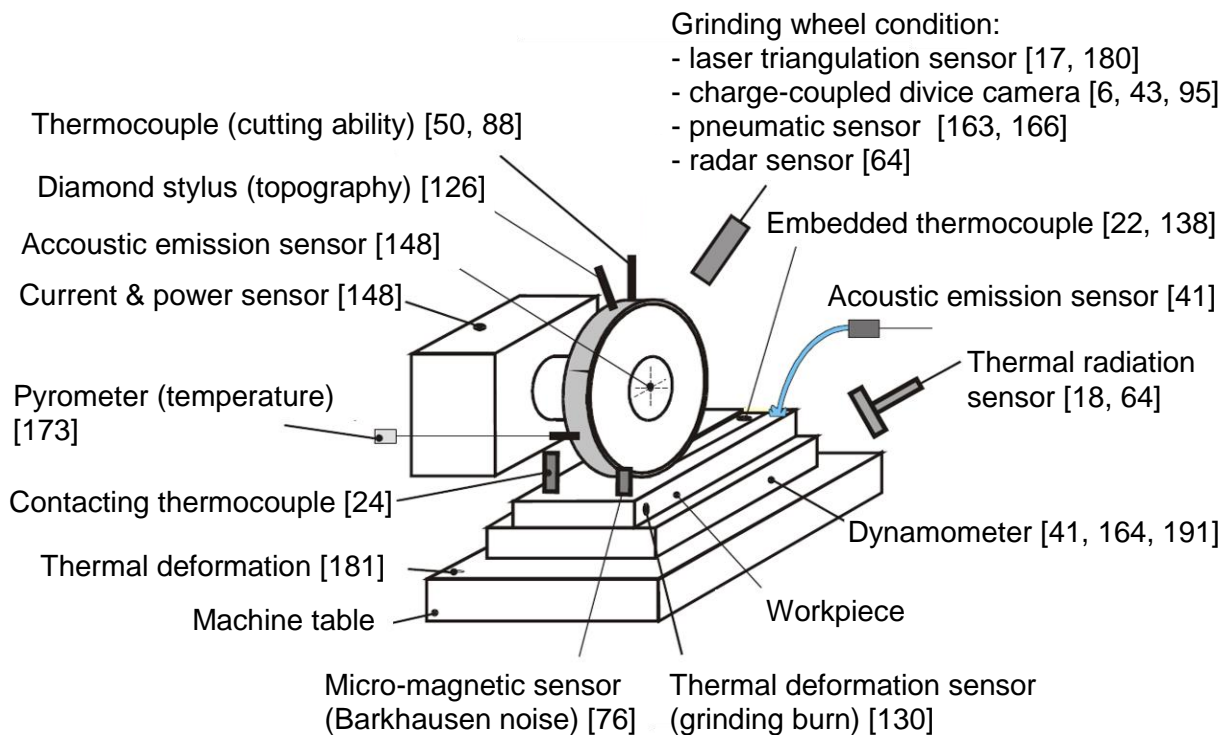


Figure 3.8: Sensors at machine or workpiece for measuring process quantities adapted from [13]

3.4 Performance measurement in turning

Similar to grinding, the main goal of performance measurement in turning is to characterize individual production costs and constraints. The individual production costs in turning consist of cost parameters, such as machine hourly costs and cost of the cutting insert, and cost quantities such as tool life and cutting time. The cutting time can be easily calculated by the specified feed per revolution, the cutting speed, and the initial and final workpiece geometry. The tool life on the other hand is not known *a priori* and must be determined experimentally by measurements. Typically, the tool life is quantified based on microscopic measurements of the inserts, such as used in [20]. Overcoming the limitations of offline measurements, online tool wear measurement based on digital images has been shown in [19].

Maximum surface roughness of the final workpiece is a typical constraint for the turning process. Similar to grinding, the surface roughness can be measured by a tactile measurement device such as for example used in [154]. And in [176] online surface roughness measurement based on laser-scattering is demonstrated.

Because measuring cost and quality quantities is sometimes challenging – especially in-process – process quantities are used to infer on these properties, in line with the approach in grinding. For example, in [23] force measurements are used to predict tool wear and in [40] an acoustic emission signal is investigated for surface roughness prediction.

3.5 Research gap

As shown in the state of the art an ideal system for autonomous parameter selection in manufacturing is able to include prior and domain knowledge to limit the number of experiments and at the same time autonomously acquire knowledge by interacting with the manufacturing process.

3.5.1 Data-driven optimization for knowledge acquisition

As identified in the state of the art, Gaussian process models and adaptive sampling are flexible and data efficient methods for the optimization of process parameters. However, only a few studies exist using Gaussian process models or adaptive sampling in grinding or turning. For optimization of a turning process, Gaussian process models have been used in combination with a full factorial design in [5]. Unfortunately, the authors do not provide any details of the specific Gaussian process model. However, a full factorial design is not a data-efficient

way to acquire knowledge. In [1] Gaussian process models have been combined with adaptive sampling for optimization of turning, where adaptive sampling showed superior performance compared to a full factorial design (details of the algorithm are presented in [142]). However, this early implementation has several shortcomings such as,

- The GP model assumes noise free experiments
- A fixed sample budget is used
- Constraints on outputs such as a maximum surface roughness are not considered
- Only material removal rate and surface roughness are considered, tool life is missing

Assuming noise free experiments, the Gaussian process model is forced to fit the measured data precisely, which leads to a poor model performance. This shortcoming is probably a consequence of the adaptation of the algorithm initially provided in [74], which is primarily designed for deterministic computer experiments. Using a fixed sample budget is also critical because too few samples lead to poor convergence and too many samples lead to a decrease in sample efficiency. Therefore, the research gap is the setup of a data-driven optimization for knowledge acquisition of expert systems in an industrial environment, avoiding the aforementioned shortcomings.

3.5.2 Quantification of process performance by sensor setup

For data-driven optimization it is necessary to provide process performance feedback. Many sensors exist for grinding and turning in general. However, the autonomous selection of process parameters for new machining tasks requires the combination of data-driven optimization with suitable sensors, which provide informative feedback on the process performance. As for example in [1], the tool life has not been considered for performance measurement in turning. Performance measurement is particularly challenging for plunge face grinding of inserts because it is a special grinding operation which has been mainly researched to improve the process understanding but not in the context of autonomous parameter selection. Therefore, for plunge face grinding it is necessary to establish a suitable performance measurement in the context of autonomous parameter selection and to combine it with appropriate sensors.

3.5.3 Prior knowledge and transfer of knowledge

The use of prior knowledge and the transfer of knowledge between similar tasks are approaches to improve the sample efficiency of data-driven optimizations. The used prior knowledge should be very general, simple to implement, and compatible with the data-driven optimization. Otherwise, one ends up with the same problems as traditional expert systems. As shown in the introduction, a common source of prior knowledge are physical or empirical models. For example, [116] demonstrates the combination of Gaussian process models with an analytical surface roughness model to improve the prediction accuracy in turning. Using this approach, they reported an improved model accuracy, especially for cases where only a few training samples are available. While the authors demonstrated data-efficient modelling of surface roughness, it is necessary to extend the use of prior knowledge to autonomous parameter selection, where it has tremendous cost saving potential.

Another approach to further increase the sample efficiency is transferring knowledge between similar cases by using the concept of similarity, as shown in eq. (3.1). However, the similarity must be determined by an expert in advance. For most practical applications it is difficult to specify similarity a priori. Accordingly, a data-driven approach is a possibility to overcome these limitations. In the Gaussian process literature learning from related tasks is often referred to multi-task learning, where correlations between different tasks are learned and used for model improvement, as shown in [161]. However, to the author's best knowledge such methods have not been published for autonomous parameter selection of turning and grinding.

3.6 Objectives

Based on the identified research gap the objectives of this thesis are:

- Quantification of the performance of grinding and turning by a sensor setup for subsequent optimization
- Establish a data-driven optimization for knowledge acquisition of manufacturing processes by improving the shortcomings of the current approaches
- Experimental demonstration of data-driven optimization for autonomous parameter selection exemplarily for longitudinal turning and plunge face grinding

- Incorporation of existing prior knowledge and transferring knowledge to further improve autonomous parameter selection for previously unexplored tasks

3.7 Outline of thesis

After a brief introduction in chapter 1, a summary on machining fundamentals in chapter 2, and an overview on the state of the art in chapter 3, chapter 4 provides an introduction to Gaussian process models and Bayesian optimization, which are used heavily throughout this thesis. Afterwards the turning process is investigated first because the process is considered simpler compared to grinding. Chapter 5 compares different optimization approaches for a simulated turning process. Using this experience, the autonomous parameter selection is demonstrated experimentally on a longitudinal turning machine in chapter 6. Building on the successful optimization of the turning process, the plunge face grinding process is investigated. Chapter 7 investigates different sensors for performance measurement in plunge face grinding of tungsten carbide. Based on the performance measurement and the tested optimization strategy, chapter 8 demonstrates autonomous parameter selection of tungsten carbide plunge face grinding. Plunge face grinding of PCBN is investigated in chapter 9, which is considered by human operators a difficult to control process and requires additional grinding wheel wear measurements. To further reduced the number of machining experiments, chapter 10 shows the incorporation of prior knowledge and the transfer of knowledge to improve data-efficiency. Finally, chapter 11 provides a short conclusion and an outlook.

4 Gaussian process models and Bayesian optimization

Before jumping to autonomous parameter selection, an introduction to Gaussian process models and Bayesian optimization is provided first. The introduction to the topic focuses on aspects, which are interesting for autonomous parameter selection for machining processes. A general introduction to Gaussian process models is given in [134] and an introduction to Bayesian optimization can be found in [150]. Parts of this chapter have been previous published in [105-109]

4.1 Gaussian process regression

According to [134], a Gaussian process can represent a distribution over functions and is a collection of random variables, which have a joint Gaussian distribution. A Gaussian process is fully defined by a mean function $m(\underline{x})$ and a covariance function $k(\underline{x}, \underline{x}')$ often referred as the kernel. Table 4.1 summarizes some typical kernels for Gaussian processes according to [134], where Γ is the gamma function, K_v is the modified Bessel function, σ_f^2 is the signal variance, and r is the distance between the input data points \underline{x} and \underline{x}' (in this case, the input data are process parameters that have to be optimized). The parameter v determines the smoothness of the function – a higher v leads to a smoother function. Throughout chapter 4 the Matern-5 kernel is used exemplarily. According to [134], the distance between the input data points \underline{x} and \underline{x}' can be calculated as follows,

$$r = \sqrt{(\underline{x} - \underline{x}')^T \underline{\underline{P}}^{-1} (\underline{x} - \underline{x}')} \quad (4.1)$$

$$\underline{\underline{P}} = \text{diag}(l_1^2, l_2^2, \dots, l_D^2) \quad (4.2)$$

where $\underline{\underline{P}}$ is a diagonal matrix containing characteristic length scale parameters l_i^2 for each input space dimension up to dimension D . The kernel function specifies the relation between the function values at process parameters \underline{x} and \underline{x}' , where for a short distance between the process parameters the corresponding function values are similar whereas for larger distances higher variations are observed.

Table 4.1: Matern and square exponential kernels according to [134]. The distance measure r is calculated following equation (4.1).

Kernel name	Formula
Matern	$k(\underline{x}, \underline{x}') = \sigma_f^2 \frac{2^{1-\nu}}{\Gamma(\nu)} (\sqrt{2\nu}r)^{\nu} K_{\nu}(\sqrt{2\nu}r)$
Matern 1 ($\nu = 1/2$)	$k(\underline{x}, \underline{x}') = \sigma_f^2 \exp(-r)$
Matern 3 ($\nu = 3/2$)	$k(\underline{x}, \underline{x}') = \sigma_f^2 \exp(-\sqrt{3}r)(1 + \sqrt{3}r)$
Matern 5 ($\nu = 5/2$)	$k(\underline{x}, \underline{x}') = \sigma_f^2 \exp(-\sqrt{5}r)\left(1 + \sqrt{5}r + \frac{5}{3}r^2\right)$
Square exponential ($\nu \rightarrow \infty$)	$k(\underline{x}, \underline{x}') = \sigma_f^2 \exp\left(-\frac{r^2}{2}\right)$

Based on a Gaussian process prior conditioned on t available measurements \underline{y}_t at process parameter points $\underline{x}_{1:t}$, predictions for an arbitrary process parameter point \underline{x}_* can be made following [134],

$$\mu_t(\underline{x}_*) = m(\underline{x}_*) + \underline{k}^T(\underline{x}_*) (\underline{\underline{K}} + \sigma_N^2 \underline{\underline{I}})^{-1} (\underline{y}_t - \underline{m}(\underline{x}_{1:t})) \quad (4.3)$$

$$\sigma_t^2(\underline{x}_*) = k(\underline{x}_*, \underline{x}_*) - \underline{k}^T(\underline{x}_*) (\underline{\underline{K}} + \sigma_N^2 \underline{\underline{I}})^{-1} \underline{k}(\underline{x}_*) \quad (4.4)$$

$$\underline{\underline{K}} = \begin{pmatrix} k(\underline{x}_1, \underline{x}_1) & \dots & k(\underline{x}_1, \underline{x}_t) \\ \vdots & \ddots & \vdots \\ k(\underline{x}_t, \underline{x}_1) & \dots & k(\underline{x}_t, \underline{x}_t) \end{pmatrix} \quad (4.5)$$

where μ_t is the posterior mean, σ_t^2 is the posterior variance, $\underline{\underline{I}}$ is the identity matrix, $\underline{m}(\underline{x}_{1:t}) = [m(\underline{x}_1) \dots m(\underline{x}_t)]^T$ is the mean function vector, $\underline{\underline{K}}$ is the covariance matrix, and $\underline{k}(\underline{x}_*) = [k(\underline{x}_*, \underline{x}_1) \dots k(\underline{x}_*, \underline{x}_t)]^T$ is the covariance vector. The measurements are assumed to be corrupted by Gaussian noise $N(0, \sigma_N^2)$, normally distributed noise with zero mean and variance σ_N^2 . If not otherwise stated, the Gaussian process prior mean function $m(\underline{x})$ is assumed zero throughout this thesis, which is a common choice in Gaussian process regression to specifying no expert knowledge. Figure 4.1 graphically illustrates the Gaussian process

regression. The left figure shows four arbitrary functions of the Gaussian process prior (dashed green lines), the Gaussian process prior mean (solid red line) and the confidence interval (shaded area). It can be seen that vastly different functions can be obtained from the same Gaussian process. The right figure shows four arbitrary functions (dashed green lines) of the posterior distribution after four experiments are available. Furthermore, the resulting predicted mean (solid red line) and the confidence interval (shaded area) are displayed, which can be calculated with equations (4.3) and (4.4). Predictions for process parameters close to the measurements show a lower uncertainty compared to predictions for process parameters far away from the measurements. For comparison, the true function (solid black line) is also shown which is typically unknown for real optimization tasks.

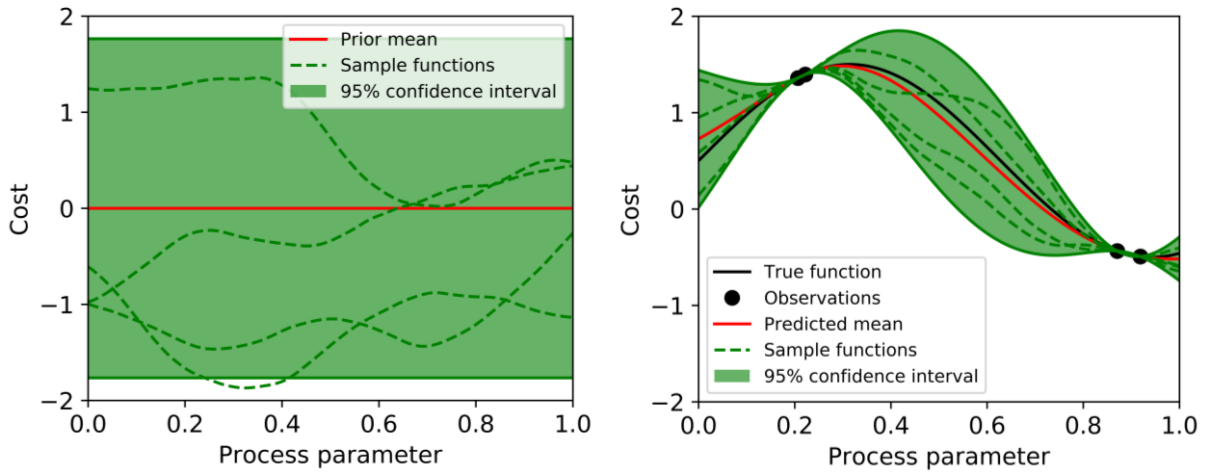


Figure 4.1: Illustration of the Gaussian process regression with a Matern 5 kernel and hyperparameters $\sigma_f^2 = 0.81$, $l_1 = 0.38$, and $\sigma_N^2 = 0$. The left figure shows exemplarily four arbitrary functions of the Gaussian process prior. The right figure shows the posterior distribution after four data points are available, where the dashed lines show four arbitrary functions and the solid red line represents the predicted mean $\mu_t(\underline{x}_*)$. The predicted mean $\mu_t(\underline{x}_*)$ is calculated using eq. (4.3). The green shaded area shows the 95% confidence interval, which is $0 \pm 2\sigma_f$ for the prior distribution and $\mu_t(\underline{x}_*) \pm 2\sigma_t(\underline{x}_*)$ for the posterior distribution. The predicted variance $\sigma_t^2(\underline{x}_*)$ is calculated using eq. (4.4).

The length scales l_i^2 in eq. (4.2), the signal variance σ_f^2 in Table 4.1, and the signal noise σ_N^2 in eq. (4.3) and eq. (4.4) are hyperparameters of the Gaussian processes regression, which can be summarized in a hyperparameter vector $\underline{\theta}$. It

is possible to specify these hyperparameters based on expert knowledge. Another method, as described in [134], is to determine the hyperparameters $\underline{\theta}^*$ based on available measurements by maximization of the marginal log likelihood $\log p(\underline{y}_t | \underline{\theta})$.

$$\log p(\underline{y}_t | \underline{\theta}) = -\frac{1}{2} \underline{y}_t^T (\underline{\underline{K}}_{\underline{\theta}} + \sigma_N^2 \underline{\underline{I}})^{-1} \underline{y}_t - \frac{1}{2} \log |\underline{\underline{K}}_{\underline{\theta}} + \sigma_N^2 \underline{\underline{I}}| - \frac{t}{2} \log 2\pi \quad (4.6)$$

$$\underline{\theta}^* = \arg \max \log p(\underline{y}_t | \underline{\theta}) \quad (4.7)$$

A $\underline{\theta}$ subscript is added to the covariance matrix in equation (4.6) to show its dependence on the hyperparameters $\underline{\theta}$ explicitly. If not otherwise stated, in this study a conjugate gradient method from the GMPL library [133] is used for the maximization of the marginal log likelihood, because preliminary tests indicated its suitability.

Figure 4.2 shows the Gaussian process regression results exemplarily for different hyperparameters. In the example the true cost function is set to $y = (x - 0.2)^2$ and displayed for illustration (dotted black line). The true cost function is evaluated at several process parameter values. The measurements are noisy observations of the true function $\bar{y} = y + \varepsilon$, where $\varepsilon \sim N(0, 5e-4)$. These measurements are the input data points to the Gaussian process regression. The red line displays the predicted mean cost and the shaded green area shows the corresponding 95% confidence interval of the cost prediction. Figure 4.2 (a) shows the Gaussian process regression for the hyperparameters maximizing the marginal log likelihood using equation (4.7). It can be seen that with these hyperparameters the fit of the data is very good. A GP regression using the same data points but a high signal noise hyperparameter is shown in Figure 4.2 (b). The prediction of the true cost function is still reasonable but shows a high overall uncertainty. Figure 4.2 (c) shows the Gaussian process regression for a short length scale hyperparameter. In this case more complex functions are also plausible candidates, which leads to high uncertainties between the measurements, where data is missing. In Bayesian optimization, short length scales lead to additional experiments and slow down the optimization. In contrast, Figure 4.2(d) shows the Gaussian process regression for a very long length scale hyperparameter. In this case the generalization from the observed measurements results in a simple (nearly linear) function for the

mean function of the Gaussian process and in low uncertainty over the whole range. In this case the true cost function is not always within the 95% confidence interval of the Gaussian process regression due to the predominant generalization. In Bayesian optimization, selecting very long hyperparameters may lead to sub-optimal parameter predictions. As pointed out in [134], an advantage of maximizing the marginal log likelihood to determine the hyperparameters is that it naturally trades off model complexity and goodness of model fit. The advantage for Bayesian optimization is that it minimizes the number of experiments while still providing a good model fit.

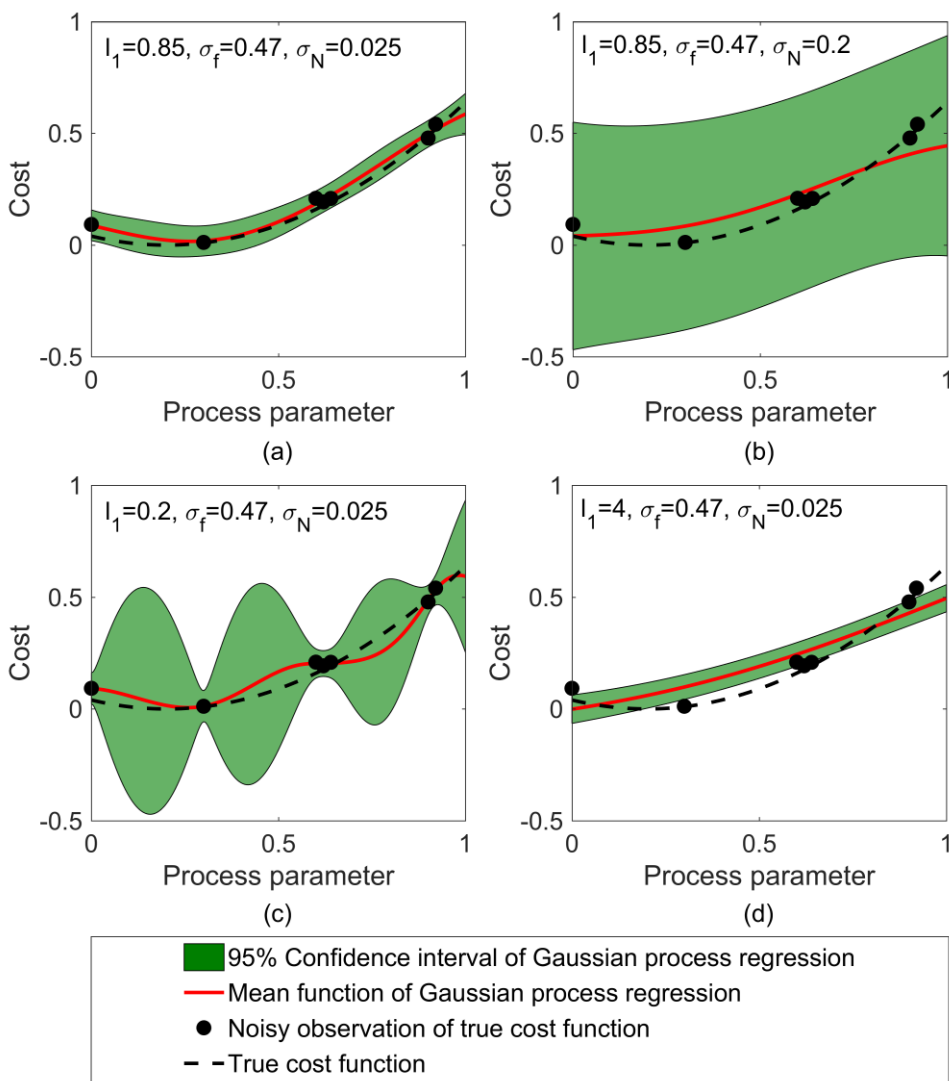


Figure 4.2: Gaussian process regression for different hyperparameters. Panel (a): hyperparameters determined by maximizing the marginal log likelihood using equation (4.7). Panel (b): results for high signal noise σ_N . Panel (c): results for short length scale parameter l_1 . Panel (d): results for long length scale parameter l_1 .

4.2 Gaussian processes for multi-task learning

Gaussian process models can be extended to learn multiple-tasks/multiple-outputs simultaneously, as investigated in detail in [4]. The motivation for such an approach is to exploit relations between tasks with the aim of improving the individual model accuracy without increasing the amount of data for the specific task. For manufacturing processes, a task corresponds to the optimization of a specific process setup. For example, in a first task the coating of the cutting tool might be from type A and in a second task it might be from type B, while the rest of the setup remains unchanged. In multi-task learning, the tasks are learned simultaneously, which allows to exploit correlation between the tasks' responses. This approach is in contrast to the conventional single-task/single-output approach, where each task is learned individually without exploiting correlations between tasks. Similar to the single task case, a Gaussian process for multi-task learning is defined as reported in [4],

$$\underline{f} \sim GP(\underline{m}, \underline{\underline{K}}) \quad (4.8)$$

where \underline{m} is a vector of mean functions for each task, and $\underline{\underline{K}}$ expresses the covariance between the different tasks.

The main difference between Gaussian processes for a single task and multiple-tasks is the specification of the covariance matrix. For the multi-task case, it is necessary to find a suitable expression for the matrix $\underline{\underline{K}}$, which specifies the relation between different tasks. The linear model of coregionalization (LMC) allows the specification of a valid covariance matrix $\underline{\underline{K}}$ by expressing the different output functions $f_d(\underline{x})$ as linear combinations of random functions as reported in [4, 52, 75],

$$f_d(\underline{x}) = \sum_{q=1}^Q \sum_{i=1}^{R_q} a_{d,q}^i u_q^i(\underline{x}) \quad (4.9)$$

where $u_q^i(\underline{x})$ are latent functions (hidden functions), $a_{d,q}^i$ are scalar coefficients, Q is the number of kernels, and R_q is the number of latent functions in each group with the same kernel. Figure 4.3 illustrates equation (4.9) graphically. Several latent functions are determined based on different kernels. Afterwards, the final functions are calculated by linear combination of the latent functions. The latent

functions $u_q^i(\underline{x})$ are used for model construction but cannot be directly measured and therefore are hidden. Only the output functions $f_d(\underline{x})$ can be measured. In the manufacturing process example, the output function $f_1(\underline{x})$ corresponds to the production cost of the first manufacturing task with cutting tool coating A and the output function $f_2(\underline{x})$ corresponds to the production cost of the second manufacturing task with cutting tool coating B.

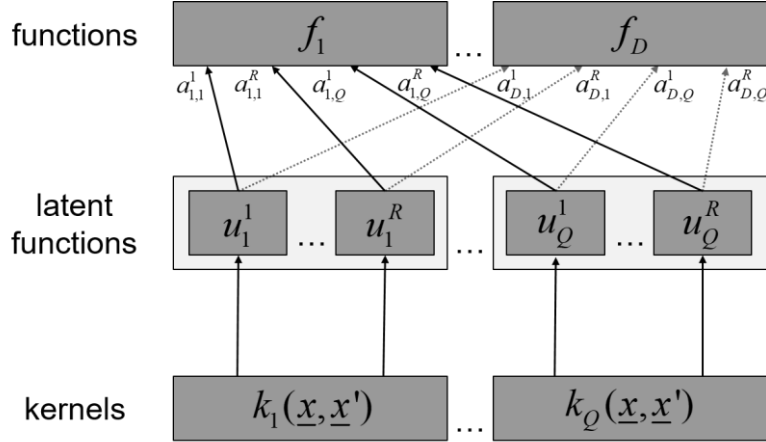


Figure 4.3: Illustration of LMC, as described in [4, 52, 75]

By using the LMC, $\underline{\underline{K}}(\underline{x}, \underline{x}')$ can be stated as in [4, 52, 75],

$$\underline{\underline{K}}(\underline{x}, \underline{x}') = \sum_{q=1}^Q \underline{\underline{B}}_q k_q(\underline{x}, \underline{x}') \quad (4.10)$$

where $\underline{\underline{B}}_q$ is the coregionalization matrix with entries $b_{d,d'}^q = \sum_{i=1}^R a_{d,q}^i a_{d',q}^i$ and rank R_q .

As shown in [4], by setting $Q=1$ the general LMC is reduced to the intrinsic coregionalization model (ICM) and by setting $R_q=1$ the general LMC is reduced to the semiparametric latent factor model (SLFM). Hence, both the ICM and the SLFM are special cases of the general LMC. As described in [25], different special cases ($\underline{\underline{B}} = \underline{\underline{I}}$ and $\underline{\underline{B}} = \underline{\underline{1}}$) can be derived from the ICM, which are illustrated in Figure 4.4. If $\underline{\underline{B}}_q$ is equal to the identity matrix as shown in the left panel of Figure 4.4, the tasks are modelled independently, but share the same kernel. The kernel only restricts the considered function space of the outputs but has no impact on the relation of the outputs. On the other hand, if all entries of the matrix $\underline{\underline{B}}_q$

are filled with 1, the outputs are perfectly related and only have different noise levels.

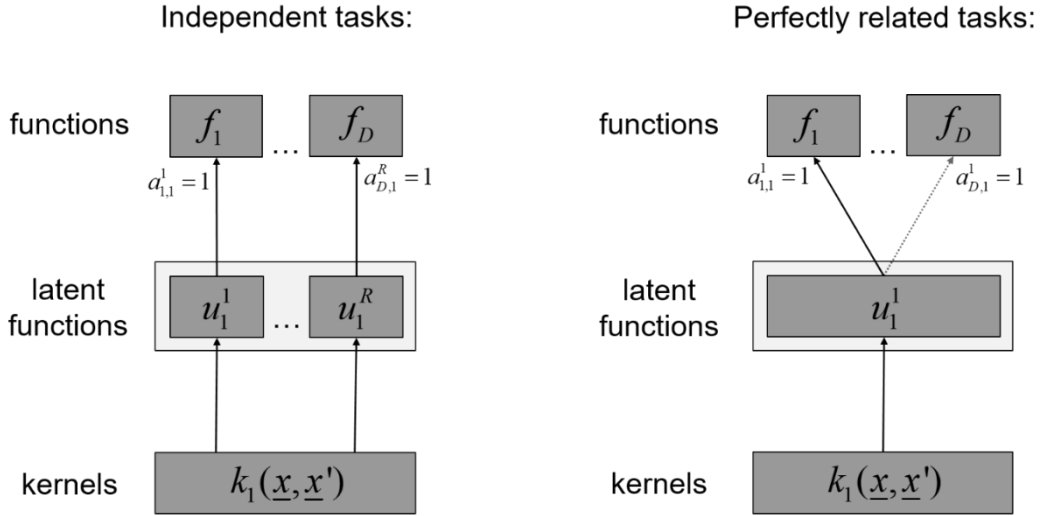


Figure 4.4: Illustration of special cases for the IMC, as described in [25]. The left panel shows the case where the tasks are modelled independently but share the same kernel. The right panel shows the case where all tasks are perfectly related.

As described in [4, 134], based on the data and the model, predictions for an arbitrary process parameter point \underline{x}_* follow a joint normal distribution $N(\underline{f}_*(\underline{x}_*), \underline{\underline{K}}_*(\underline{x}_*, \underline{x}_*))$.

$$\underline{f}_*(\underline{x}_*) = \underline{\underline{K}}_{x_*}^T \left(\underline{\underline{K}}(\underline{\underline{X}}, \underline{\underline{X}}) + \text{diag}(\underline{\sigma}_N^2) \otimes \underline{\underline{I}}_N \right)^{-1} \underline{y} \quad (4.11)$$

$$\underline{\underline{K}}_*(\underline{x}_*, \underline{x}_*) = \underline{\underline{K}}(\underline{x}_*, \underline{x}_*) - \underline{\underline{K}}_{x_*} \left(\underline{\underline{K}}(\underline{\underline{X}}, \underline{\underline{X}}) + \text{diag}(\underline{\sigma}_N^2) \otimes \underline{\underline{I}}_N \right)^{-1} \underline{\underline{K}}_{x_*}^T \quad (4.12)$$

For simplicity, the prior mean functions \underline{m} are assumed zero. The measured output vector is $\underline{y} = (y_{1,1}, \dots, y_{N,1}, \dots, y_{1,D}, \dots, y_{N,D})^T$, where D is the number of tasks and N is number of data samples per task, assumed to be the same for all outputs for notation simplicity. The measurements of each output are assumed to be corrupted with an individual Gaussian noise with zero mean and variance $(\underline{\sigma}_N^2)_d$.

The matrix $\underline{\underline{K}}(\underline{\underline{X}}, \underline{\underline{X}})$ has dimensions $ND \times ND$ and the matrix $\underline{\underline{K}}_{x_*}$ has dimensions $D \times ND$. Both matrices are calculated based on equation (4.10). Further details on the calculation are provided in the Appendix A. $\underline{\underline{I}}_N$ is the identity matrix with dimensions $N \times N$, $\underline{\underline{X}}$ are the input points for all

measurements of all tasks, and \otimes is the Kronecker product. The Kronecker product of $\text{diag}(\underline{\sigma}_N^2) \otimes \underline{I}_N$ multiplies each element of the matrix $\text{diag}(\underline{\sigma}_N^2)$ (dimensions $D \times D$) with matrix \underline{I}_N (dimensions $N \times N$), which results in a matrix with dimensions $ND \times ND$. For multi-task learning the prediction in eq. (4.11) and (4.12) is given as a joint normal distribution. The prediction of a single function $f_d(\underline{x}_*)$ at a test parameter point \underline{x}_* as for the single output case, corresponds to the marginal distribution of the joint normal distribution. For the prediction of the single function $f_d(\underline{x}_*)$, the mean is $\mu_d(\underline{x}_*) = (\underline{f}_*(\underline{x}_*))_d$ and the variance is $\sigma_d^2(\underline{x}_*) = (\underline{\underline{K}}_*(\underline{x}_*, \underline{x}_*))_{d,d}$, which directly follows from the properties of a joint normal distribution, as listed in [135].

The LMC has a number of hyperparameters collected in the vector $\underline{\theta}$, such as the elements of each coregionalization matrix $\underline{\underline{B}}_q$, the signal noise vector $\underline{\sigma}_N^2$, and the parameters for each kernel $k_q(\underline{x}, \underline{x}')$. By using Matern kernels, each kernel has length scale parameters l_i^2 for each input dimension and a signal variance parameter σ_f^2 . The hyperparameters can be computed by maximizing the marginal log likelihood, similar to equation (4.7) for the single output case, as described in [4, 134].

$$\begin{aligned} \log p(\underline{y} | \underline{\underline{X}}, \underline{\theta}) &= -\frac{1}{2} \underline{y}^T \left(\underline{\underline{K}}(\underline{\underline{X}}, \underline{\underline{X}}) + \text{diag}(\underline{\sigma}_N^2) \otimes \underline{I}_N \right)^{-1} \underline{y} \\ &\quad - \frac{1}{2} \log |\underline{\underline{K}}(\underline{\underline{X}}, \underline{\underline{X}}) + \text{diag}(\underline{\sigma}_N^2) \otimes \underline{I}_N| - \frac{ND}{2} \log 2\pi \end{aligned} \quad (4.13)$$

$$\underline{\theta}^* = \arg \max \log p(\underline{y} | \underline{\underline{X}}, \underline{\theta}) \quad (4.14)$$

4.3 Gaussian process classification

Gaussian processes can also be applied to classification tasks such as binary classification with two outcomes. An application is to classify a manufacturing process as stable or unstable. The main difference is that outputs of the Gaussian process regression are in the interval $(-\infty, \infty)$, while outputs in Gaussian process classification are probabilities in the interval $[0,1]$, as pointed out in [134]. Therefore, the general idea of Gaussian process classification is to use a Gaussian process prior over a latent function $f_i(\underline{x})$ and use a response function to transform

the latent function to valid probabilities, as described in [134]. A typical approach is called *probit regression* and uses the cumulative Gaussian distribution of a standard normal distribution $F(Z) = \frac{1}{\sqrt{2\pi}} \int_{-\infty}^Z \exp(-t^2/2) dt$ as a response function, as explained in [134].

Making predictions is more challenging for Gaussian process classification than for Gaussian process regression because the posterior distribution in classification is non-Gaussian and therefore analytically not traceable, as pointed out in [134]. Instead, one needs to use approximation methods such as *expectation propagation* [115] or sampling methods such as *Markov chain Monte Carlo* [122] to make predictions. In this study expectation propagation is applied for prediction and calculation of the marginal log likelihood because sampling methods increase the computational effort drastically. Details on calculating the marginal log likelihood and on making predictions using the expectation propagation algorithm are provided in Appendix B.

4.4 Bayesian optimization

Once a GP model of the objective is available, in Bayesian optimization an acquisition function is used to determine the candidate parameters where the next experimental trial is conducted. In general, the acquisition function provides an implicit trade-off between process parameters which are associated with a high uncertainty (exploration), and process parameters with a low predicted value (exploitation) [150]. Various acquisition functions can be used in Bayesian optimization such as *expected improvement* [117], *probability of improvement* [93], *upper confidence bounds* [159], and *predictive entropy search* [63]. In [48] good performance is demonstrated for constraint optimization based on an expected improvement acquisition function. As shown in [62], predictive entropy search is able to outperform expected improvement for constraint optimization, but this comes at the cost of increased complexity, potential numerical instabilities and analytical intractability. Hence, in a conservative approach the expected improvement acquisition function is used in this thesis.

For an unconstrained cost minimization task, the expected improvement function can be calculated following [74, 117],

$$a_{EI}(\underline{x}) = E[\max(C_{min} - f(x), 0)] \quad (4.15)$$

where C_{min} is the so far lowest measured cost. By using a Gaussian process model for $f(x)$, equation (4.15) stays analytically traceable and the expected improvement can be calculated following [74, 117],

$$a_{EI}(\underline{x}) = (C_{min} - \mu_{t,co}(\underline{x}))F(Z) + \sigma_{t,co}(\underline{x})\phi(Z) \quad (4.16)$$

$$Z = \frac{C_{min} - \mu_{t,co}(\underline{x})}{\sigma_{t,co}(\underline{x})} \quad (4.17)$$

where $\mu_{t,co}(\underline{x})$ is the predicted mean cost after t measurements obtained by Gaussian process regression using equation (4.3), $\sigma_{t,co}^2(\underline{x})$ is the predicted variance of the cost after t measurements obtained by Gaussian process regression using equation (4.4), $F(Z)$ is the cumulative standard normal distribution $F(Z) = 1/\sqrt{2\pi} \int_{-\infty}^Z \exp(-t^2/2) dt$, and $\phi(Z)$ is the probability density function of a standard normal distribution $\phi(Z) = 1/\sqrt{2\pi} \exp(-Z^2/2)$. A standard normal distribution is a normal distribution with zero mean and standard deviation of one. The acquisition function is displayed exemplarily for a cost minimization problem in Figure 4.5(a) using the Gaussian process regression from Figure 4.2(a). Based on the acquisition function the next experiment is conducted at a process parameter of 0.25, which maximizes the acquisition function.

Most machining operations require fulfilling constraints such as workpiece quality, process or safety constraints. As proposed in [48], the expected improvement acquisition function can be extended to constrained Bayesian optimization (CBO),

$$a_{EIC}(\underline{x}) = a_{EI}(\underline{x}) \prod_{i=1}^n p_{f,i}(\underline{x}) \quad (4.18)$$

where $a_{EI}(\underline{x})$ is the expected improvement without constraints (4.16), n is the number of constraints, and $p_{f,i}(\underline{x})$ is the probability that the constraint i is fulfilled. For the constrained case the best observed value C_{min} is the minimal measured cost value, which fulfills all constraints - and not the absolute minimal measured cost as in the case without constraints. For the classification case, where the result of the constraint is binary such as a stable process or an unstable process,

the probability that the constraint i is fulfilled is calculated directly by Gaussian process classification. For the regression case, where the constraint is not allowed to exceed a specific value such as a maximum surface roughness, the probability that the constraint i is fulfilled can be calculated following [48],

$$p_{f,i}(\underline{x}) = \frac{1}{\sigma_{t,c_i}\sqrt{2\pi}} \int_{-\infty}^{c_{\max,i}} \exp\left(\frac{-(t - \mu_{t,c_i}(\underline{x}))^2}{2\sigma_{t,c_i}^2(\underline{x})}\right) dt \quad (4.19)$$

where $c_{\max,i}$ is the maximum allowed value for constraint i , $\mu_{t,c_i}(\underline{x})$ is the predicted mean of constraint i after t iterations calculated using (4.3), and $\sigma_{t,c_i}^2(\underline{x})$ is the variance of the constraint i after t iterations calculated using (4.4). Following [48, 74, 117], the next experiment is conducted for process parameters \underline{x}_{next} , which maximize the constrained expected improvement acquisition function.

$$\underline{x}_{next} = \arg \max a_{EIC}(\underline{x}) \quad (4.20)$$

The acquisition functions can have multiple optima, as shown in [74]. Hence, throughout this thesis for a one-dimensional input space a grid-based evaluation is used for the optimization of the acquisition function with approximately 10'000 equally distributed parameters. For a two-dimensional input space, random search (generated by a Sobol sequence [158]) is used instead with 30'000 points because, as shown in [10], random search is more data-efficient than the commonly used grid search approach for multiple dimensions, especially for cases where the outputs are not equally sensitive to all input parameters.

Figure 4.5(b) shows exemplarily the result of a Gaussian process regression for a constraint quantity. In a real application, the quantity might be surface roughness of the workpiece or the temperature during the machining process and must stay below a specified limit, which depends on the requirements such as the final workpiece quality. In this example, the limit is set to 250. The probability that the constraint is fulfilled is displayed in Figure 4.5(c) and can be calculated using equation (4.19) and the Gaussian process regression of the constraint, as displayed in Figure 4.5(b). Finally, the constrained expected improvement acquisition function is displayed in Figure 4.5(d) and can be calculated according to equation (4.18), using the Gaussian process regression of the cost (displayed in Figure 4.2(a)) and the Gaussian process regression of the constraint (displayed in Figure

4.5 (b)). The constrained expected improvement acquisition function is maximal for a process parameter value of 0.61, which is the next experimental parameter value. The constrained expected improvement acquisition function favors higher process parameters than the acquisition function without considering constraints because according to the Gaussian process regression of the constraint the probability that low process parameters fulfill the maximum allowed constraint of 250 is low. After the next experiment is conducted at a process parameter value of 0.61, the optimization procedure is repeated with the newly available measurements until a maximum number of iterations or a stopping criterion is reached.

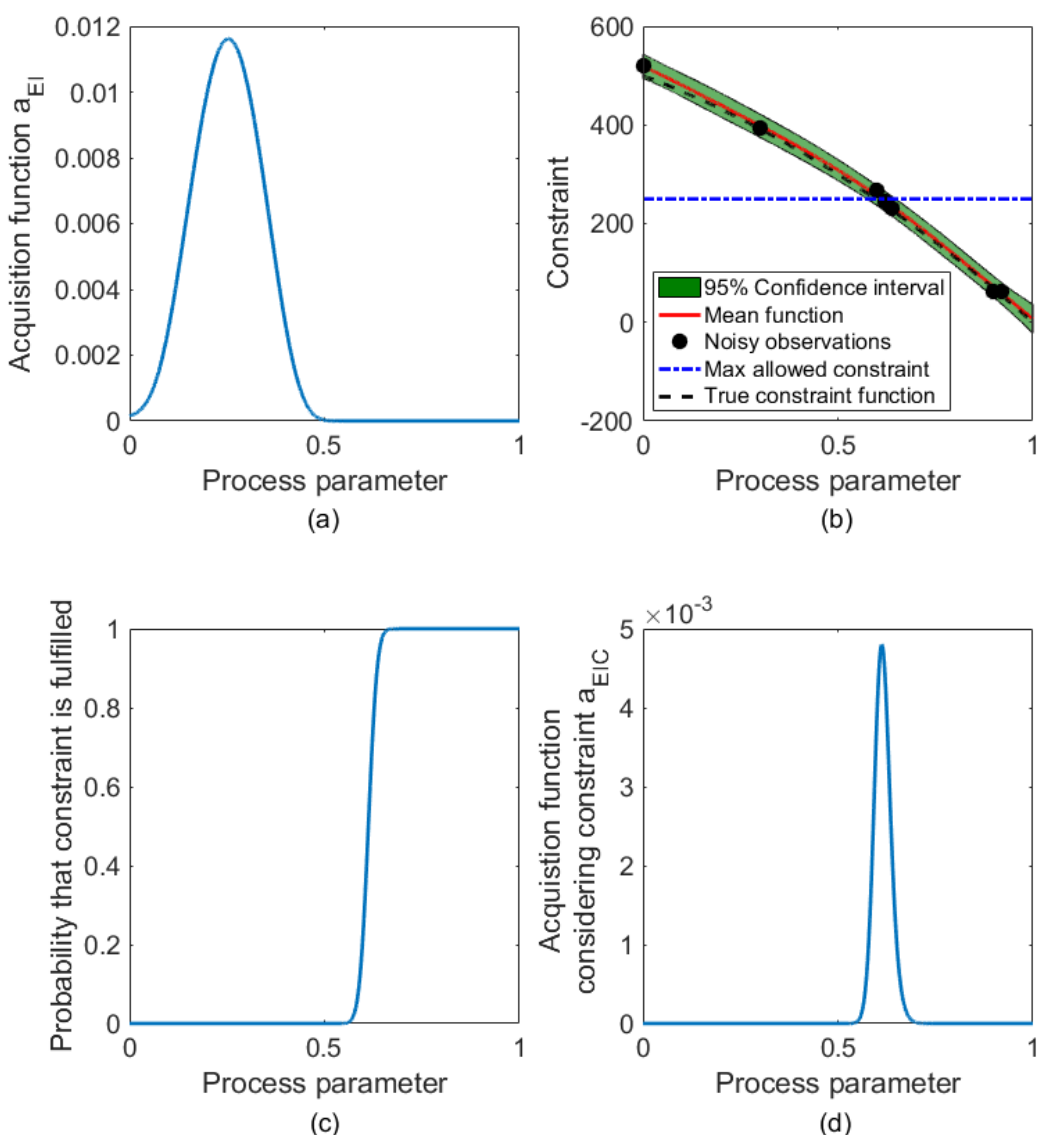


Figure 4.5: Panel (a) shows the calculation of the acquisition function without considering constraints using equation (4.16) and the Gaussian process regression model of the cost as displayed in Figure 4.2(a). Panel (b) shows the Gaussian process regression

model of the constraint exemplarily, calculated by maximizing the marginal log likelihood. Panel (c) shows the probability that the constraint is fulfilled, calculated using equation (4.19) and the Gaussian process regression of the constraint, as displayed in panel (b). Panel (d) shows the result of the acquisition function considering constraints, which can be calculated using equation (4.18).

Different stopping criteria can be used in practice. A simple and often used stopping criterion is to limit the maximum number of iterations, as applied in [48]. For real optimization problems with unknown objective and constraint functions it is infeasible to a priori specify the number of iterations until convergence is reached. As a result, this approach is limited to optimization tasks, where the optimization budget is fixed. For optimization tasks without a fixed budget, [175] proposed to limit the number of experiments based on the estimated uncertainty at the predicted optimal parameter values \underline{x}_{opt} ,

$$\sigma_{t,co}(\underline{x}_{opt}) < \varepsilon_{stop} \quad (4.21)$$

where ε_{stop} is a predefined threshold value. Another stopping criteria has been proposed by [74], which can be calculated as follows.

$$\frac{\max(a_{EI})}{C_{\min}} < \varepsilon_{stop} \quad (4.22)$$

In this case the algorithm uses the maximum expected improvement normalized with the current best value as a stopping criterion, which must be below a certain threshold value ε_{stop} . A summary of the Bayesian optimization procedure is displayed in Figure 4.6.

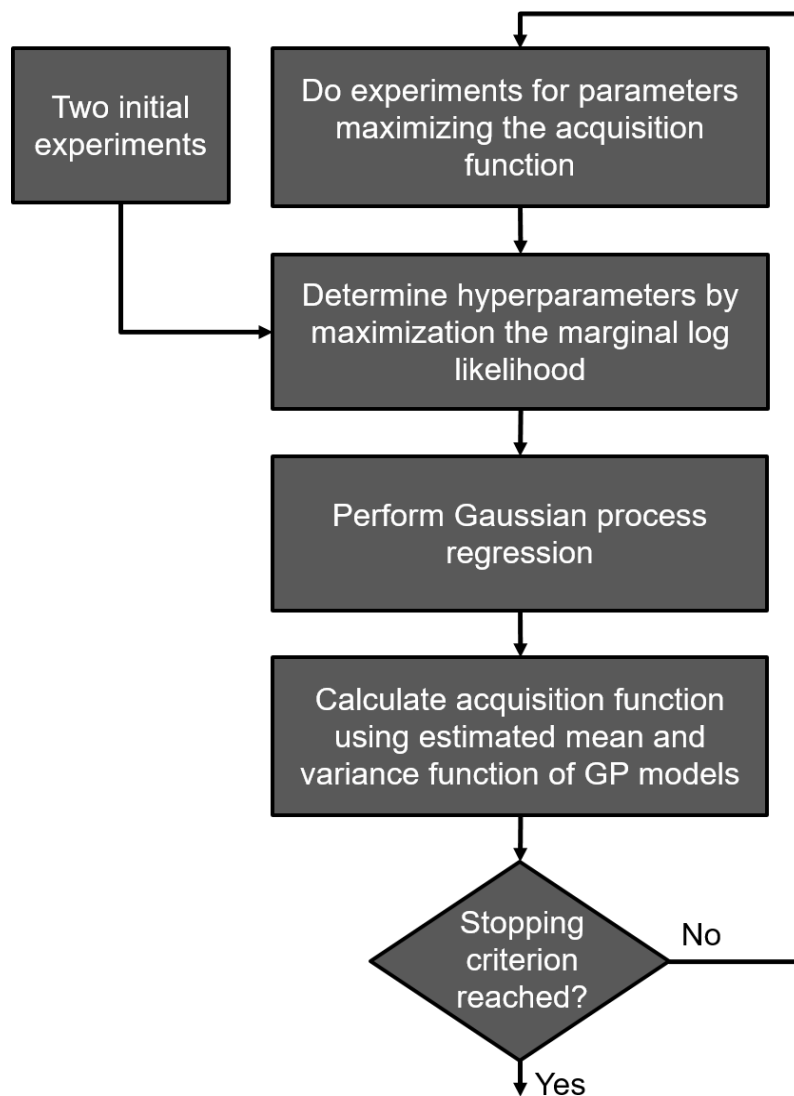


Figure 4.6: Procedure of Bayesian optimization

5 Optimization of simulated turning process

The autonomous parameter selection is first tested in a simulated turning environment before switching to an experimental optimization. In this section constrained Bayesian optimization is compared to unconstrained Bayesian optimization in addition to the comparison of different kernel functions. Part of this chapter has been previously published in [106].

5.1 Methodology

The optimization task in this section is to produce high quality turning parts at minimal individual production costs. High quality workpieces must fulfill certain quality constraints, which in this section correspond to the surface roughness R_a . The maximum allowed surface roughness $R_{a,\max}$ is assumed to be $0.7 \mu\text{m}$. The production costs are determined by the production time and the tool life T . In this chapter, the cutting speed v_c and feed per revolution f are the unknown machining parameters to be optimized, and the depth of cut is fixed at 0.5 mm.

5.1.1 Simulation environment

An empirical model for the turning process from [78] is used to test parameter tuning. The model from [78] is derived using Taguchi method and response surface methodology for finishing hard turning of cylindrical AISI 52100 bearing steel bars with a diameter of 41 mm and a length of 300 mm using a cubic boron nitride (CBN) tool.

$$T = 127.5365 - 0.84629v_c - 144.21f + 0.001703v_c^2 + 0.3656v_cf \quad (5.1)$$

$$R_a = 0.9094 - 0.010035v_c + 7.0877f + 0.000034v_c^2 - 0.018969v_cf \quad (5.2)$$

The range of parameter values ($100 \text{ m/min} \leq v_c \leq 200 \text{ m/min}$ and $0.08 \text{ mm/rev} \leq f \leq 0.16 \text{ mm/rev}$), where this model can be applied, is also used as the optimization domain. Furthermore, the diameter D and the length l of the workpiece were assumed to be equal as in [78]. The individual production costs C_{FE} were defined as follows,

$$C_{FE} = t_c(\underline{x}) \left(C_{MH} + \frac{C_w}{T(\underline{x})} \right) \quad (5.3)$$

$$t_c = \frac{lD\pi}{v_c f} \quad (5.4)$$

where t_c is the cutting time, C_w are the tool wear costs, and C_{MH} are the machine hourly costs. For the optimization, it is assumed that the machine hourly costs are 40 U/h and the tool wear costs are 50 U. Figure 5.1 shows an overview of the simulation environment.

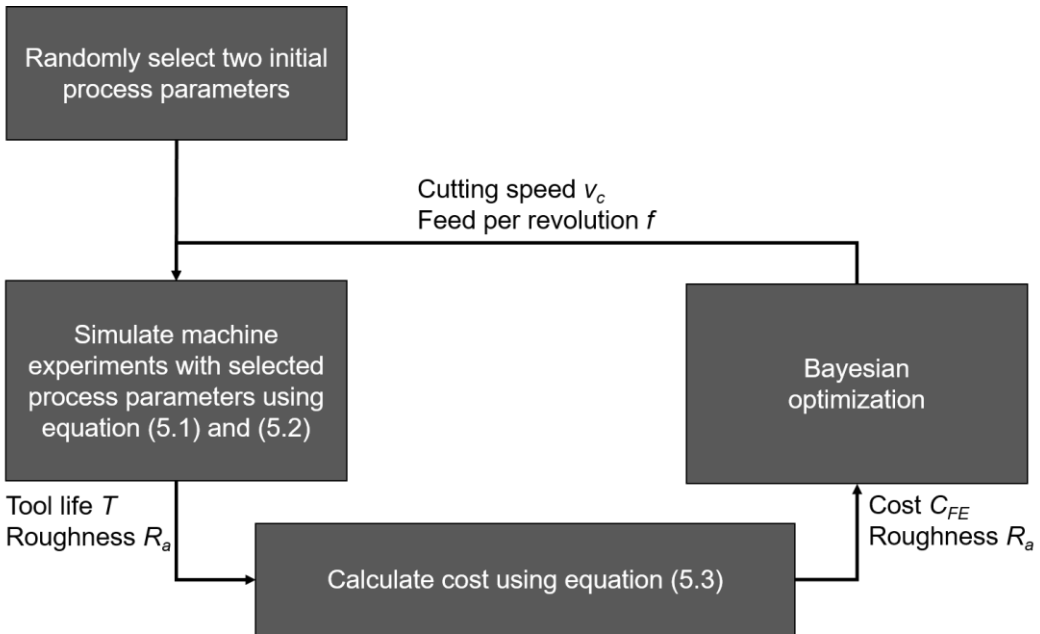


Figure 5.1: Overview simulation environment

5.1.2 Convergence of optimization

Convergence of the optimization is evaluated based on a comparison with the true minimal cost $C_{t,\min}$. The true minimum of the cost is,

$$C_{t,\min} = \min_{\underline{x} \in X} C_{FE}(\underline{x}) \text{ s.t. } R_a(\underline{x}) < R_{a,\max} \quad (5.5)$$

where the cost and roughness are evaluated based on (5.2) and (5.3). The minimum of the true objective is obtained using a grid-based evaluation, where the model is tested for evenly distributed parameter combinations with an increment of 0.1 m/min for the cutting speed and 0.001 mm/rev for the feed per revolution. The optimal parameters of the true function are a feed per revolution of 0.131 mm/rev and a cutting speed of 163.4 m/min. The error of the optimization is defined as $\epsilon_t = |C_{FE}(\underline{x}_{opt}) - C_{t,\min}|$, where $C_{FE}(\underline{x}_{opt})$ is the cost

evaluated for the best estimated parameters of the optimization. Similarly, the relative error is defined as $\epsilon_R = \epsilon_t / C_{t,\min}$.

5.1.3 Unconstrained Bayesian optimization

In the conventional Bayesian optimization approach, the objective function is defined without constraints. This can be achieved by defining the optimization problem as a utility U maximization problem.

$$\underline{x}_{\max} = \arg \max_{\underline{x} \in X} U(\underline{x}) \quad (5.6)$$

In the case where the workpiece fulfills the quality constraints, the utility is calculated as the earnings from workpiece sale E minus the individual production costs C_{FE} . In the case where the workpiece quality is not acceptable, the utility is negative because workpieces cannot be sold and production costs are generated.

$$U(\underline{x}) = \begin{cases} E - C_{FE}(\underline{x}), & \text{for } R_a \leq R_{a,\max} \\ -C_{FE}(\underline{x}), & \text{for } R_a > R_{a,\max} \end{cases} \quad (5.7)$$

The price of the raw material is neglected and it is assumed that the individual production costs are equal to the total production costs for simplicity, as it would only shift the curve by a constant value. The earning is assumed to be 10 U, which only affects the utility of the workpieces that fulfill the surface roughness constraint.

A single GP model is used to estimate the utility score, and the expected improvement acquisition function (4.16) is used to determine the parameters for the next cutting trial. The formulation of equation (4.16) slightly changes for a maximization task compared to a minimization task. However, instead of maximizing the utility one can minimize the negative utility. The optimal parameters \underline{x}_{opt} are defined as the maximum of the estimated mean utility function which is calculated using equation (4.3). Figure 5.2 summarizes the unconstrained Bayesian optimization approach.

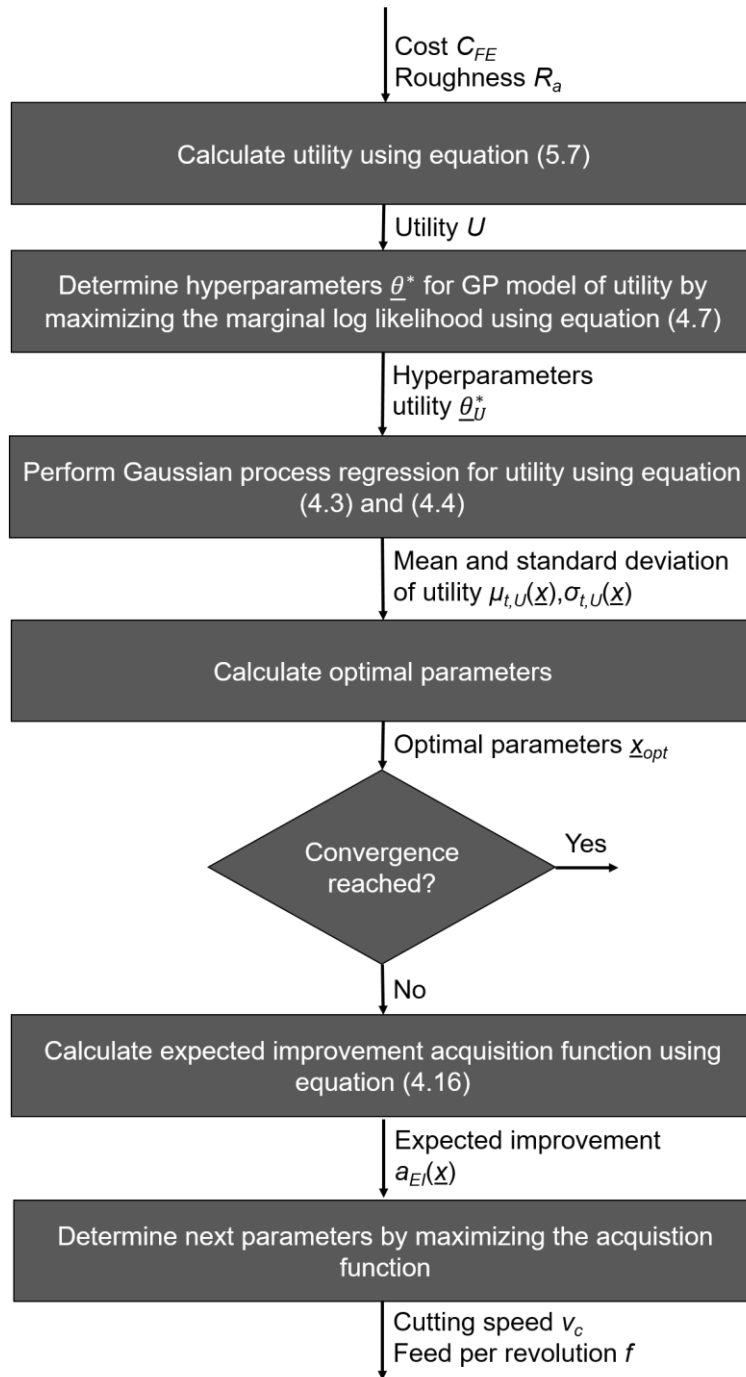


Figure 5.2: Flow diagram of unconstrained Bayesian optimization

5.1.4 Constrained Bayesian optimization

The second approach is the minimization of the individual production costs subjected to constraints on surface roughness:

$$\underline{x}_{\min} = \arg \min_{\underline{x} \in X} C_{FE}(\underline{x}), \text{ s.t. } R_a(\underline{x}) < R_{a,\max} \quad (5.8)$$

Two GP models are needed for optimization – one for the surface roughness constraint and one for the cost function. The parameters of the next cutting trial

5 | Optimization of simulated turning process

are determined using the constrained expected improvement acquisition function (4.18). The estimated optimal parameters are defined as the parameters which minimize the estimated mean cost $\mu_{t,co}$ and result in an estimated mean surface roughness $\mu_{t,Ra}$ which is below the maximum allowed roughness $R_{a,max}$:

$$\underline{x}_{opt} = \arg \min \mu_{t,co}(\underline{x}), \text{ s.t. } \mu_{t,Ra}(\underline{x}) < R_{a,max} \quad (5.9)$$

Figure 5.3 summarizes the constrained Bayesian optimization approach.

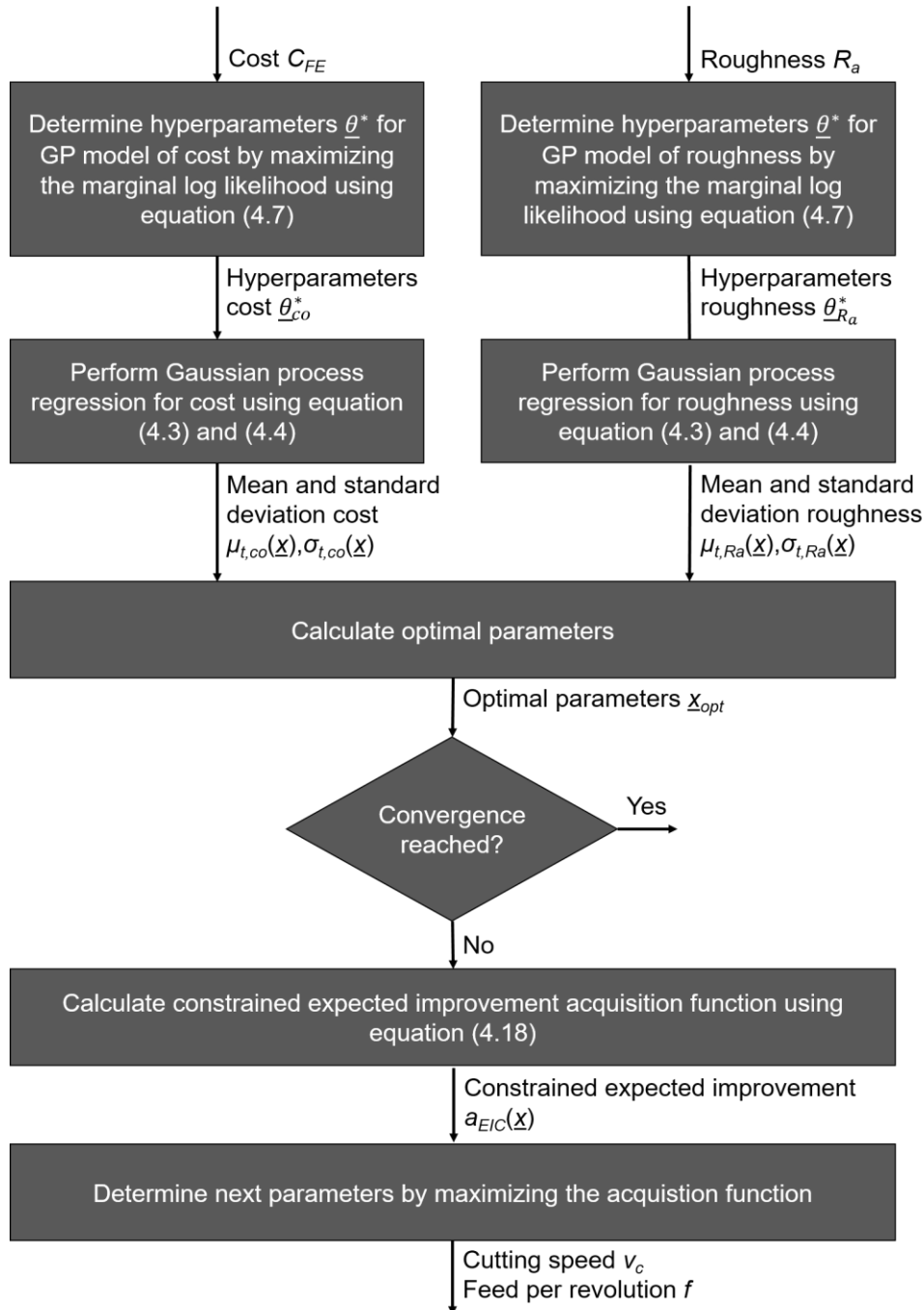


Figure 5.3: Flow diagram of constrained Bayesian optimization

5.2 Simulation results

The convergence results for Bayesian optimization and constrained Bayesian optimization are presented in Figure 5.4 and Figure 5.5. For CBO, the 95% confidence interval of the estimated optimal cost is reduced very fast and the estimation is very certain about the best point after 10 iterations. The results of the estimation are confirmed by the error ε_t , which decreases also very fast for CBO. In contrast to this very good result for CBO, BO does not achieve full convergence. For BO, the uncertainty of the estimated best point fluctuates and stays high for all iterations. The convergence behavior is confirmed by the error ε_t .

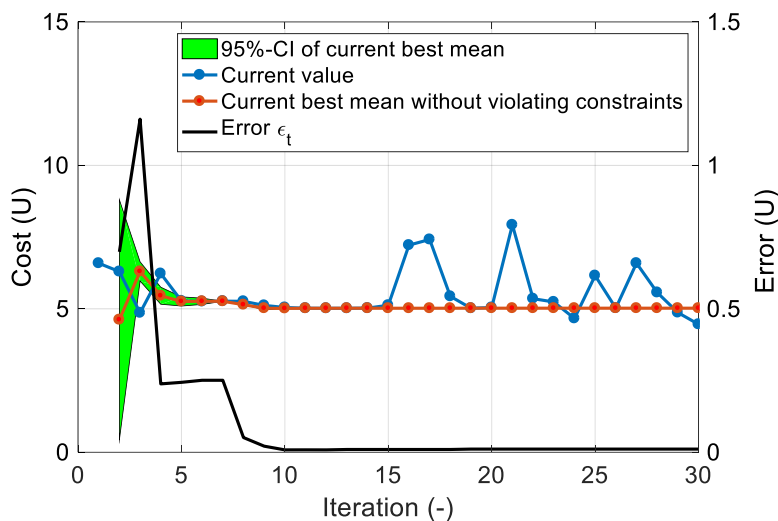


Figure 5.4: Convergence of constrained Bayesian optimization with Matern 5 kernel

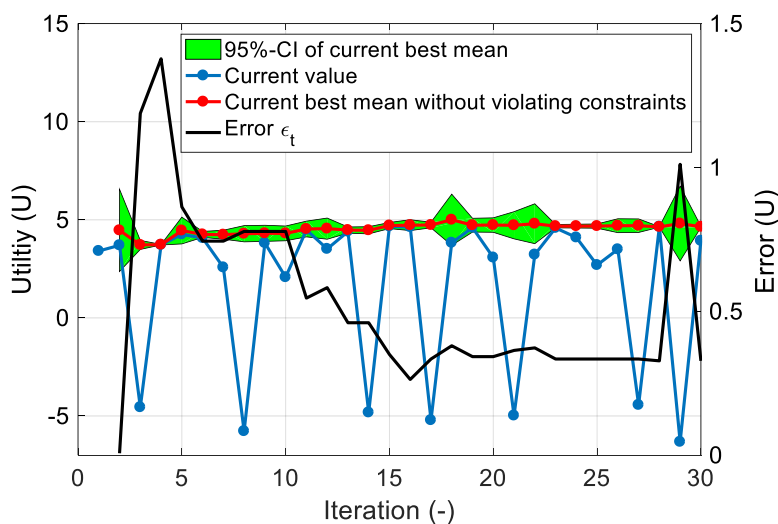


Figure 5.5: Convergence behavior of Bayesian optimization without constraints and Matern 5 kernel

The resulting costs for estimated optimal parameters of BO and CBO with different kernels were compared to the true optimal cost. To keep the results comparable all experiments are started with two identical turning parameter configurations. For the CBO case the same kernel is used for the surface roughness and the cost GP model – it would also be possible to model the surface roughness and cost with different kernels. Figure 5.6 shows the error after 30 iterations for both methods and different kernel functions. The estimated optimal parameters of CBO lead to a cost much closer to the true minimal cost than BO for all kernels. For CBO, square exponential, Matern 3 and Matern 5 kernels show a very small error (below 0.1%) and the largest error is obtained for the Matern 1 kernel. This behavior is typical because the smoothness of the considered functions decreases from squared exponential to Matern 5 to Matern 1 kernel, which leads to a slower convergence of the Matern 1 kernel compared to the other kernels.

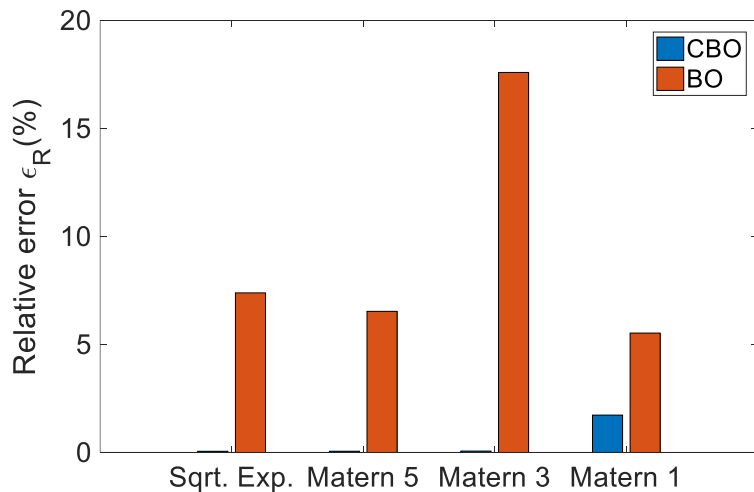


Figure 5.6: Convergence comparison of Bayesian optimization without constraints (BO) and constrained Bayesian optimization (CBO) for different kernel functions

After 30 iterations, the predicted mean cost and mean surface roughness function of the CBO is very close to the true function (5.2) and (5.3). Figure 5.7 shows the true utility function and the predicted mean utility function of the Gaussian process regression used for BO. The sudden jump in utility, which is caused due to the surface roughness constraint, is not modelled precisely by the Gaussian process model. Therefore, the worse performance of BO compared to CBO can be explained by limitations of the tested Gaussian process models, which are unable to model jumps or discontinuities precisely.

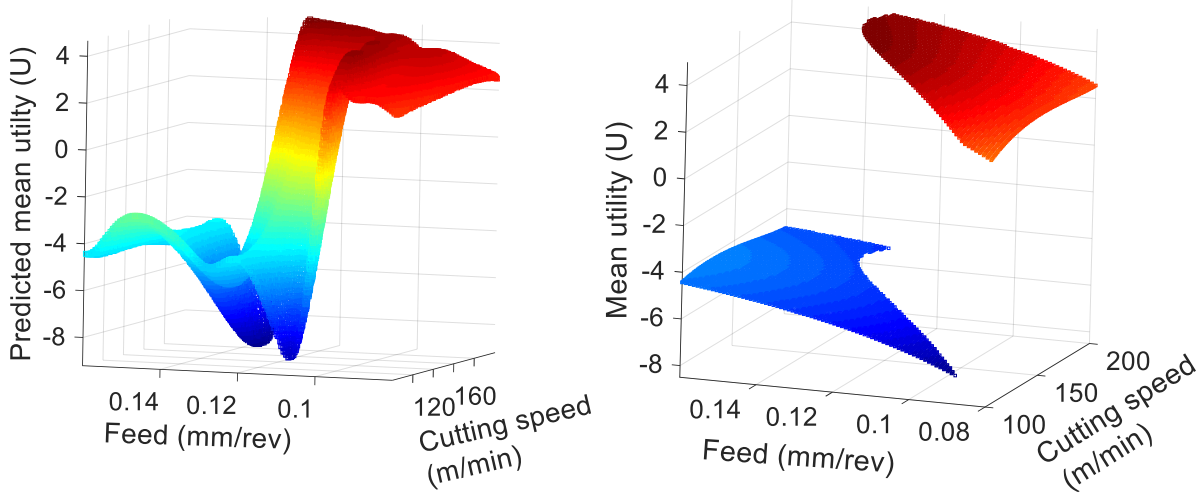


Figure 5.7 Left: Predicted mean utility of Gaussian process regression used for Bayesian optimization without constraints after 30 iterations with a Matern 5 kernel. Right: True utility function calculated from equation (5.7).

5.3 Conclusion

In conclusion, constrained Bayesian optimization showed a superior performance compared to the standard Bayesian optimization approach for a typical turning optimization task, as a consequence of Gaussian process model limitations to accurately model jumps or discontinuities. It might be possible to improve the modelling of jumps or discontinuities by using a neural network kernel, as shown in [134]. However, this comes at the cost of an increase in model complexity, typically increasing the number of iterations Bayesian optimization needs to solve such problems. Therefore, it is recommended to set up the optimization task in a way to avoid discontinuities in the modelled functions. Furthermore, for the simulated turning optimization task, the influence of the kernel selection on the results of constrained Bayesian optimization is small.

6 Optimization of longitudinal turning

After constrained Bayesian optimization outperformed conventional Bayesian optimization for parameter selection of a simulated turning process, the constrained Bayesian optimization approach is tested experimentally. Part of this chapter has been previously published in [109].

6.1 Methodology

6.1.1 Optimization task and cost calculation

The optimization task in this chapter is to produce turning parts with minimal individual production costs C_{FE} and produce workpieces which fulfill the roughness constraint $R_{a,max}$:

$$\underline{x}_{\min} = \arg \min_{\underline{x} \in \chi} C_{FE}(\underline{x}), \text{ s.t. } R_a(\underline{x}) < R_{a,max} \quad (6.1)$$

Where \underline{x} is a vector of the optimized parameters cutting speed v_c and feed per revolution f . In this section the individual production costs were calculated as follows,

$$C_{FE}(\underline{x}) = t_c(\underline{x}) \cdot \left(C_{MH} + \frac{C_I + t_i(C_{MH} + C_o)}{T(\underline{x})} \right) \quad (6.2)$$

where t_c is the cutting time and T is the tool life. The individual production costs combine cost of machining time and tool replacement costs. The used cost and constraint parameters are listed in Table 6.1.

Table 6.1: Cost and constraint parameters for optimization

Parameter	Description	Value
C_{MH}	Machine hour-rate	60 U/h
C_I	Cost per cutting edge	10 U
t_i	Time to change worn out insert	10 min
C_o	Operator cost per hour	100 U/h
$R_{a,max}$	Maximum roughness	0.8 μm

6.1.2 Experimental set-up

The used feedstock are steel bars made of 1.4125 (AISI440C, X105CrMo17) with an initial diameter of 7 mm. The longitudinal turning is performed with constant depth of cut of 0.3 mm. The bars are cut 6 times with a cutting length of 10 mm for each cut. This results in a final workpiece of length 10 mm and a final diameter of 3.4 mm. As shown in Figure 6.1, a CNC-Lathe (Deco Sigma 8 made by Tornos SA) is used for the experiments. The machine is equipped with an automatic bar feeder Robobar SBF-210 from Tornos SA. As cooling fluid Blasomill 15 mineral oil from Blaser Swisslube AG with a constant flow rate of 5.8 l/min is used. The cutting insert type VCGX-FN 120302 from Diametal AG, made of coated cemented carbide (Diametal specification: carbide M10/30 with coating D60, type number 388948) with a corner radius of 0.2 mm is used. The tool is mounted in a 12 x 12 mm, right-hand tool holder of type SVAC 90° from Diametal AG. The roughness R_a of the machined parts is measured parallel to the axis of the cylinder using a MarSurf PS1 (from Mahr). The roughness values of all available parts are measured. In a conservative approach the average of the 5% highest roughness values is used. The tool life of the inserts is determined by maximum flank wear land width measurements using a Leica DCM3D microscope. The tool is considered worn out if $VB_{B,\max} > 0.07$ mm. In this study tool life and roughness measurements are conducted by an operator.



Figure 6.1: Turning machine Deco Sigma 8

The maximum cutting speed is limited at 80 m/min in order to avoid vibrations in the bar feeder. Based on recommendations from the tool manufacturer Diametal AG [33] the maximum feed per revolution is set to 0.1 mm/rev, which is half the tip radius of the indexable insert per revolution. The minimal parameters ($f_{min} = 0.01$ mm/rev and $v_{c,min} = 10$ m/min) are selected to provide a wide range while still avoiding very slow experiments.

6.1.3 Optimization implementation

The optimization is implemented in MATLAB using the GPML library [133] for Gaussian process regression and [48] for constrained Bayesian optimization. Matern 5 kernels (see Table 4.1) are used to model the covariance cost and roughness function because in section 5 their suitability for turning applications has been demonstrated and they are a common choice. As specified in equation (4.1) and (4.2), different length scale parameters for cutting speed and feed per revolution are used because it is known that feed per revolution and cutting speed influence cost and roughness differently. As introduced in section 4, the marginal log-likelihood is maximized to select the hyperparameters of the GP model, which balances data fit and model complexity. The next experiment is determined by maximizing the constrained expected improvement acquisition function (4.18), as proposed by [48].

Figure 6.2 summarizes the workflow used for on-machine optimization. Data collected from the turning process is used to calculate the cost of the current experiment. These results are utilized to update the GP cost model. Roughness measurements of the workpiece are used to update the GP roughness model. The estimations of both GP models are used by the constrained Bayesian optimization algorithm to determine the next measurement point. This procedure is repeated until convergence is reached. Some experiments with slow cutting speed and slow feed per revolution took very long while already violating the required roughness constraints. To shorten the experiments, they were stopped when the roughness value was 20% higher than $R_{a,max}$ and the share of cost to replace the insert was below 10% of the individual production costs.

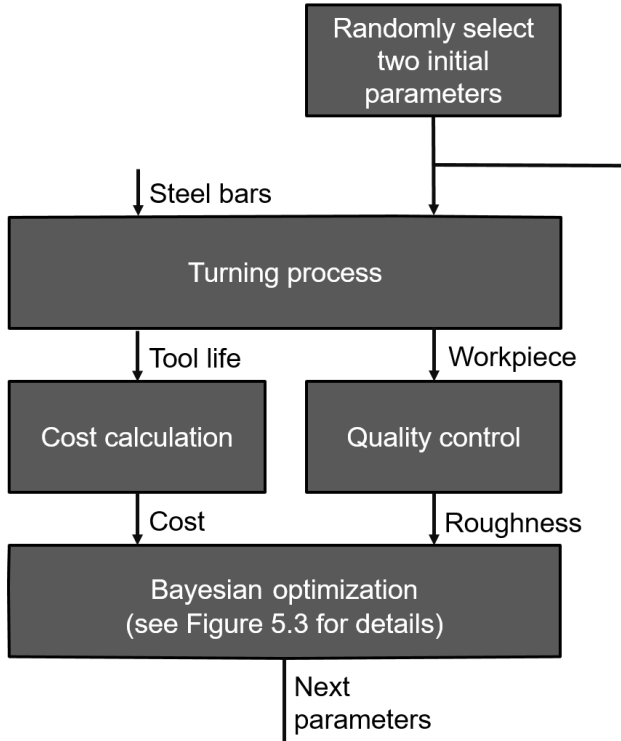


Figure 6.2: Workflow of Bayesian optimization in turning

6.1.4 Convergence criterion

The best experimental point is defined where the posterior mean cost $\mu_{t,co}$ is minimal and the posterior mean roughness $\mu_{t,Ra}$ fulfills the maximum allowed roughness $R_{a,max}$.

$$\underline{x}_{opt} = \arg \min \mu_{t,co}(\underline{x}), \text{ s.t. } \mu_{t,Ra}(\underline{x}) < R_{a,max} \quad (6.3)$$

Similar to [175], the cost uncertainty of the estimated optimal parameters \underline{x}_{opt} is used as a measure of convergence,

$$2\sigma_{t,co}(\underline{x}_{opt}) < \varepsilon_{stop} \quad (6.4)$$

where $\sigma_{t,co}(\underline{x}_{opt})$ is the standard deviation at the current best mean and ε_{stop} is the convergence limit. The model estimates that 95% of all samples conducted at the optimal values will be within $\mu_{t,co}(\underline{x}_{opt}) \pm \varepsilon_{stop}$. To improve the robustness of the convergence criterion, convergence is only reached if three consecutive values are below the convergence limit. The value for the convergence limit should be set as close as possible to the combined process and measurement uncertainty because the uncertainty of the estimated cost and roughness cannot be minimized below

this value as the convergence criterion cannot be met if the combined uncertainty is higher than the convergence limit. The convergence limit is set to 0.15 U which corresponds to 10% of an assumed final cost of 1.5 U. Full convergence can be reached when the convergence limit ε_{stop} is fulfilled, the predicted optimal cutting speed varies within less than 0.5 mm/min over three iterations and the predicted feed per revolution varies within less than 0.003 mm/rev over three iterations.

6.2 Experimental results

Figure 6.3 shows the results of the on-machine optimization. Both initial random parameters violate the roughness constraint. The algorithm used the third and fourth experiments to explore edges of the design space. The third measurement point fulfills the surface roughness constraint but at a high cost of 5.23 U. Most of the experiments between 5th and 12th iteration are located near the estimated optimal parameters. Full convergence is reached after 11 iterations, corresponding to optimal cutting speed of 16.1 m/min and optimal feed per revolution of 0.026 mm/rev. The maximum of the expected improvement also confirms convergence after 11 iterations. The estimated optimal cutting speed is rather low because the cost to manually change an insert is assumed to be high (compare with Table 6.1). To validate the convergence criterion additional experiments were performed. The 12th experiment fulfilled the roughness constraint and showed the lowest measured cost of 2.22 U. This measurement point is very close to the estimated optimal parameters. The algorithm used the experiments 13 to 16 to explore regions with high uncertainty (high feeds per revolution and high cutting speeds). From the 9th to the 16th iteration the estimated optimal speed was within an interval of 0.5 m/min width and the estimated optimal feed was within an interval of 0.003 mm/rev width. It might be that the current measured cost is below the estimated minimal cost because the measured cost might be low, but the constraint is not fulfilled for this experiment and can therefore not be considered optimal (see for example iteration 13 in Figure 6.3). Furthermore, it can be seen that the confidence interval of the prediction increases from the 4th to the 5th experiment. This is caused by updating the Gaussian process model with new available measurements. Figure 6.3(right) shows the experiments for which the constraint was fulfilled, and those, where it was exceeding the critical value $R_{a,max}$. It can be seen that adaptive sampling performs as expected – many experiments are performed close to the optimum and parameter values in other regions are only sampled sparsely.

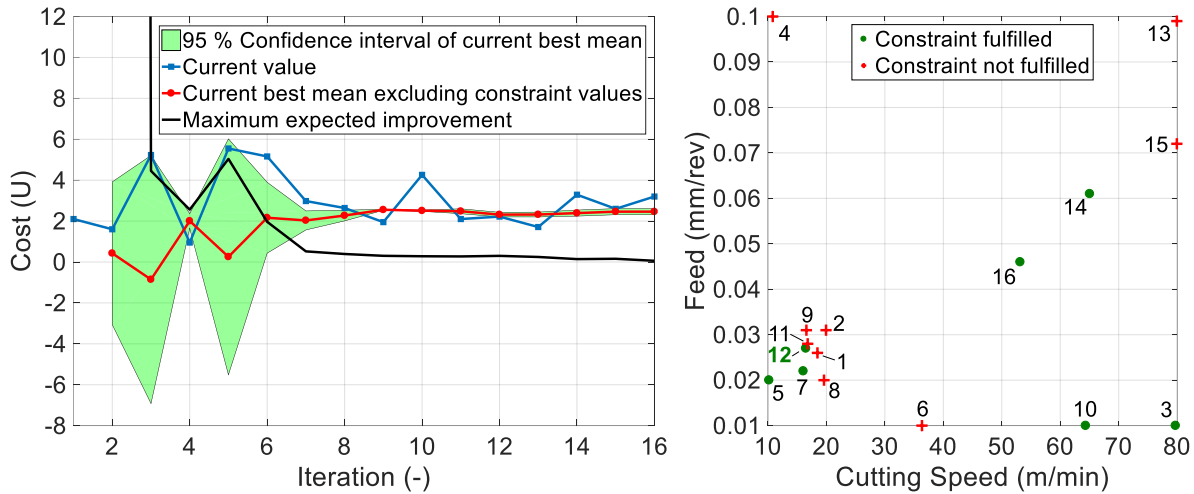


Figure 6.3 left: Convergence of on-machine optimization. Right: Conducted experiments as a function of feed per revolution and cutting speed. Experiment with lowest cost was the 12th experiment.

Figure 6.4 shows the predicted mean and the twofold standard deviation, corresponding to a 95% confidence interval of roughness and cost from the on-machine cutting trials. At low cutting speeds the production costs are high because of the slow process, while at high cutting speeds the production costs increase due to high wear. At high feeds per revolution the production costs decrease since more parts can be produced during the lifetime of the tool. The roughness depends on the feed per revolution and cutting speed. A higher feed per revolution leads to a higher surface roughness, in line with the kinematic surface roughness equation (2.4). At cutting speeds between 20 m/min and 50 m/min the roughness and the cost increase due to built-up edge on the tool. The cost is increased by a reduction of the tool life caused by built-up edge on the tool. The influence of the built-up edge on the surface roughness and tool life is known in literature, see [81] for comparison. In general, the uncertainties of the predictions are smaller close to available measurement points and increase for points further away from measurements, as shown in the bottom of Figure 6.4. The highest cost and roughness uncertainties are reached in an area where the estimated mean roughness is much higher than the allowed roughness.

The presented results demonstrate the applicability of Bayesian optimization for process set-up in turning. A promising direction to further automate the process set-up is the use of a handling system to exchange workpiece and tool between the machine and the measurement equipment and connect the tool wear and roughness measurement with the machine to exchange data. It might even be

possible to measure roughness and tool wear on-line, such as demonstrated in [176] for roughness and in [19] for tool wear.

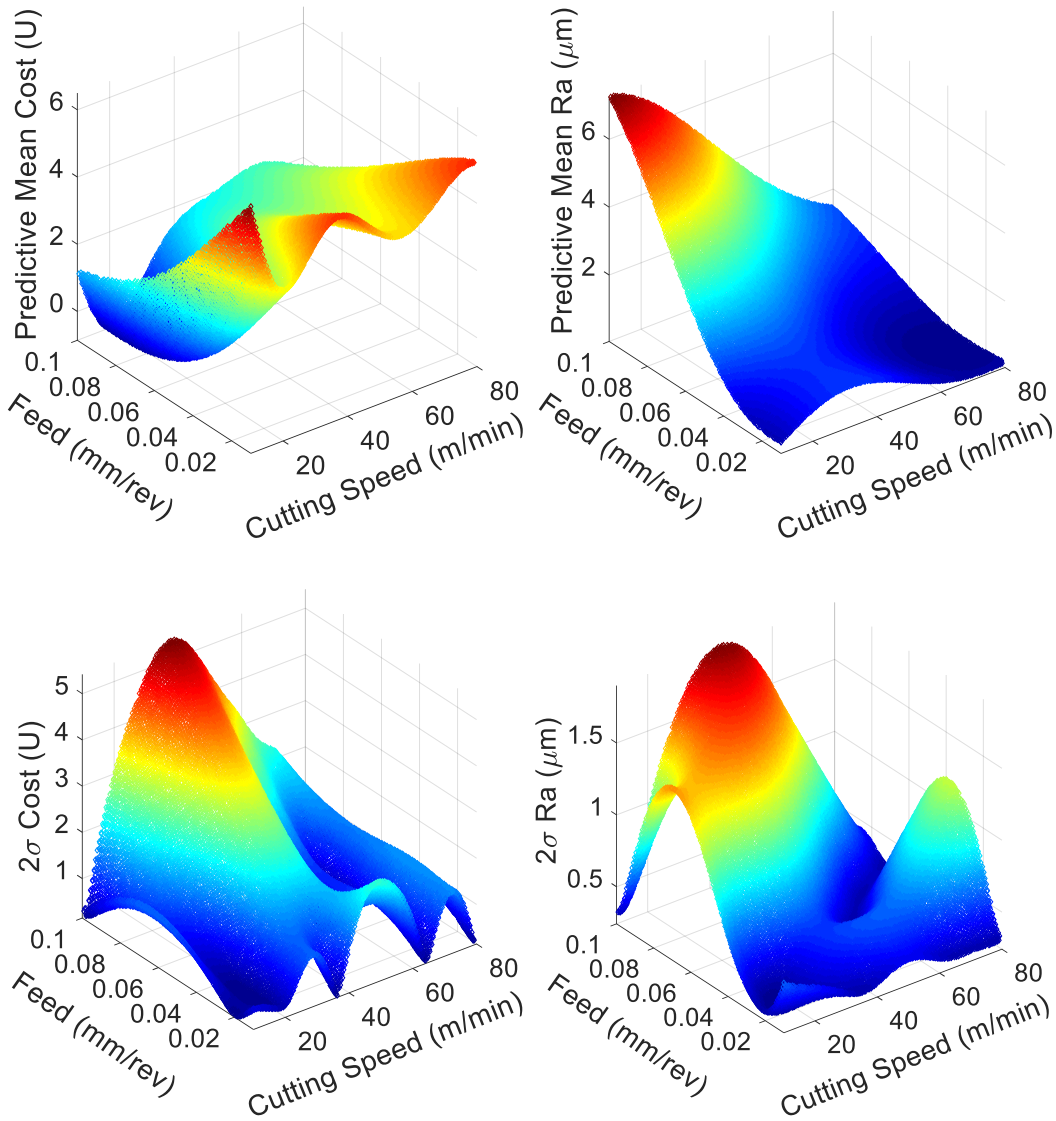


Figure 6.4: Predicted mean cost (top left), predicted mean roughness (top right), twofold standard deviation of cost (bottom left), and twofold standard deviation of roughness (bottom right) after 16 experiments

The experimental data can also be used to estimate optimal process parameters for different system variables and constraint requirements (see Table 6.2). Only the time to change an insert, the machine operator cost, and the allowed surface roughness are changed - the other parameters are the same as those listed in Table 6.1. The first parameter set corresponds to the baseline parameters as specified in Table 6.1. First the cost parameters are changed assuming an automatic change of the insert instead of a manual change. In this case it is assumed that the machine operator cost is reduced from 100 U/h to 0 U/h and the time to change an insert is

reduced from 10 min to 30 sec. The algorithm recommends a higher cutting speed which is expected, since according to the Taylor equation (2.5) tool wear increases with an increase in cutting speed and changing a worn-out tool is less costly for an automatic machine. The estimated optimal cutting speed is very close to the upper cutting speed limit of the optimization domain, which is selected to avoid bar feeder vibrations. Hence, in this case the cutting speed is limited by bar feeder vibrations. Another scenario is the loosening of the maximum roughness constraint from 0.8 μm to 1.2 μm . In that case the algorithm recommends an increase in feed per revolution, in line with the increase of the kinematic surface roughness, as higher feeds per revolution correspond to higher surface roughness according to equation (2.4).

Table 6.2: Estimated optimal process parameters for different constraint requirements and system variables

Cost & constraint parameters	Estimated optimal parameters	Estimated cost (U)
$C_O = 100 \text{ U/h}$ $t_i = 10 \text{ min}$ $R_{a,max} = 0.8 \mu\text{m}$	$f = 0.026 \text{ mm/rev}$ $v_c = 16.1 \text{ m/min}$	$2.46^{\pm 0.15}$
$C_O = 0 \text{ U/h}$ $t_i = 0.5 \text{ min}$ $R_{a,max} = 0.8 \mu\text{m}$	$f = 0.071 \text{ mm/rev}$ $v_c = 79.8 \text{ m/min}$	$0.88^{\pm 0.09}$
$C_O = 100 \text{ U/h}$ $t_i = 10 \text{ min}$ $R_{a,max} = 1.2 \mu\text{m}$	$f = 0.037 \text{ mm/rev}$ $v_c = 18.4 \text{ m/min}$	$1.14^{\pm 0.24}$

7 Performance measurement for grinding of tungsten carbide inserts

In the previous chapter it has been demonstrated that Bayesian optimization combined with Gaussian process models is suitable for process parameter selection for longitudinal turning. To extend the optimization approach to other processes, plunge face grinding of tungsten carbide is investigated. In the past, plunge face grinding has been mostly investigated to improve the process understanding and not for parameter optimization. Therefore, this chapter focuses on the systematic measurement of cost and constraints in plunge face grinding of tungsten carbide cutting inserts, which can be used in a subsequent optimization. Parts of this chapter have been previously published in [104, 107, 108].

7.1 Experimental set-up

7.1.1 Grinding operation

Figure 7.1 shows a picture of the used plunge face grinding machine for grinding of cutting inserts. The grinding wheel rotates in counterclockwise direction. The rotational speed and the diameter of the grinding wheel specify the cutting speed. The grinding wheel can be moved in X-direction, which is the direction of the axial feed rate during grinding. To ensure a uniform wear of the grinding wheel, the grinding wheel is oscillated during grinding along the Y-direction with 1 Hz during grinding and 1.5 Hz during spark-out. The spark-out time is set sufficiently large to ensure reduction of residual grinding forces. The hard metal-bonded grinding wheel shows a limited self-sharpening effect. Hence, a dressing wheel is used for conditioning. The workpiece is clamped using a clamping device, which can rotate the workpiece along the B axis. Furthermore, the workpiece can be rotated along the C axis. An initially quadratic insert made of tungsten carbide is ground on two opposite sides, where on each side 2.25 mm of workpiece material is removed. The flow rate of the cooling lubricant is controlled manually by a lever and the angle between the nozzle and the grinding wheel is also adjusted manually. In this thesis, the flow rate and the angle between the cooling nozzle and the grinding wheel were set before the experimental run by an experienced operator. During the experimental runs, these parameters were kept constant. Table 7.1 summarize the specific grinding conditions.

The error of the final workpiece geometry is influenced by the thermal distortion of the grinding machine and the abrasive layer thickness of the grinding wheel, which experiences wear during the grinding operation. In this thesis the geometrical error of the workpiece was not considered in the parameter optimization because the used grinding machine allows adaptive correction of the geometrical error. The grinding machine is equipped with a sensor measuring the final workpiece dimension (see Figure 7.1). The sensor measurements of each workpiece then serve as corrective feedback for the grinding action. With the grinding parameters used in this thesis and the automatic insert handling switched on, the measurement interval is typically below 1 min, which allows frequent corrective adaption. For workpieces with a higher geometrical complexity or a long grinding time it might be beneficial to consider the geometrical error of the final workpiece in the optimization.

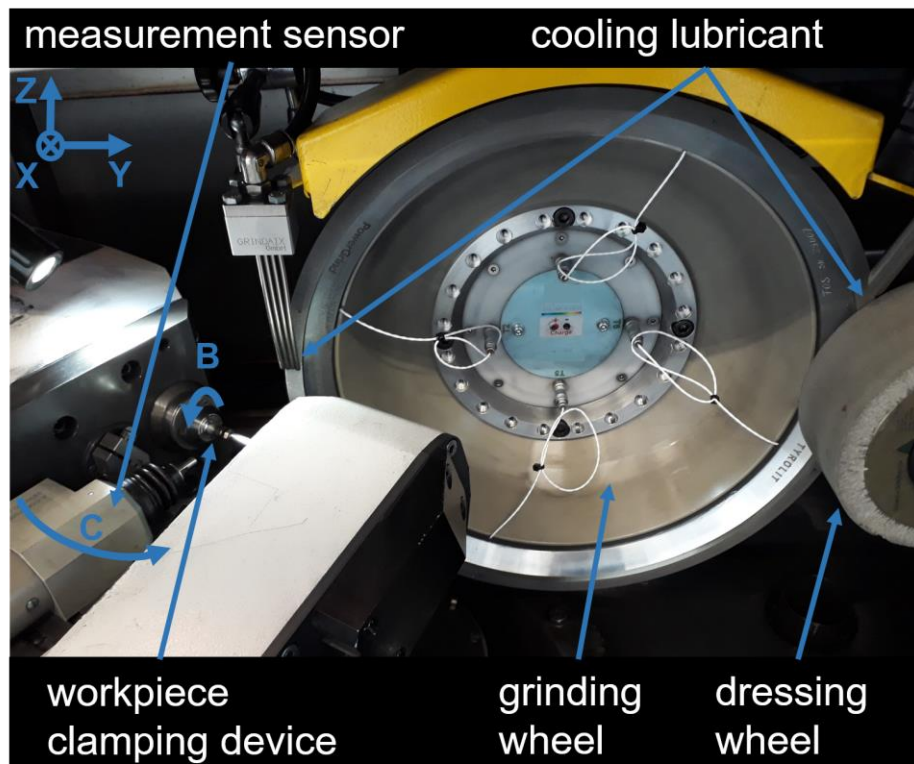


Figure 7.1: Overview of plunge face grinding machine

Table 7.1: Experimental conditions for performance measurement

Property	Setup
Grinding machine	Agathon DOM Semi
Grinding wheel	Metal-bonded, diamond abrasive grains (Tyrolit D46C100M717)
Insert material	Tribo S25, tungsten carbide, grain size 2.5 µm, HV30 1470
Initial insert geometry	14.5 mm x 14.5 mm x 4.76 mm
Final insert geometry	10 mm x 14.5 mm x 4.76 mm
Cooling lubrication	Blasogrind HC 5 with constant flow rate
Oscillation frequency	1 Hz during grinding, 1.5 Hz during spark-out
Dressing wheel	Tyrolit 89A 240 J5 AV217, aluminum oxide abrasive
Dressing parameter	Infeed 0.1 mm, grinding wheel speed 6 m/s, dressing wheel speed 12 m/s, feed rate 0.5 mm/min, spark-out time 1 sec

7.1.2 Grinding burn

Grinding burn is inspected optically after grinding. Workpieces with grinding burn show a distinct black coloring of the final workpiece surface (see Figure 7.2). This approach is a simple approach for burn detection, which is widely used in industry. The main disadvantages of the method are that it is a subjective measurement and damage induced by grinding burn in the subsurface regions cannot be detected. Other methods for grinding burn detection exist, as introduced in section 3.3.2. However, the disadvantage of the commonly used nital etching is that it is a subjective measurement, and the disadvantage of the more sophisticated Barkhausen noise measurements is that it needs calibration and referencing, as reported in [76]. Using a Hall probe or X-ray diffractometry increases the measurement time and measurement complexity. Therefore, the simple inspection method is considered sufficient, as this approach is common practice in an industrial environment. In case of higher surface quality requirements, more sophisticated methods are recommended.

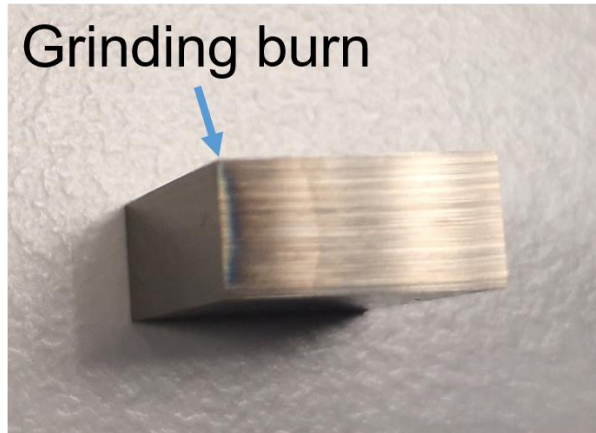


Figure 7.2: Optical detection of grinding burn

7.1.3 Temperature measurement

The grinding temperature is measured at the contact zone between grinding wheel and workpiece by use of an optical measurement system (FOS Messtechnik). The optical measurement system consists of four evenly distributed fibers which are embedded in the grinding wheel with an orientation perpendicular to the abrasive layer surface. The temperature signal is processed on the rotating cup wheel and transmitted wirelessly to a receiver unit outside the grinding machine. The receiver unit is connected to a measurement computer, where the data is post-processed. Figure 7.3 illustrates the temperature measurement setup. The measurement system has a measurement range between 200 and 660°C. The emissivity of the workpiece is not measured. Therefore, the temperature readings can only be considered as relative measurements. However, a relative measurement is sufficient in this study because the final objective is to determine a threshold temperature for grinding burn detection.

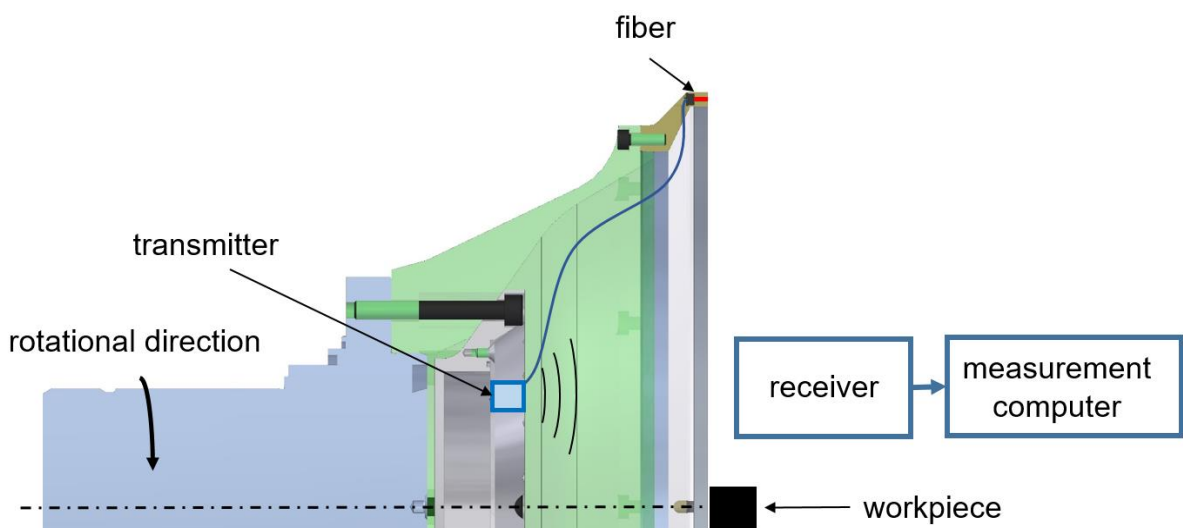


Figure 7.3: Experimental setup of temperature measurement

7.1.4 Gas measurement

The gas concentration in the machining area is measured using a metal-oxide gas sensor (Sensirion SGP30). The sensor system is able to detect total volatile organic compounds (TVOC) and can provide a CO₂ equivalent, which corresponds to the greenhouse gas emissions of the test gas. Originally, the sensor is designed for indoor air quality measurements. To protect the sensor from cooling lubricant, it is placed in a housing as shown in Figure 7.4. The sensor system is placed vertically inside the grinding machine in which the inlet is at the bottom and the outlet is at the top. A ventilator inside the housing is used to provide a steady circulation of the ambient process chamber gases. The gas enters the housing on the bottom and is guided through plates as fluid separators to the gas sensor. Afterwards, the gas leaves the housing through a U-shaped tube to protect the sensor from cooling fluid.

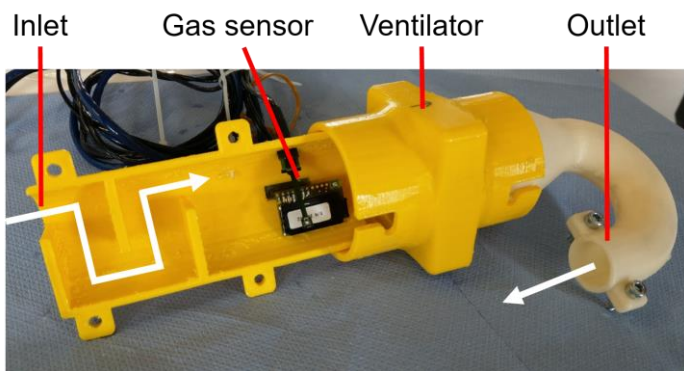


Figure 7.4: Experimental setup of a gas sensor

7.1.5 Surface roughness measurement

The surface roughness of the ground workpiece is measured transversally to the grinding direction using a tactile measurement device (Taylor Hobson Form Talysurf Series 2) with a tip radius of the measurement probe of 2 µm and a cut-off wavelength of $\lambda_c = 0.8$ mm. The measurement length is reduced to 3.5 mm, since the total length of the workpiece was only 4.76 mm. The roughness was measured on both ground sides of the insert and subsequently averaged.

7.2 Results of performance measurement

7.2.1 In-process detection of grinding burn

Figure 7.5 shows a comparison of in-process grinding burn detection based on maximum temperature measurements and on maximum gas concentration measurements. The experiments were conducted for different cutting speeds, feed rates, and wheel wear states of the grinding wheel. The temperature sensor is able

to distinguish grinding burn and no grinding burn with a 100% success rate. No grinding burn was observed for maximum temperature readings below 585°C. All temperature readings above the threshold value showed grinding burn. For process optimization, the measured temperature can be used as a constraint value and the maximum allowed temperature is determined to be 585°C.

The maximum gas concentrations are correlated with the maximum grinding temperatures as shown in Figure 7.5. An increase in maximum temperature leads to an increase in maximum gas concentration. The sharp peak at high temperatures is caused by the measurement range of the temperature sensor, which is limited to 660°C. Physically the positive correlation between gas concentration and temperature can be explained by the chemical reaction speed because the chemical reaction speed depends on the Arrhenius equation $k = Ae^{-E_A/(RT)}$, as described in [92]. The components of the Arrhenius equation are rate constant k , Arrhenius factor A , activation energy E_A , temperature T , and universal gas constant R . Therefore, higher temperatures lead to higher reaction speeds [92]. However, the current gas concentration does not only depend on the reaction speed but also on reaction time and the concentration of components, as explained in [92]. Especially the reaction time is critical for grinding burn detection because having the same maximum temperature for a very short time or a very long time influence the measured maximum gas concentration, while the maximum temperature is the same. Therefore, for the gas measurements no clear threshold limit for burn detection can be determined. A threshold limit of 2000 ppm detects all workpiece grinding burns but is a very conservative approach with respect to the grinding burn limit. A threshold of 6000 ppm is able to detect cases without wrongly classifying successful grinding operations as failures. A threshold limit of 6000 ppm can be seen as a limit for very extreme cases. Hence, the gas sensor is a low-cost alternative for grinding burn detection with reduced sensitivity.

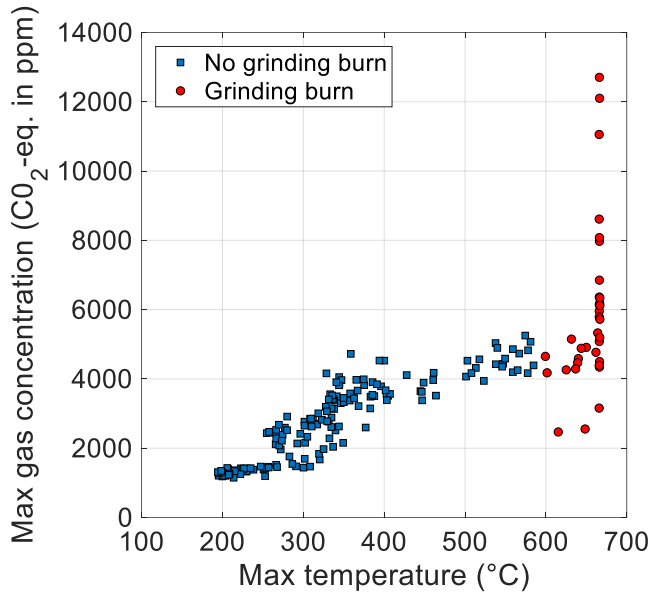


Figure 7.5: Comparison between measured maximum gas concentration and maximum temperature for in-process detection of grinding burn

7.2.2 Grinding burn and surface roughness constraint

Figure 7.6 shows the influence of feed rate and cutting speed on grinding burn for grinding the first side of the test insert directly after dressing. In general, grinding burn is favored by high feed rates and high cutting speeds. In general, high feed rates lead to a higher material removal rate, which increases the power demand and total heat dissipation. Without changing the axial feed rate, higher cutting speeds decrease the uncut chip thickness, according to eq. (2.6). As explained in [137], decreasing the uncut chip thickness increases the specific grinding energy (energy required to remove a unit volume of material). Due to a feed rate step size of 5 mm/min between measurements, an uncertainty bound is introduced as shown in gray. The measurements at cutting speeds of 18 m/s and 24 m/s show the same grinding burn boundary while the measurements at cutting speeds of 12 m/s and 30 m/s confirm the general trend that grinding burn is favored by high cutting speeds. However, due to the uncertainty introduced by the measurement discretization, the measurements still support a linear trend of the grinding burn boundary.

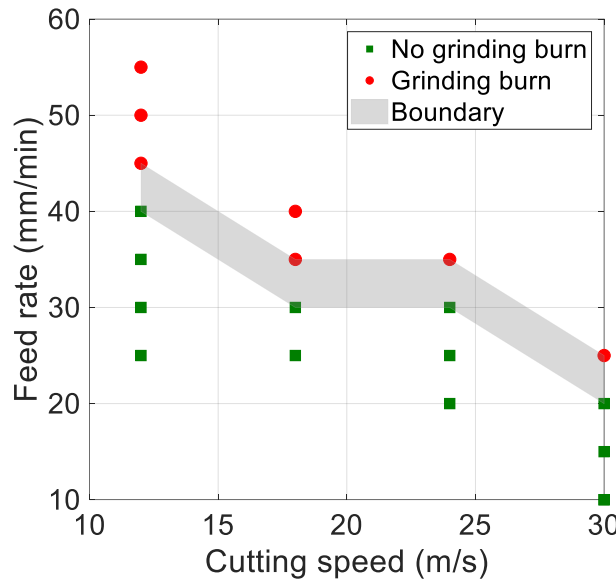


Figure 7.6: Measured grinding burn limit of a freshly dressed plunge face grinding process

Figure 7.7 shows the workpiece surface roughness as a function of cutting speed and feed rate. An increase in cutting speed leads to a decrease in surface roughness of the workpiece. This is in line with the findings of [7]. For the feed rate no general trend can be observed.

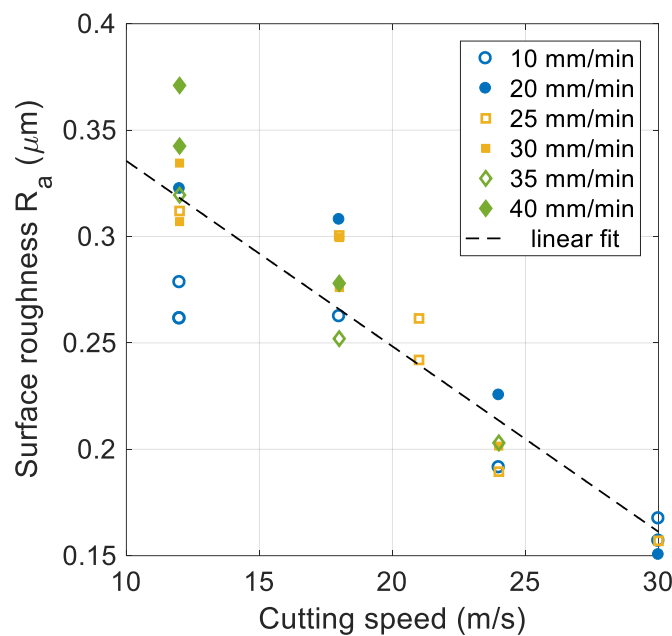


Figure 7.7: Surface roughness of workpiece ground with a freshly dressed wheel for different feed rates and cutting speeds

7.2.3 Maximum dressing interval

Grinding costs are influenced by maximum dressing intervals. To measure the maximum dressing interval, a freshly dressed wheel is used for grinding until grinding burn occurred. Figure 7.8 shows a typical temperature reading as a function of ground inserts for a full experimental run with constant input parameters. In general, the temperature is strongly influenced by the accumulated removed material volume, where towards the end of an experimental run the temperature increases. The second side of the 7th insert does not fulfill the constraint, resulting in grinding burn. Accordingly, the measured maximum dressing interval for this parameter set is 6.5 inserts. Depending on the grinding task, considering workpiece handling time may lead to positive natural numbers as optimal dressing intervals instead of positive real numbers due to time-saving of dressing and workpiece handling parallelization. The time-saving of dressing and workpiece handling parallelization is typically a few seconds. However, the actual time-saving depends on many factors such as the handling system, handling parameters, grinding time, dressing time, and movement speed of the grinding wheel. In this study, additional time caused by workpiece handling was neglected because it is considered short compared to the dressing time and strongly depends on the actual handling system and corresponding parameters.

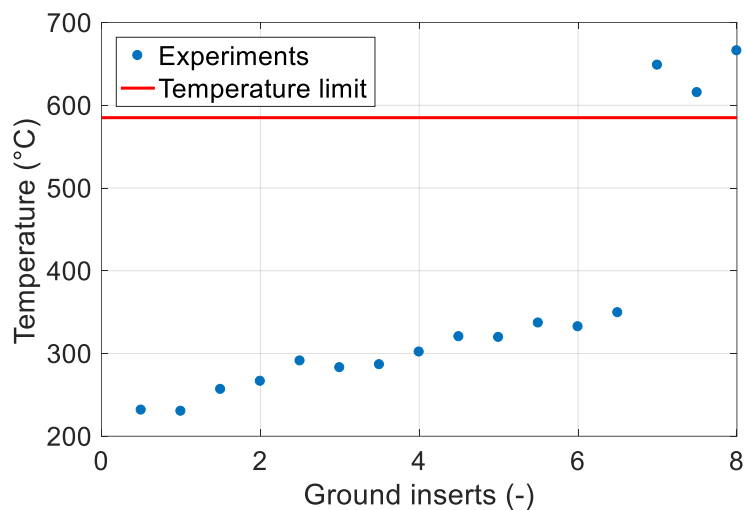


Figure 7.8: Typical temperature measurement as a function of ground inserts for a cutting speed of 24 m/s and a feed rate of 10 mm/min. The last side which fulfills the temperature constraint is the first side of plate 7. Therefore, the maximum dressing interval is 6.5 inserts.

The maximum number of ground inserts until grinding burn occurred is used for comparison, which can be seen in Figure 7.9. After eight inserts, the experiment

was stopped to avoid unnecessarily long experiments. This limits the number of ground inserts for some experiments with low cutting speeds and low feed rates (yellow bars in Figure 7.9). Nevertheless, general trends influencing the number of maximum ground inserts can be observed. An increase in feed rate and an increase in cutting speed lead to a reduced number of maximum ground inserts because for higher feed rates and higher cutting speeds the grinding operation is already started at higher temperatures. Due to higher initial temperatures smaller changes in wheel sharpness are sufficient to reach the temperature limit and therefore the maximum dressing interval is reduced for higher feed rates and higher cutting speeds.

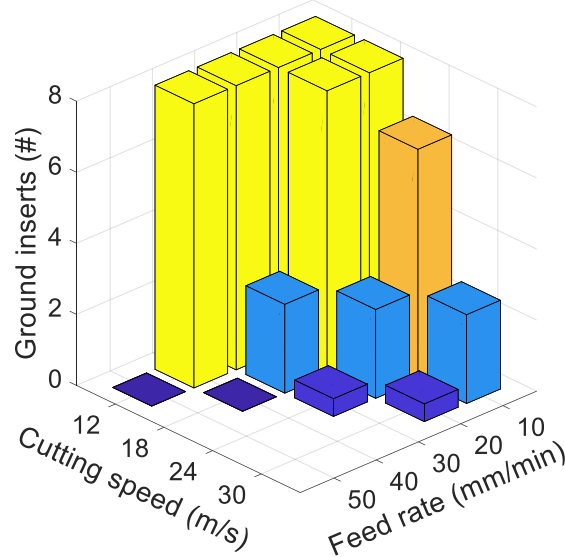


Figure 7.9: Maximum dressing interval until temperature exceeds maximum

7.3 Conclusions

The measurements show that there are tradeoffs for the feed rate and the cutting speed. Slow feed rates lead to high production costs due to a time-consuming manufacturing process, whereas fast feed rates favor grinding burn and lead to short dressing intervals, which requires frequent redressing. High cutting speeds also favor grinding burn and lead to short dressing intervals but improve the surface roughness quality. Hence, an optimization of the process parameters feed rate and cutting speed is required to balance grinding time, dressing interval, surface roughness, and grinding burn. Furthermore, the embedded temperature measurement was able to accurately classify grinding burn, while the gas sensor provided a lower accuracy. Despite the higher costs for the embedded temperature sensor, it is chosen for further optimization tasks due to a higher grinding burn classification accuracy.

8 Optimization of plunge face grinding of tungsten carbide

In the previous chapter performance measurement of the plunge face grinding of tungsten carbide cutting inserts is shown. In this chapter the performance measurement is combined with constrained Bayesian optimization for autonomous process parameter selection. Part of this chapter has been previously published in [107, 108] and filed for patenting in [12].

8.1 Methodology

8.1.1 Experimental setup

The used grinding setup is specified in Table 8.1 and is similar to the grinding setup in chapter 7. Only the dressing wheel is slightly changed from Tyrolit 89A 240 J5 AV217 to Tyrolit 89A 240 L6 AV217 due to unavailability of the previous dressing wheel. The new dressing wheel is slightly harder and has a slightly higher porosity.

Table 8.1: Experimental conditions for process optimization

Property	Setup
Grinding machine	Agathon DOM Semi
Grinding wheel	Metal-bonded, diamond abrasive grains (Tyrolit D46C100M717)
Insert material	Tribo S25, tungsten carbide, grain size 2.5 µm, HV30 1470
Initial insert geometry	14.5 mm x 14.5 mm x 4.76 mm
Final insert geometry	10 mm x 14.5 mm x 4.76 mm
Cooling lubrication	Blasogrind HC 5 with constant flow rate
Oscillation frequency	1 Hz during grinding, 1.5 Hz during spark-out
Dressing wheel	Tyrolit 89A 240 L6 AV217, aluminum oxide abrasive
Dressing parameter	Infeed 0.1 mm, grinding wheel speed 6 m/s, dressing wheel speed 12 m/s, feed rate 0.5 mm/min, spark-out time 1 sec

The temperature sensor, which has been introduced in chapter 7 is used for burn detection. The measured temperature of the first ground side after dressing is a constraint in the optimization procedure because in general the grinding

temperature increases during grinding due to grinding wheel dulling (compare with Figure 7.8). This leads to a workpiece quality, which is not fulfilled for the current and the following workpieces.

The surface roughness is measured transversal to the grinding direction using a tactile measurement device as in chapter 7. Due to availability, the tactile measurement device is changed from Form Talysurf Series 2 to Form Talysurf 120 L both from Taylor Hobson. A measurement tip radius of $2 \mu\text{m}$ and a wavelength cut-off of $\lambda_c = 0.8 \text{ mm}$ is used. The evaluation length was reduced to 4 mm because the total thickness of the insert was only 4.76 mm. In general, the roughness of both ground sides per insert is measured and averaged. If grinding burn occurred on a ground side the roughness was not measured on this side. Instead, the roughness measurement was repeated at a different location on the other ground side, where grinding burn did not occur. The measured roughness varies from insert to insert with no clear trend. Therefore, in a conservative approach, the maximum measured roughness value of one optimization run, grinding with a freshly dressed wheel until grinding burn occurred, was considered as a constraint for the optimization.

8.1.2 Cost calculation

Grinding costs cannot be measured directly with a single sensor because they are composed of process-related quantities such as grinding time and grinding wear, and of economic quantities such as machine hourly costs and cost of the grinding wheel. The individual production costs to grind one insert C_{FE} are calculated based on grinding time costs, dressing time costs, cost of grinding wheel wear during dressing, and cost of dressing wheel wear during dressing.

$$C_{FE}(v_c, v_{fa}) = C_{MH} \frac{s \cdot a_{pg}}{v_{fa}} + \left(C_{MH} t_d + \frac{C_{gw} a_{d,gw}}{a_{gw}} + \frac{C_{dw} a_{d,dw}}{a_{dw}} \right) \frac{V_g}{V_w(v_c, v_{fa})} \quad (8.1)$$

The axial feed rate v_{fa} , and the removed workpiece material until the wheel is dull V_w depend on the selected input parameters axial feed rate v_{fa} and cutting speed v_c , which are the process parameters used in Bayesian optimization. The other cost parameters are constants as summarized in Table 8.2. The macroscopic grinding wheel wear during dressing was considered and the macroscopic

grinding wear during grinding was neglected. This assumption is reasonable because, as described in [112], it is known that metal bonded grinding wheels hold the diamond grains very strongly, resulting in a high abrasive wear resistance whereby self-sharpening is limited. The limited self-sharpening of the grinding wheel requires redressing of the grinding wheel, which is assumed to be the main cause of macroscopic grinding wheel wear. The macroscopic grinding wheel wear during dressing $a_{d,gw}$ was assumed to be 1 μm . Macroscopic grinding wheel wear during dressing is determined by the dressing parameters, which were fixed in this study and not considered in the optimization. In this study, macroscopic grinding wheel wear during dressing can be considered as a weight in the cost function. The spark-out time for each grinding operation was not considered for cost calculation because it was held constant in this study and therefore it only shifts the cost function up by a constant value without influencing the optimal parameters.

Table 8.2: Parameters for cost calculation

Parameter	Description	Value
V_g	Removed material per workpiece	310.6 mm^3
s	Number of ground sides	2
a_{pg}	Infeed per side	2.25 mm
t_d	Dressing time	19 sec
a_{gw}	Abrasive layer thickness of grinding wheel	4 mm
$a_{d,gw}$	Macroscopic grinding wheel wear during dressing	1 μm
a_{dw}	Thickness of dressing wheel	65 mm
$a_{d,dw}$	Wear of dressing wheel during dressing	0.1 mm
C_m	Machine hourly cost	100 U/h
C_{gw}	Cost of grinding wheel	1500 U
C_{dw}	Cost of dressing wheel	95 U

8.1.3 Optimization Implementation

The objective in this study is to find the process parameters minimizing the individual production costs C_{FE} and to fulfill the maximum temperature constraint ϑ_{max} and the maximum surface roughness constraint $R_{a,max}$.

$$\underline{x}_{min} = \arg \min C_{FE}(v_c, v_{fa}), \text{ s.t. } \begin{array}{l} \vartheta(v_c, v_{fa}) < \vartheta_{max} \\ R_a(v_c, v_{fa}) < R_{a,max} \end{array} \quad (8.2)$$

The maximum allowed temperature was set to 585°C because in section 7.2.1 experiments with 194 insert sides grinding burn has been classified with a 100% success rate using this temperature measurement system and the same workpiece-wheel combination. The roughness limit depends on the grinding application. In the special case of plunge face grinding of inserts the allowed roughness limit is a trade secret of each insert manufacturer. In this study, the roughness was limited to $R_{a,max} = 230$ nm, which leads to typical optimal cutting parameters. The algorithm was implemented in MATLAB using the GPML library [133] for Gaussian process regression. A flow diagram of the implementation is shown in Figure 8.1. The optimization is started with two experiments at random process parameters within the input optimization domain. The optimization domain for the Bayesian optimization was set based on experience to a minimal feed rate of 10 mm/min and a maximum feed rate of 40 mm/min. The minimal cutting speed was set to 12 m/s and the maximum cutting speed was set to 30 m/s. In this way, a typical cutting speed range for plunge face grinding of tungsten carbide inserts was covered. To avoid unnecessary long experimental runs, the run was stopped after 8 inserts if the maximum temperature was not previously exceeded. For those cases the cost was calculated based on the eight inserts. After calculating the cost per part at the measured process parameter values and determining the hyperparameters, three Gaussian process regressions are calculated, to model the cost, the temperature, and the roughness.

Based on the obtained probabilistic predictions at different (not previously probed) values of the process parameters, the optimal parameters that fulfill (8.2) can be calculated based on the obtained probability distributions for the cost, temperature and roughness. Using stochastic models allows for probabilistic statements about the fulfillment of the constraint limits. As discussed in detail in [151], the optimal parameters $\underline{x}_{opt} = (v_{c,opt}, v_{fa,opt})$ are calculated as the parameters,

which minimize the expected cost $\mu_{t,co}(v_c, v_{fa})$ after t experiments – calculated using equation (4.3) – and fulfill the roughness and temperature constraints with probabilities higher than user defined values $p_{Ra,min}$ and $p_{g,min}$.

$$\underline{x}_{opt} = \arg \min \mu_{t,co}(v_c, v_{fa}), \text{ s.t. } \begin{aligned} p_{f,g}(v_c, v_{fa}) &\geq p_{g,min} \\ p_{f,Ra}(v_c, v_{fa}) &\geq p_{Ra,min} \end{aligned} \quad (8.3)$$

The minimal probability that a constraint is fulfilled can be chosen freely and depends on the requirements. For example, many parts for the aviation industry will require a high minimal probability that the constraints are fulfilled. On the other hand, if one produces disposable products (products for single use), it might be reasonable to accept a lower minimal probability that the constraints are fulfilled. The probability $p_{f,i}$ that the constraint i is below its maximum allowed value $c_{max,i}$ can be calculated for temperature $p_{f,g}$ and roughness $p_{f,Ra}$ by using equation (4.19) and the maximum allowed temperature value $g_{max} = 585^\circ\text{C}$ and the maximum allowed roughness value $R_{a,max} = 230 \text{ nm}$. In general, it is possible to specify separate minimal probabilities for temperature and roughness. In this study, the parameters $p_{g,min}$ and $p_{Ra,min}$ were set equal for simplicity.

Afterwards the optimal parameters can be used to assess convergence as proposed in section 6.1.4 and equation (6.4). Full convergence is reached, when the stopping criterion ε_{stop} is below 0.04 U over three consecutive iterations, the optimal feed rate changes within an interval of 0.4 mm/min, and the optimal cutting speed changes within an interval of 0.2 m/s. If convergence is not reached, the next experimental parameters will be determined based on maximizing the constrained expected improvement acquisition function, as specified in equation (4.20), and the optimization continues.

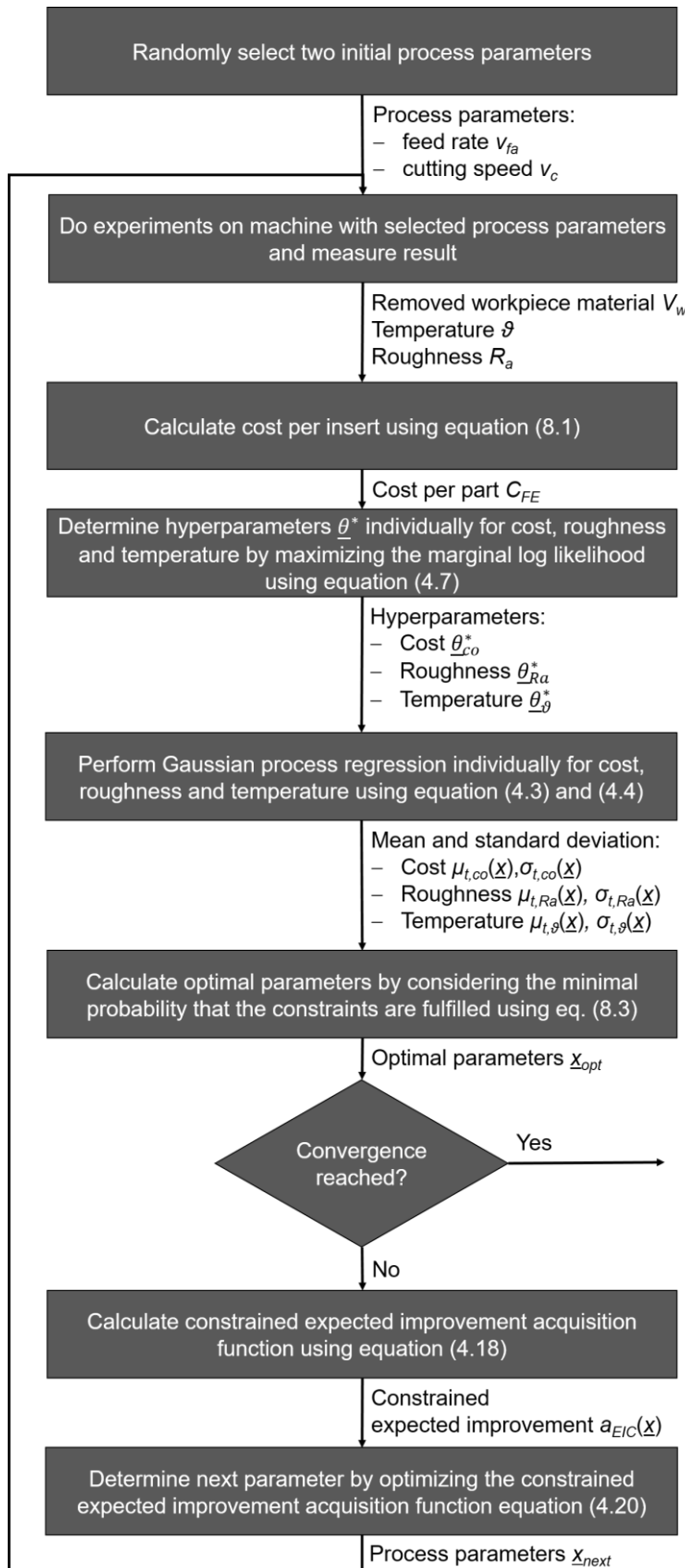


Figure 8.1: Flow diagram of optimization implementation

8.2 Results

Figure 8.2 presents the on-machine optimization. Convergence was judged for a minimal allowed probability of quality defects of 0.5 ($p_{Ra,min} = p_{\theta,min} = 0.5$). The

first two experiments are conducted at random points in the parameter space to initialize the optimization. The first and the second experiment do not fulfill the constraints, therefore the algorithm does not approach convergence after these experiments. However, the proposed trial for the third measurement is at high cutting speeds and low feed rates, which reduces both surface roughness and temperature. The third measurement fulfills the constraints. The blue line on Figure 8.2 shows the current measured cost values. Experimental points explored due to high model uncertainty often result in high current measured costs, for example iterations 4, 7, and 9. In such cases, often the constraints are not fulfilled. Until the 8th iteration the uncertainty of the prediction is reduced drastically. After the 8th iteration, the uncertainty remains low until full convergence is reached after 12 iterations. Experimentally, the best parameters are obtained at the 10th iteration with a cutting speed of 24.3 m/s, a feed rate of 11.7 mm/min, and a dressing interval of 7.5 inserts. After the 10th iteration, a slight increase in the cost and the uncertainty is observed, however within the convergence limits. In this study, convergence is reached after 12 iterations. The number of iterations is influenced by the complexity of the objective and constraint functions. Simple functions follow global trends, which can be modelled with a large length scale hyperparameter, resulting in a minimal number of iterations. On the other hand, complex functions will show very localized behaviors, which correspond to short length scales, and consequently require more iterations.

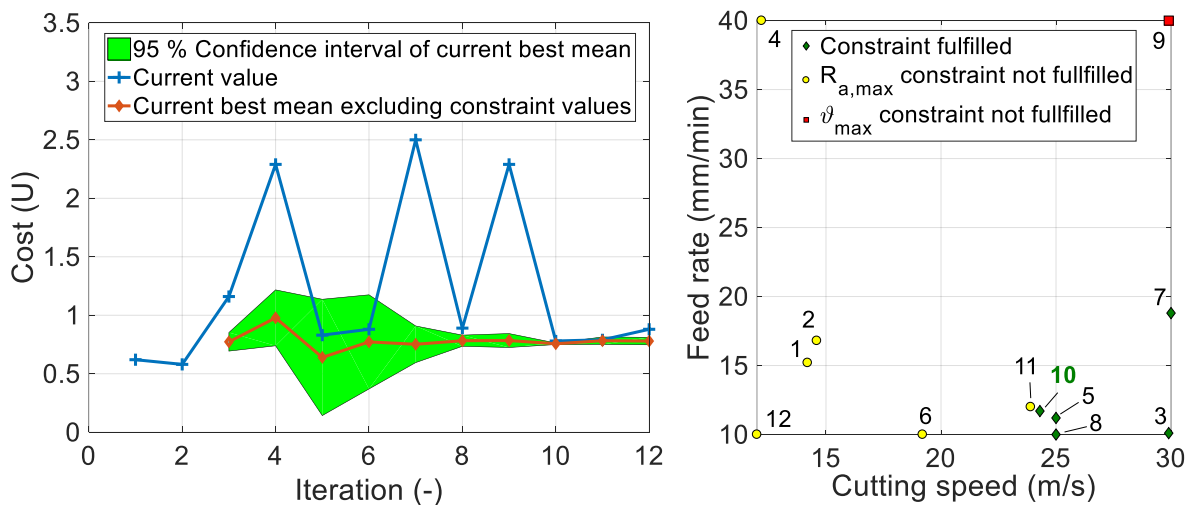


Figure 8.2 left: Convergence of Bayesian optimization with a maximum allowed probability of quality defects $p_{Ra,min} = p_{g,min} = 0.5$. Right: Conducted experiments for 12 iterations. Experiment with lowest cost and fulfilled constraints was 10th experiment.

Figure 8.3 shows the predicted mean and twofold standard deviation after 12 iterations for cost, roughness and temperature. The predicted cost is high for low feed rates because the operation is time consuming. On the other hand, higher feed rates lead to shorter dressing intervals, which results in high dressing costs. Optimal parameters are a trade-off between these two costs. After 12 experiments, the model uncertainty in the high feed rate range (above 25 m/min) is higher than the uncertainty corresponding to low feed rate. Considering the high predicted costs for these parameters, the uncertainty is still moderate. The variation of the uncertainty is mainly influenced by the availability of measurements close to the prediction. For predictions far away from measurements the uncertainties are high, whereas for predictions close to measurements the uncertainties are low. The roughness mostly depends on the cutting speed. An increase in cutting speed reduces the surface roughness whereas the feed rate only influences the roughness minimal. This is in line with the findings in section 7.2.2 for plunge face grinding with a similar setup, where an extensive series of experiments was conducted. The predicted uncertainty of the roughness is between 19.7 and 33.4 nm, which is 9 and 15% of the maximum allowed roughness. An increase in feed rate or cutting speed leads to higher temperatures, again confirming the results reported in section 7.2.2. The predicted temperature uncertainty is between 59.5 and 76.5°C which is between 10 and 13% of the maximum allowed temperature. The temperature uncertainty is higher for high feed rates because only a limited number of experiments were conducted at high feed rates, due to high total costs at high feed rates. In such cases, the recommended process parameter configuration by the BO algorithm for the next trials moves to process parameters corresponding to lower costs, and the more unfavorable regions of the parameter space are not extensively explored. Figure 8.4 shows a comparison of the model predictions and the measured values after 12 iterations. The model shows very good agreement with the measured data.

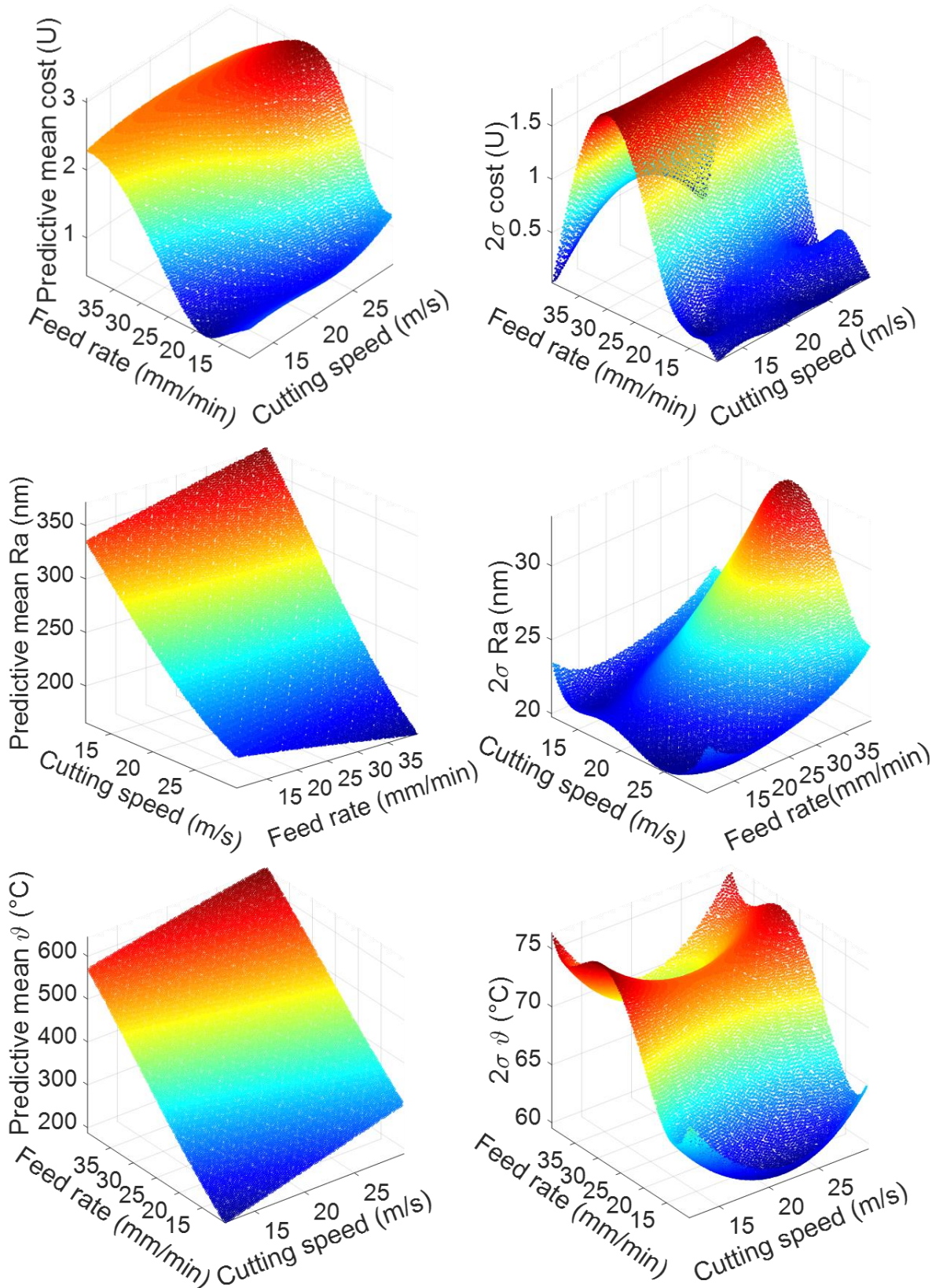


Figure 8.3: Predicted mean cost (top left), cost twofold standard deviation (top right), predicted mean roughness (middle left), roughness twofold standard deviation (middle right), predicted mean temperature (bottom left), and temperature standard deviation (bottom right) after 12 iterations.

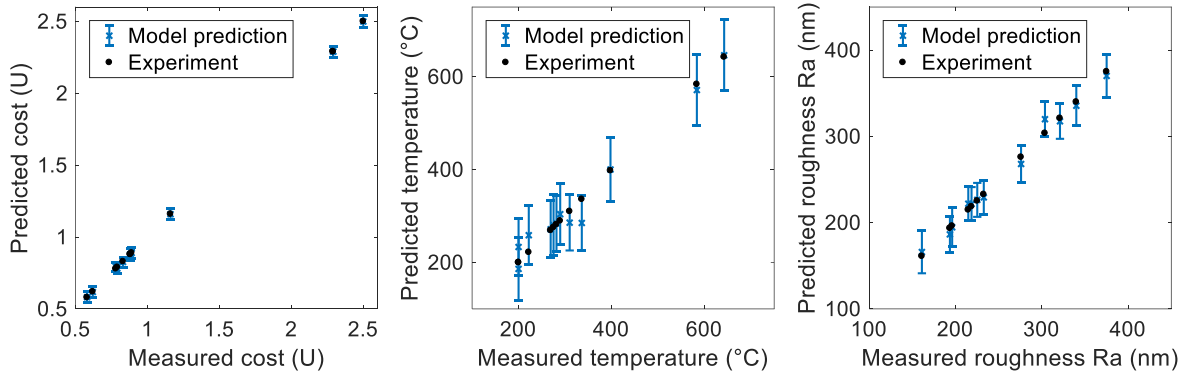


Figure 8.4: Comparison of model predictions with 95% confidence interval and measured temperature, roughness, and cost values after 12 iterations.

Table 8.3 shows optimal parameters for several different values of $p_{Ra,min}$ and $p_{g,min}$ computed from equation (8.3) after 12 iterations. The algorithm recommends an increase in cutting speed when the minimal probabilities that the constraints are fulfilled $p_{Ra,min}$ and $p_{g,min}$ are increased, without a large modification of the feed. An increase in cutting speed leads to lower surface roughness and less probability to violate the surface roughness constraint. As expected, increasing the minimal probability that the constraints are fulfilled results in higher production costs.

Table 8.3: Optimal predicted parameters after 12 iterations with different minimal probabilities that the temperature and roughness constraints are fulfilled. The predicted optimal costs and the predicted 95% confidence interval of the optimal costs is also given.

Minimal probability that constraints are fulfilled (%)	Optimal parameters	Costs (U)
50	$v_{fa,opt} = 12.0 \text{ mm/min}, v_{c,opt} = 23.8 \text{ m/s}$	0.78 ± 0.04
84.1	$v_{fa,opt} = 11.8 \text{ mm/min}, v_{c,opt} = 25.2 \text{ m/s}$	0.83 ± 0.05
97.7	$v_{fa,opt} = 11.4 \text{ mm/min}, v_{c,opt} = 26.8 \text{ m/s}$	0.92 ± 0.07
99.9	$v_{fa,opt} = 11.6 \text{ mm/min}, v_{c,opt} = 28.8 \text{ m/s}$	1.08 ± 0.13

9 Optimization of plunge face grinding of PCBN

Building on the optimization of plunge face grinding of tungsten carbide cutting inserts, in this chapter the grinding of PCBN cutting inserts is investigated. PCBN is a difficult to grind material, which typically leads to a fast deterioration of the grinding wheel cutting ability. Therefore, during grinding of PCBN cutting inserts the grinding wheel is typically conditioned simultaneously to the grinding operation. This grinding strategy contrasts with the intermittent dressing approach, which is commonly used for grinding tungsten carbide inserts. Continuous conditioning of the grinding wheel typically results in a high grinding wheel wear. Therefore, this chapter investigates grinding wheel wear measurement and subsequent optimization of axial grinding feed rate and conditioning feed rate. The optimization objective in this chapter is to reduce the individual production cost while achieving a stable grinding process. The definition for a stable grinding process is motivated by the judgement of human operators. They consider grinding processes unstable if the normal grinding force increases rapidly and exceeds a certain threshold value. Therefore, a grinding process is considered stable if the grinding normal force stays below 300 N for grinding four inserts consecutively after dressing of the grinding wheel. A maximum number of four inserts is chosen to reduce the number of inserts. In preliminary tests an unstable process typically resulted in a rapid increase of the normal grinding force and exceeding the threshold value of 300 N within four inserts. Part of this chapter has been filed for patenting in [149].

9.1 Methodology

9.1.1 Grinding setup and machine

The mechanical setup of the grinding machine is the same as in the previous chapters 7 and 8 with details of the grinding setup listed in Table 9.1. In this chapter the grinding task is to grind a quadratic PCBN insert on four sides evenly, resulting in a smaller but again quadratic insert. The conditioning procedure is specified by discrete steps, where each step consists of an infeed amount which is followed by a waiting time. Dividing the total infeed amount by the total time results in an average conditioning feed rate, which is used to specify the conditioning operation. The optimization is performed for axial grinding feed rates between 1 and 12 mm/min and average conditioning feed rates between 0 and 0.01 mm/s. The parameters are varied between experimental runs but they

stay fixed during a single run. Each experimental run is started with a freshly dressed wheel to provide the same initial conditions for all experiments. Standardly, the grinding machine estimates the grinding normal force based on measurements of the drives, which are used to judge the stability of the process.

Table 9.1: Grinding process specification

Property	Specification
Insert material	Element six DHA650, solid PCBN, CBN content 65%, CBN size $< 4 \mu\text{m}$, binder TiC/TiN, Vickers hardness $34.5 \pm 2.5 \text{ GPa}$
Initial insert geometry	10 mm x 10 mm x 3.2 mm
Final insert geometry	9 mm x 9 mm x 3.2 mm
Grinding machine	Agathon DOM Semi
Grinding wheel	Diamond grains with a vitrified bond (D10V from Tyrolit)
Dressing wheel	Aluminum oxide grains with ceramic bond (89A03202H5AV83 from Tyrolit)
Grinding parameters	Cutting speed 12 m/s, spark out time 3 sec, oscillation frequency grinding 1 Hz, and oscillation frequency spark out 1.5 Hz
Dressing parameter	Infeed 0.4 mm, cutting speed of the grinding wheel 12 m/s, cutting speed of the dressing wheel 8 m/s, feed rate of dressing wheel 0.3 mm/min, and the spark out time 2 sec.
Conditioning parameters	Cutting speed of grinding wheel 12 m/s, cutting speed of the dressing wheel 2 m/s, and average conditioning feed rate varied
Cooling lubricant	Blasogrind GTC 7 from Blaser Swisslube with constant flow rate

9.1.2 Measurement fiber

The wear measurement is based on a device developed originally for the monitoring of civil structures such as tunnels, bridges, dams, and power plants, as presented in [69]. Figure 9.1 shows the grinding wheel wear measurement which relies on low-coherence interference. The measurement system consists of a reference fiber and a measurement fiber. The measurement fiber is embedded inside the grinding wheel perpendicular to the grinding surface and the reference fiber is located on the back of the grinding wheel. For the length measurement, the optical signal of a light source is split, one signal is travelling through the

measurement fiber and the other through the reference fiber. The optical signal travelling through the reference fiber is reflected at the end by a mirror and the optical signal propagating through the measurement fiber is reflected at the end of the fiber. The measurement fiber is continuously shortened as the grinding wheel wears due to grinding, dressing, and conditioning. The length of the measurement fiber is calculated based on the reflections using a spectrum analyzer, part of the SOFO Lite reading unit (Smartec SA, measurement resolution 2 μm). Finally, the length of the measurement fiber is recorded five times and averaged by the measurement computer. The first measurement is taken at least one minute after stopping the grinding wheel and cooling lubricant to reduce the influence of cooling lubricant on the measurement. The difference in length between the measurement before and after an operation is the wear of the grinding wheel. In the current prototype setup, the optical cable is connected manually before and after each operation to measure the wear of the grinding wheel. To improve the industrial applicability, it is proposed to transmit the optical signal via a rotary joint from the rotating part to the non-rotating part, such as presented in [157], or to integrate the SOFO Lite reading unit in the grinding wheel and transmit the data through a wireless connection to the measurement computer, similar to the wheel integrated temperature measurement, as shown in section 7.1.3.

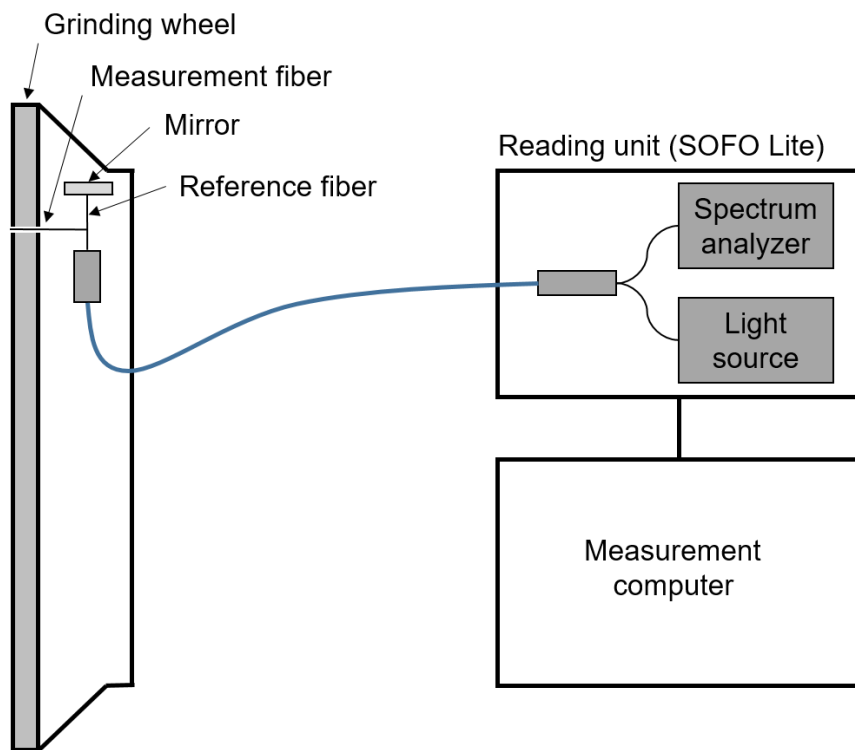


Figure 9.1: Experimental set-up of wheel integrated wear measurement

9.1.3 Microscopic reference measurement

The results of the wear measurements using the low-coherence interferometry were compared and validated against microscopic measurements. To measure the wear with a 3D microscope image reconstruction method, a rectangular pocket with approximately 5 mm length and 2 mm width is lasered into the grinding wheel abrasive layer. The bottom surface of the pocket serves as a reference and the top surface is the abrasive layer of the grinding wheel. Microscopic measurements are performed using the TOOLInspect microscope from Confovis with the focus variation method and a magnification of 10. A typical microscopic measurement is shown in Figure 9.2.

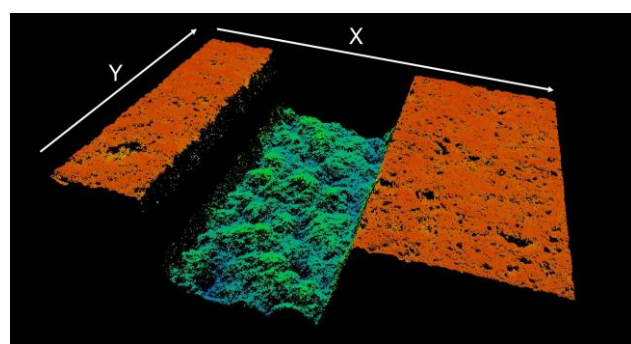


Figure 9.2: Microscopic 3D measurement of reference

The software MountainsMap 7 from Digital Surf is used to evaluate the height difference between the abrasive layer and the reference layer. The measured profiles in X-direction were averaged over the whole evaluation length in Y-direction. The resulting average profile is shown in Figure 9.3. The blue line represents the average profile and the orange area represents the area used for calculating the step size between the upper and lower surface. In this way a mean height of the step between the abrasive surface and the reference surface can be calculated. The grinding wheel wear finally can be calculated as the difference between the step height before and after an operation.

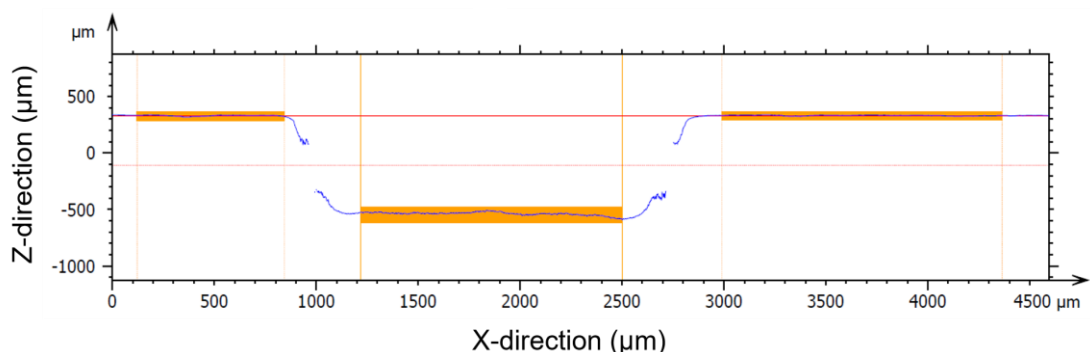


Figure 9.3: Average profile of microscopic reference measurement

9.1.4 Optimization objective and cost calculation

The optimization objective is to find the process parameters \underline{x}_{\min} , which minimize the individual production cost C_{FE} and result in a stable grinding process.

The individual production cost C_{FE} are calculated based on grinding time costs, cost of grinding wheel wear, and cost of dressing wheel wear,

$$C_{FE}(v_{fa}, v_{co}) = C_{MH} t_g(v_{fa}) + a_{co}(v_{fa}, v_{co}) \left(\frac{RC_{gw}}{a_{gw}} + \frac{(1-R)C_{dw}}{a_{dw}} \right) \quad (9.1)$$

where v_{fa} is the axial grinding feed rate, v_{co} is the average conditioning feed rate, t_g is the grinding time, a_{co} is the conditioning distance, and R is the ratio between grinding wheel wear and conditioning distance. The ratio R is similar to the common G ratio but is inverted and used for conditioning and not for grinding. The other cost parameters are listed in Table 9.2. In a first approach, the grinding wheel wear caused by grinding is neglected and the wear is assumed to be caused by the conditioning process alone. The optimal parameters are not influenced by a constant grinding wear independent of the process parameters because it only shifts the cost by a constant value. Only a significantly changing wear for different process parameter such as a change in feed rate values would result in a shift of optimal parameters. Making this assumption reduces the experimental effort and allows to decouple the cost and constraint measurements. The individual production cost can be measured without using inserts and only requires determining the wear ratio R experimentally. After close to optimal parameters are found, this assumption is tested.

Table 9.2: Cost parameters for optimization

Parameter	Description	Value
a_{gw}	Abrasive layer thickness of the grinding wheel	5.8 mm
a_{dw}	Thickness of the dressing wheel	59 mm
C_{MH}	Machine hourly cost	100 U/h
C_{gw}	Cost of grinding wheel	1900 U
C_{dw}	Cost of dressing wheel	100 U

9.1.5 Optimization implementation

A flowchart of the optimization is given in Figure 9.4. The individual production cost is calculated analytically according to equation (9.1) after measuring the ratio R based on conditioning experiments. The analytical calculation of the cost is different compared to the previous chapters where the cost has been modelled with Gaussian process regression using the available cost measurements. After performing the conditioning experiments, it is unclear whether selected process parameters result in a stable or an unstable process. Therefore, a Gaussian process model is needed to model the process stability similar to the constraints in the previous chapters. The probability for process stability as a function of process parameters is predicted by Gaussian process classification. As described in section 4.3 and Appendix B, probit regression is used and predictions are calculated by the expectation propagation approximation method. The use of Gaussian process classification is also in contrast to the previous chapters using Gaussian process regression. As for the regression case in previous chapters, a zero mean function and a Matern 5 covariance function is used. The hyperparameters of the Gaussian process are determined by maximizing the marginal log likelihood, as described in section 4.3. Having obtained a model for the process stability, the next experiment is selected based on the constrained expected improvement equation (4.18) by multiplying the probability for a stable process with the expected improvement a_{EI} . The parameters maximizing the constrained expected improvement are used in the subsequent experiment. The expected improvement is calculated similar to equation (4.15),

$$a_{EI} = \max((C_{\min} - C_{FE}), 0) \quad (9.2)$$

where C_{\min} is the lowest measured cost which results in a stable process and C_{FE} is the individual production cost calculated according to equation (9.1). This approach slightly differs from the previous formulation because the individual production cost C_{FE} is deterministic and not modelled by a Gaussian process. The predicted optimal parameters show the lowest cost and result in a stable grinding process with a probability of 95%. Having obtained optimal parameters, convergence is reached when the optimal parameters vary less than 0.001 mm/s in average conditioning feed rate and 0.3 mm/min in axial feed rate for three consecutive experiments, similar to the previous approach as described in section 6.1.4. The optimization is implemented in MATLAB using the GPML library [133] for Gaussian process classification.

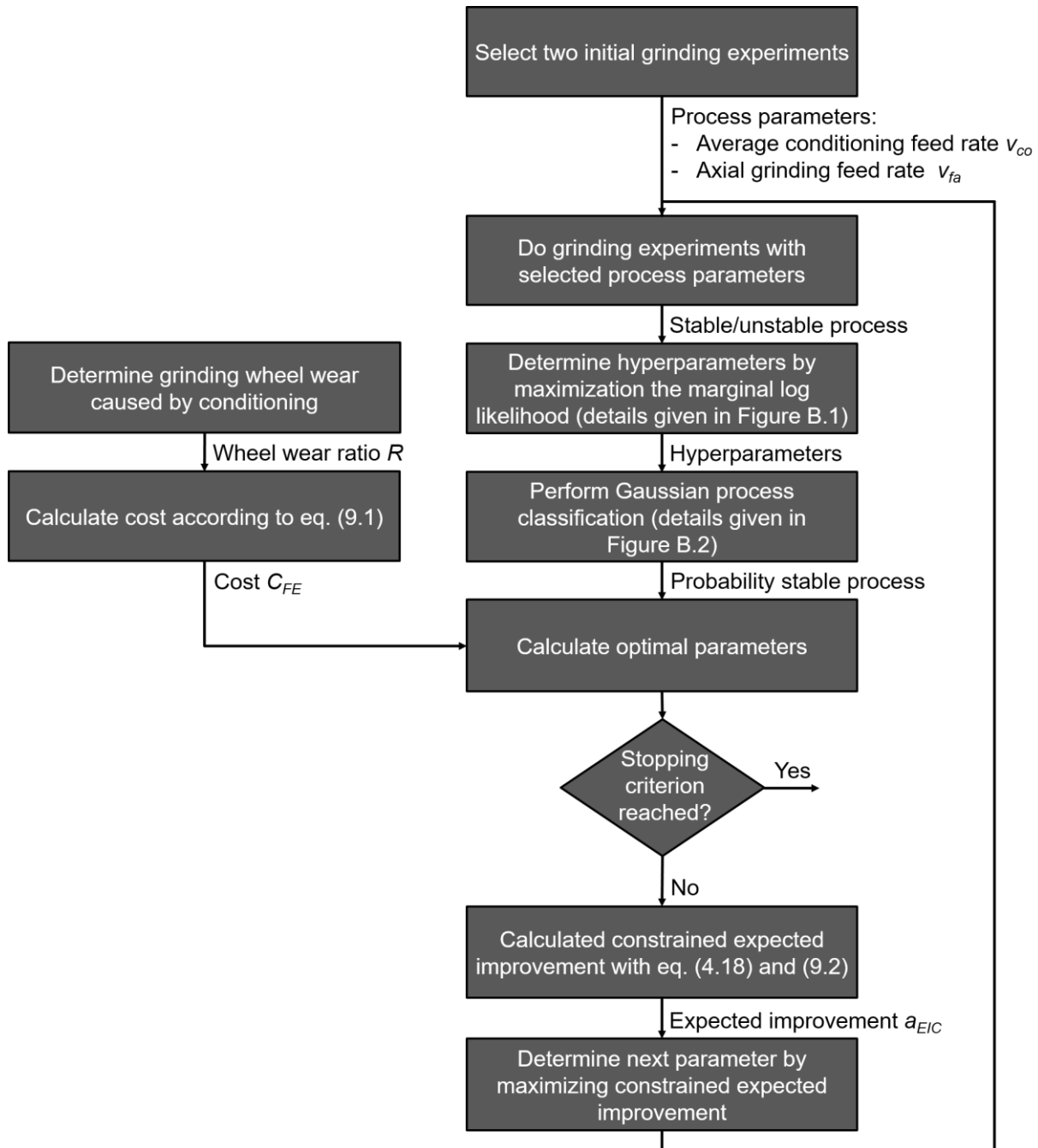


Figure 9.4: Flowchart of PCBN grinding optimization

9.2 Results

9.2.1 Validation of wear sensor

In a first step, interferometric wear measurements are compared to established microscopic wear measurements. For these experiments the grinding wheel is conditioned with different parameters and the grinding wheel wear is measured by both measurement principles. A comparison of the results obtained by the two measurement principles is shown in Figure 9.5. The overall agreement between the wear measurement by the optical fiber and the microscopic wear measurement

is good, with an empirical standard deviation of 7.5 μm . In total two fibers were embedded in the grinding wheel. However, only one fiber showed a reliable reading and was used for wear measurement in this study. To investigate the cause of the unreliable sensor, the results of 20 measurements at different abrasive layer heights, each measurement consisting of 5 repetitive measurements, are compared for both sensors. The fiber showing an unreliable reading showed fluctuations for repetitive measurements of up to 48 μm and an average fluctuation of 12.6 μm . These fluctuations are much larger compared to the properly working sensor which showed an average fluctuation of 4.8 μm and a maximum fluctuation of 11 μm . Increasing the number of sensors in future might improve the overall accuracy compared to the current approach with one functioning sensor because localized wear effects are averaged.

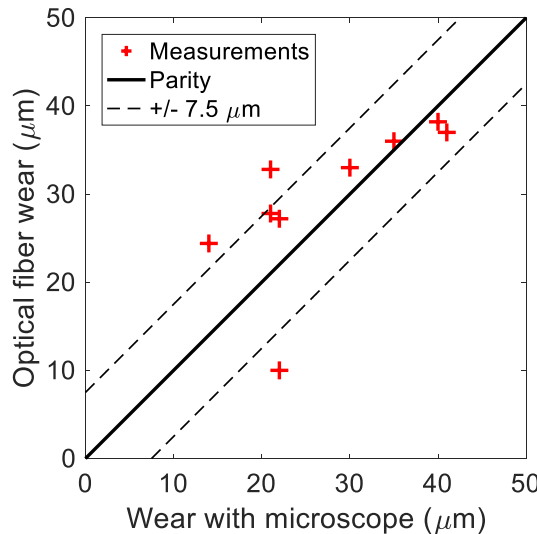


Figure 9.5: Comparison of wear measurement with integrated fiber and microscopic reference measurement

9.2.2 Wear and grinding costs

Figure 9.6 shows the grinding wheel wear caused by conditioning on the left hand side. For these measurements different conditioning infeed and waiting time combinations are tested, which result in different average conditioning feed rates. Specifically, the following combinations are tested: conditioning infeed 10 μm and waiting time 1 sec, conditioning infeed 1 μm and waiting time 1 sec, and conditioning infeed 1 μm and waiting time 0.1 sec. These three combinations are tested for conditioning distances around 1, 2, and 3 mm. However, no significant effect of the average conditioning feed rate on the grinding wheel wear is measured. The variation at each conditioning distance can be fully explained by

measurement noise. The R ratio between grinding wheel wear and conditioning distance is calculated by a linear fit and results in 1.15%.

After the grinding wheel wear caused by conditioning is known, the grinding costs per part can be determined by equation (9.1). The results of the cost calculations are illustrated in the right panel of Figure 9.6. As expected, the grinding costs are lowest for fast axial feed rates and slow average conditioning feed rates. For slow axial feed rates the costs are heavily influenced by the axial feed rate and less sensitive to the average conditioning feed rates. For fast axial feed rates the effect of the average conditioning feed rate increases.

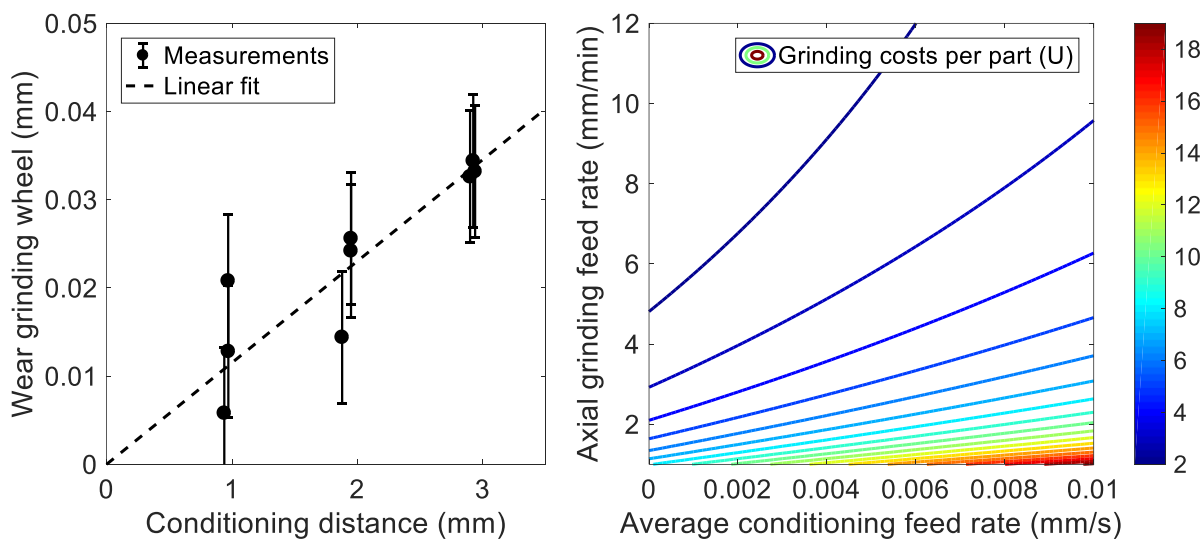


Figure 9.6 Left: Grinding wheel wear caused by conditioning. Right: Grinding cost per part for PCBN grinding

9.2.3 Grinding optimization

The result of the optimization is illustrated in Figure 9.7. The optimization is started with two initial experiments. The first experiment results in a stable grinding process but at high costs and the second experiment results in an unstable process. From the second to the eighth experiment the process is unstable, as the algorithm tests for parameters with low costs. The biggest improvement in cost is achieved between the ninth and eleventh experiment, where all measurements resulted in stable grinding processes. During these tests the cost is reduced by an increase in axial feed rate and a reduction of the average conditioning feed rate. After the eleventh experiment, the tested parameters again result in an unstable grinding process. These experiments reduce the model uncertainty and confirm that close to optimal parameters are found. Convergence is reached after 13 experiments with a predicted optimal axial feed rate of 3.5 mm/min and an

optimal average conditioning feed rate of 0.0066 mm/s. These parameters are very close to the eleventh experiment with an axial feed rate of 3.7 mm/min and an average conditioning feed rate of 0.0064 mm/s.

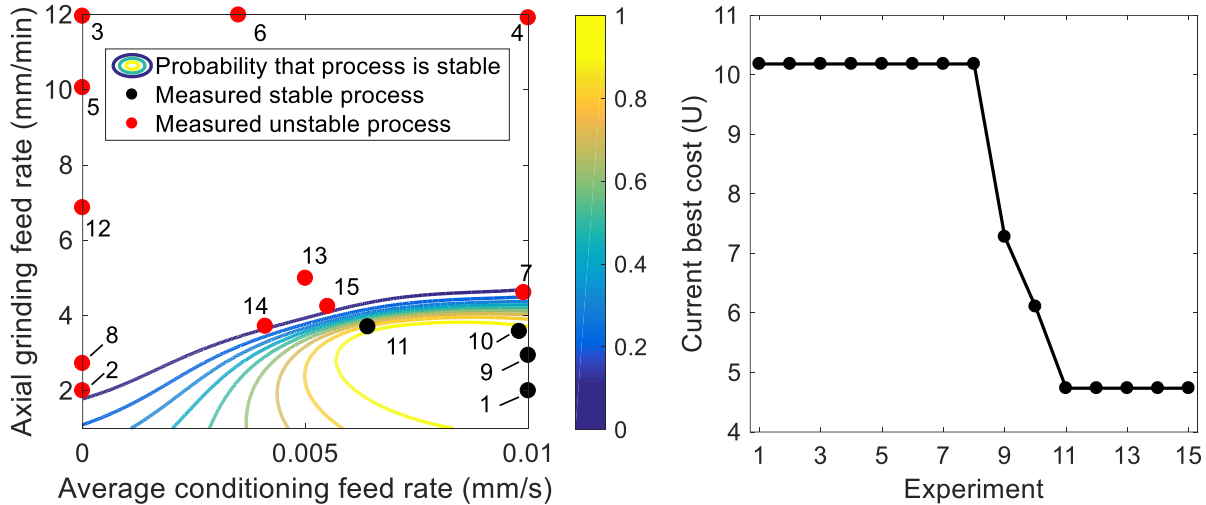


Figure 9.7: Optimization of PCBN grinding process. Left: Conducted experiments with stability prediction of Gaussian process classification after 15 iterations. Right: Current best cost of the optimization.

9.2.4 Wear of grinding and conditioning

The grinding cost used for optimization included the grinding wheel wear caused by conditioning but not the grinding wheel wear caused by grinding. Therefore, the grinding wheel wear is measured during the optimization runs. Figure 9.8 shows the grinding wheel wear for all experiments which resulted in stable grinding processes. The measured grinding wheel wear can be fully explained by wear caused by conditioning for the ninth, tenth, and eleventh experiment. For the first experiment the measured grinding wheel wear is smaller than the wear expected by conditioning. This indicates a higher measurement error for this experiment but does not indicate additional wear caused by grinding. Therefore, all these experiments support the initial assumption that the grinding wheel wear is mainly caused by conditioning and the wear caused by grinding is low. Furthermore, experiment eleven shows the lowest measured grinding wheel wear, confirming the optimization results.

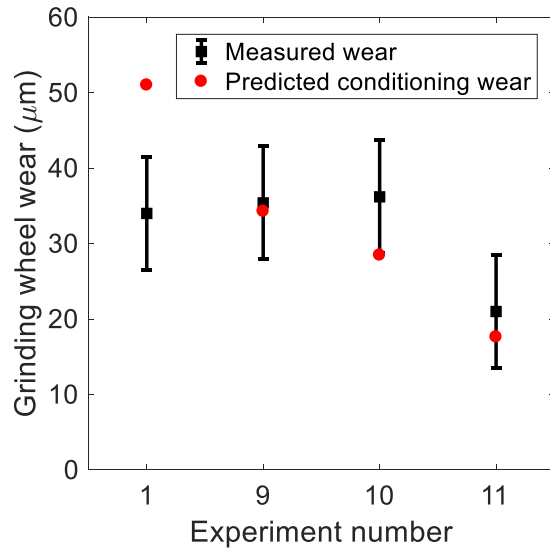


Figure 9.8: Comparison of measured wear during optimization and predicted conditioning wear

9.3 Discussion and conclusion

The investigations show that measuring the wear of the grinding wheel is possible by means of interferometry, and that reflections at the end of the measurement fiber are sufficient for signal analysis. The potential advantages of the investigated interferometric wear measurement system are that it only needs a small installation space, allows fast in-process wear measurement, and does not require human intervention. However, the robustness and accuracy of the tested wear measuring system has potential for improvement. The brakeage of the measurement fiber caused by grinding wheel wear is random and happens locally. Therefore, in future it might be beneficial to include multiple sensors to average this effect and thereby increase the measurement accuracy. Multiple sensors also ease the filtering of inaccurate readings such as happened for the second sensor in this study. Another source of uncertainty might be introduced by disturbances caused by the cooling lubricant which disturbs the optical signal. In this study, the influence of the cooling lubricant was minimized by waiting at least one minute between stopping the grinding wheel and cooling lubricant and measuring grinding wheel wear. However, additional measures such as a more sophisticated post-processing of the data, including cooling lubricant effects, might be beneficial to further reduce the uncertainty.

The optimization of axial grinding feed rate and average conditioning feed rate for grinding of PCBN cutting inserts was successfully demonstrated by using a deterministic cost function, Gaussian process classification to model process

stability and Bayesian optimization. The optimization approach reduced the grinding costs by around 50% compared to the cost of the first experiment, conducted with conservative parameters. Compared to the previous chapters the use of Gaussian processes was demonstrated for binary classification and thereby extending the previous regression cases. Furthermore, this chapter shows the incorporation of a precalculated deterministic cost function within the general Bayesian optimization framework.

10 Prior knowledge and transfer of knowledge

In the previous chapters autonomous parameter selection is demonstrated using constrained Bayesian optimization for longitudinal turning of 1.4125 steel bars and plunge face grinding of PCBN and tungsten carbide inserts. Gaussian process regression and Gaussian process classification without utilizing expert knowledge or transfer of knowledge have been used for process modelling. This chapter focuses on extensions of the current approach to further improve the autonomous parameter selection, by incorporating prior knowledge and transfer of knowledge. Part of this chapter is published in [105].

10.1 Methodology

10.1.1 Experimental setup

The experiments are performed for longitudinal turning on a Swiss GT 32 turning machine from Tornos, shown in Figure 10.1. The machine is equipped with an automatic bar feeder Robobar SBF 326 from Tornos, which handles round bars made of 1.4125 martensitic stainless steel with an initial diameter of 20 mm and a length of 3 m. During the cutting operation, the diameter of the bar is reduced from 20 to 7 mm in 13 steps with a fixed depth of cut of 0.5 mm over a length of 20 mm. In this chapter, the feed per revolution is fixed to 0.05 mm/rev and only the cutting speed is optimized. During cutting Blasomill 15 from Blaser Swisslube is used as a cooling lubricant with a constant flow rate for all experiments. The cutting operations are performed using carbide inserts from Diametal (carbide M10/30, coating D30, geometry DCGX-FR070301, corner radius of 0.1 mm, and article number 236157) mounted on a right-hand tool holder Topdec SDACR from Diametal. The tool life of the cutting tool is determined based on $VB_{B,\max}$ measurements using a Leica Wild M10 microscope, whereby a tool with $VB_{B,\max} \geq 100 \mu\text{m}$ is considered worn out.



Figure 10.1: Picture of turning machine

10.1.2 Optimization task and cost calculation

In this chapter, the aim of the optimization is to find the cutting speed, which minimizes the individual production costs.

$$v_{c,\min} = \arg \min \left(\ln(C_{FE}(v_c)) \right) \quad (10.1)$$

The cutting speed is optimized over a large domain between 10 and 175 m/min. The upper bound of the cutting speed is selected based on the maximum rotational speed of the turning machine, reached during the final longitudinal cutting step. A wide range of cutting speeds results in costs that are different by orders of magnitudes. Having these large cost differences, accurate modelling typically requires short length scale parameters of the Gaussian process, which generally slows down optimization. Therefore, the logarithm of the individual production cost is modelled and optimized. By optimizing in the log space, the Gaussian noise is also changed from a normal to a log-normal distribution. The advantage of the log-normal distribution is that the predicted cost is always positive, which matches reality. The individual production costs C_{FE} are calculated as follows,

$$C_{FE} = t_c \left(C_{MH} + \frac{C_I}{T} \right) \quad (10.2)$$

and the cutting time t_c for multiple cuts can be calculated as shown below.

$$t_c = \sum_{i=1}^{n_{cuts}} \frac{lD_i \pi}{v_c f} \quad (10.3)$$

In this chapter, the machine hour-rate C_{MH} is assumed to be 90 U/h and the cost per cutting edge C_l is assumed with 10 U.

10.1.3 Modelling

The optimization is implemented in Python and uses the GPy library [54] for Gaussian process models. The aim of all Gaussian process models is to accurately model the production costs as a function of cutting speed. Four Gaussian process model versions are tested:

- Model 1 - standard model without expert knowledge (benchmark)
- Model 2 - model with fixed hyperparameters, determined from similar optimization tasks to transfer knowledge
- Model 3 - model with non-zero prior mean function, incorporating knowledge from available empirical or analytical models
- Model 4 - model based on multi-task learning, modelling several tasks together and transfer knowledge by utilizing correlations between different tasks

Figure 10.4 illustrates the four Gaussian process model variants.

The standard Gaussian process model (Model 1) uses a zero prior mean function and determines the hyperparameters by maximizing the marginal log likelihood based on available data points, as specified in equation (4.7). Throughout this chapter the maximization of the marginal log likelihood is performed by using the quasi-Newton method by Broyden, Fletcher, Goldfarb, and Shanno (BFGS) with 1000 restarts. Details of the BFGS method are given in [124].

Instead of determining the hyperparameters by maximizing the marginal log likelihood, the hyperparameters can be fixed based on expert knowledge, which is investigated as a possible alternative in Model 2.

The informative prior mean function of Model 3 can be specified based on known physical or empirical models. Therefore, the Taylor equation, as introduced in equation (2.5), is used to model the tool life as a function of the cutting speed. The tool life predictions are then used in combination with equation (10.2) to calculate the individual production costs. The resulting deviation between the

measured cost and the prediction based on the Taylor equation is modelled by a standard Gaussian process model using a Matern 5 kernel. This corresponds to a two-step approach. The parameters of the Taylor equation are determined first by ordinary least squares using the *scikit-learn* library [129]. Afterwards, the hyperparameters of the Gaussian process model are determined by maximizing the marginal log likelihood, as specified in equation (4.7). The two-step approach is chosen to make the results comparable to standard curve fitting techniques based solely on the Taylor equation, which is identical to the first modelling step.

For transferring knowledge between different tasks, Model 4 uses multi-task learning. As introduced in section 4.2, different multi-task learning models exist. In this chapter, the general idea of the used multi-task approach is to determine a common model for all tasks and model individual deviations to this model independently. Thus, a linear model of coregionalization, as specified in equation (4.9) and (4.10), is used. The used model is based on two Matern 5 kernels, resulting in two coregionalization matrices $\underline{\underline{B}}_1$ and $\underline{\underline{B}}_2$. The first coregionalization matrix $\underline{\underline{B}}_1$ is filled with ones and the hyperparameters of the associated Matern 5 kernel are free. In this way, the combination of coregionalization matrix $\underline{\underline{B}}_1$ and the corresponding kernel models the fully related share of the task outputs. For the second coregionalization matrix and associated kernel, the coregionalization matrix is $\underline{\underline{B}}_2 = \text{diag}(\kappa)$, the length scale hyperparameter of the kernel is free and the signal variance of the kernel is fixed to one because the signal variance is fully captured by the coregionalization matrix $\underline{\underline{B}}_2$. By specifying a diagonal coregionalization matrix, the outputs are modelled independently but share the same hyperparameters. The specifications of $\underline{\underline{B}}_1$ and $\underline{\underline{B}}_2$ are identical to the special cases shown in Figure 4.4. The hyperparameters of the multi-task model are determined by maximizing the marginal log likelihood, as specified in equation (4.14).

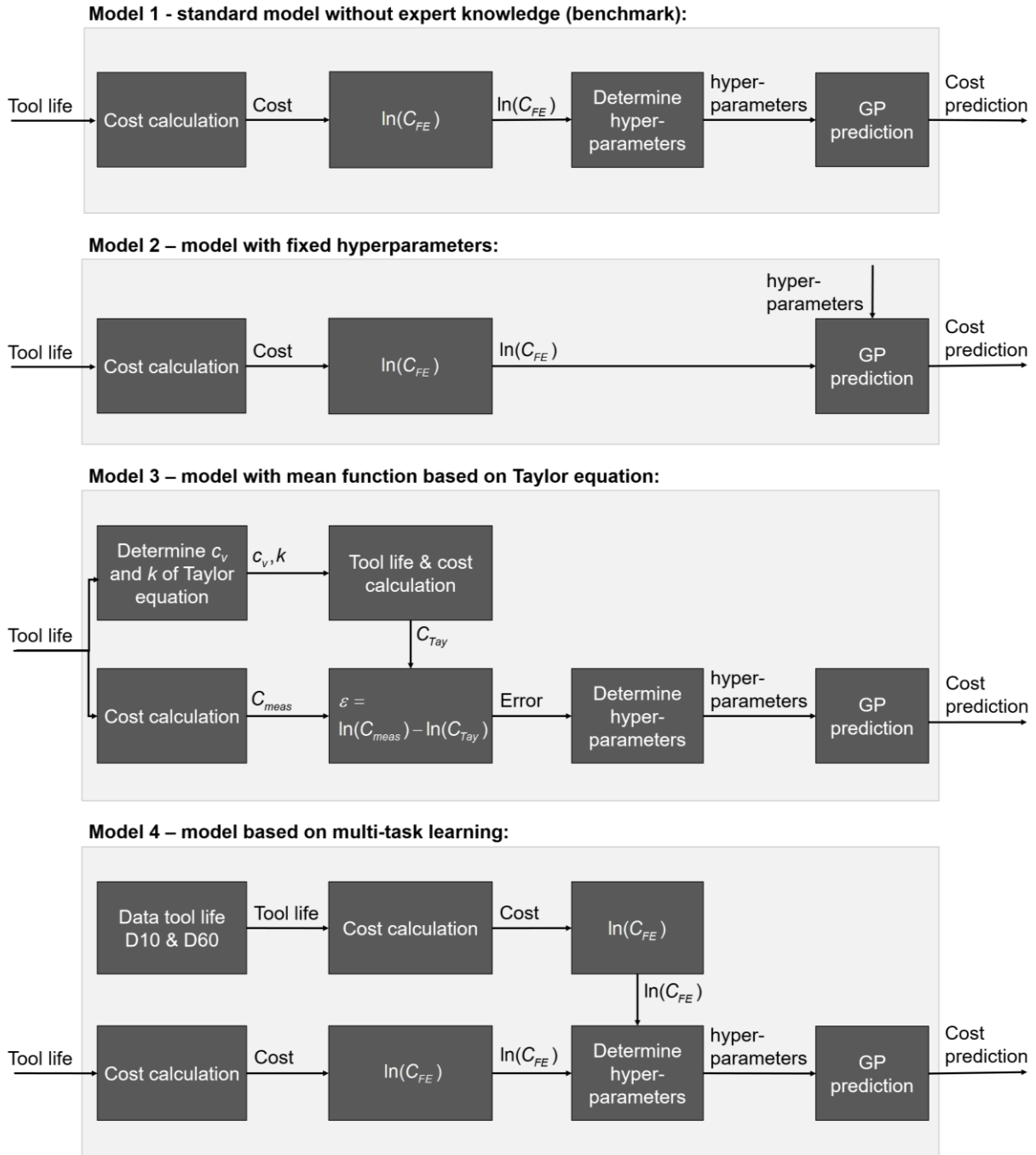


Figure 10.2: Overview of tested Gaussian process model variants. The different Gaussian process variants are a standard Gaussian process, a Gaussian process with fixed hyperparameters, a Gaussian process with a prior mean function based on the Taylor equation, and a multi-task learning model.

The benchmark model (Model 1) and the model based on a non-zero prior mean function (Model 3) do not need additional information. For the multi-task learning model (Model 4) measurements from other tasks are necessary and the model with fixed hyperparameters (Model 2) requires the specification of the hyperparameters, which can also be achieved by using measurements from other

tasks. Figure 10.3 shows available results for optimization tasks using carbide cutting inserts with coating D10 and D60, which serve as prior knowledge for the current optimization task. The current optimization task is slightly different from the previous optimization tasks. In the current setup the carbide insert is coated with D30 instead of D10 or D60 – the rest of the setup remained unchanged. For the fixed hyperparameter case, the hyperparameters of the D60 coating determined by maximizing the marginal log likelihood utilizing all D60 measurements are reused for the D30 case, which are $l_{1,D60} = 0.975$, $\sigma_{f,D60}^2 = 17.02$, and $\sigma_{N,D60}^2 = 0.015$. These hyperparameters correspond to a normalized cutting speed between zero and one. For the multi-task learning approach, the available observations from the D10 and the D60 coating are used together with the new observations from the D30 coating for model updating, as specified in equation (4.14), and for prediction, as specified in equation (4.11) and (4.12).

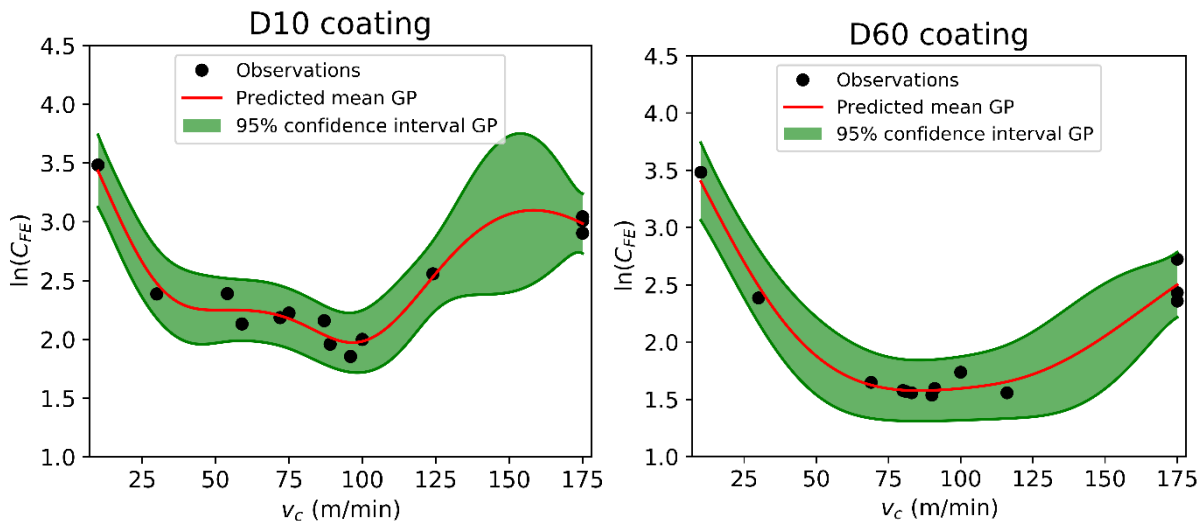


Figure 10.3: Gaussian process regression for coating D10 and D60

10.1.4 Optimization procedure

The different Gaussian process models are tested within the general optimization procedure, as shown in Figure 10.4. Each optimization is started with two initial experiments. When the parameters are determined by maximizing the marginal log likelihood, the initial experiments should be chosen in an area, which allow a good characterization of the function shape. In Bayesian optimization, knowing the maximum gradient of the function allows to determine the smallest length scale of the Gaussian process model, which improves robustness of the optimization. Thus, the initial cutting speeds are set to 10 m/min and 30 m/min

because this region is the expected maximum slope of the cost. This selection is especially useful for the standard Gaussian process model.

Each experiment is started with a fresh cutting insert, used for manufacturing until it is considered worn out following the $VB_{B,\max}$ criterion. For low cutting speeds it might take very long until the tool reaches the $VB_{B,\max}$ criterion, while the time costs are already very high. To avoid unnecessary long experiments, the experiments are stopped when the contribution of the cost for the cutting time exceeds 95% of the total cost. In this case, the cost is calculated as the average between the time cost alone, assuming an infinite tool life, and the cost, which would occur if the insert is assumed worn out directly after the next workpiece is manufactured.

Having obtained the measurements, the Gaussian process model can be used to calculate the optimal parameters and assess convergence of the optimization. Similar to section 6.1.4, convergence is reached when over three consecutive iterations the change in the optimal predicted cost $\mu(x_{opt})$ is less than 5%, the variance at the optimal predicted parameter is $2\sigma(x_{opt})/\mu(x_{opt}) < 25\%$, and the optimal cutting speed varies less than 15 m/min. If convergence is not reached, the cutting speed maximizing the expected improvement acquisition function, as specified in equation (4.16), is used as the next test parameter. In total four individual optimization runs have been performed. To reduce the total number of experiments for the optimization runs, measurements from previous optimization runs are reused when a measurement is available within ± 2 m/min of the requested cutting speed value that is not used during this run yet.

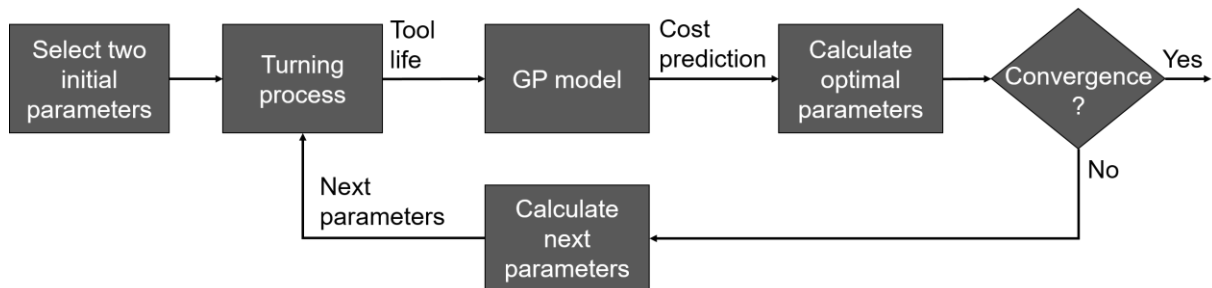


Figure 10.4: Flowchart of the general optimization procedure. The GP model can be represented by one of the four model variants as illustrated in Figure 10.2.

10.2 Experimental results

Figure 10.5 left shows the model prediction after 10 experiments for the standard Gaussian process model without expert knowledge. The observations (black dots) are acquired by the Bayesian optimization procedure, as specified in Figure 10.4. After the two initial experiments at cutting speeds of 10 m/min and 30 m/min, the algorithm requests an experiment at the maximum cutting speed of 175 m/min because based on the two available experiments the model expects a decrease in cost for an increase in cutting speed. Having these three data points, the algorithm explains the data by a nearly linear model with a high length scale parameter and a high noise level, where the cost decreases slightly for higher cutting speed. Considering only these three data points, without additional information, the prediction is reasonable, but the model is too simple for the investigated process. Due to the simple initial model a cutting speed of 175 m/min is investigated four times until the model reduces the noise estimation to an adequate level and is able to distinguish between noise and signal. The following experiments are selected close to the optimum. After 10 experiments the algorithm reaches convergence.

In addition to the observations, which are used by the Gaussian process regression, several validation points are shown, which are not used by the Gaussian process regression. It can be seen that all validation points are within the predicted confidence interval. The uncertainty prediction close to the data points is mainly explained by noise, whereas the uncertainty between measurement points is a combination of noise and uncertainty due to missing data. It can be observed that for high cutting speeds above 150 m/min the cost is more scattered. In the Gaussian process model the noise is assumed to be identical for all cutting speeds. Therefore, this approximation causes the model to overestimate the noise for lower cutting speeds. It would be possible to use a different likelihood which reflects the heteroscedasticity of the data (different noise levels for different process parameters), such as shown in [51, 121]. However, such approaches usually increase the model complexity and are typically analytically intractable. Consequently, approximation methods such as expectation propagation, as shown in [121], or computationally expensive sampling methods such as Markov chain Monte Carlo, as shown in [51], are needed. Due to the increased complexity and the good performance obtained by the simple model, no attempts have been made to improve the model. However, the use of a tailored likelihood might be an interesting direction for future research.

Figure 10.5 right shows the result for fixed hyperparameters (Model 2) instead of determining the hyperparameters by maximizing the marginal log likelihood. The two initial experiments are again at cutting speeds of 10 m/min and 30 m/min. As for the case without prior knowledge the next experiment is performed at the highest cutting speed of 175 m/min. However, the algorithm does not test high cutting speeds again because it is able to directly distinguish between noise and signal. Afterwards the algorithm selects parameters close to the optimum and reaches convergence after 6 experiments. The resulting posterior prediction of the standard Gaussian process model and the model with fixed hyperparameters is very similar after convergence but the model with fixed hyperparameters needs 6 experiments instead of 10 experiments, which reduces the experimental effort significantly.

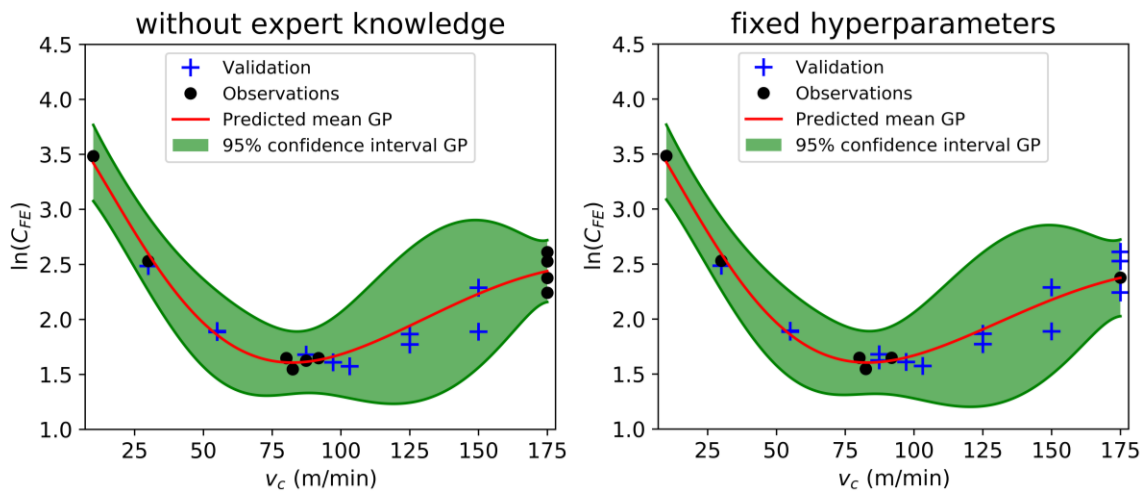


Figure 10.5 Left: Result of Bayesian optimization after 10 experiments using a standard Gaussian process model without expert knowledge (Model 1). Right: Result of Bayesian optimization after 6 experiments using fixed hyperparameters (Model 2).

Another investigated approach is the specification of a non-zero prior mean function (Model 3), as displayed in Figure 10.6. At least two tool life measurements at different cutting speeds are required to fit the Taylor equation. In this case the optimization is again started at cutting speeds of 10 m/min and 30 m/min. However, the experiment at the lowest cutting speed of 10 m/min takes very long without reaching the end of the tool life. Hence, the 95% criterion for the cost is reached before the insert is worn out and no tool life is measured for this experiment. To obtain a second measurement for the tool life, the third experiment is conducted at 175 m/min as requested by the optimization with the standard Gaussian process model (Model 1). After these three experiments, two

tool life measurements are available and a prior mean function based on the Taylor equation can be calculated. Afterwards the algorithm starts to sample close to the optimum and converges after 6 experiments. As shown on the left of Figure 10.6, the Taylor equation shows a high error between measurements and predictions. Especially the tool life measurements at low cutting speeds influence the quality of the Taylor equation fit negatively. The tool life is reduced at low cutting speeds due to build up edge of the tool, as described in [81]. This effect is not captured by the Taylor equation and reduces the quality of the model fit. It would be possible to improve the Taylor equation fit by carefully choosing the range of cutting speeds where the Taylor equation is valid. However, no such attempt has been made in this study because the main objective is to demonstrate the combination of existing models describing general trends with Gaussian process models capturing the deviation between measurements and the existing models. As shown on the right of Figure 10.6, using the predicted tool life by the Taylor equation for cost calculation alone leads to high model errors. Although the Taylor equation fit is not very good, the data is explained well by the Gaussian process model using the cost calculated by the Taylor equation as a mean function. Therefore, the deviation between the cost predicted by the Taylor equation and the cost determined experimentally is modelled accurately by the Gaussian process model. Moreover, compared to the standard approach, the data-efficiency of the optimization is improved by using a Gaussian process model with a mean function based on the Taylor equation. Some of the validation points are outside the 95% confidence interval for cutting speeds of 175 m/min. This is again a result of the Gaussian likelihood, assuming identical noise for all cutting speeds. However, for this case, the model predicts the data very well near the optimum because more data is available in this range and a cutting speed of 175 m/min is only sampled once.

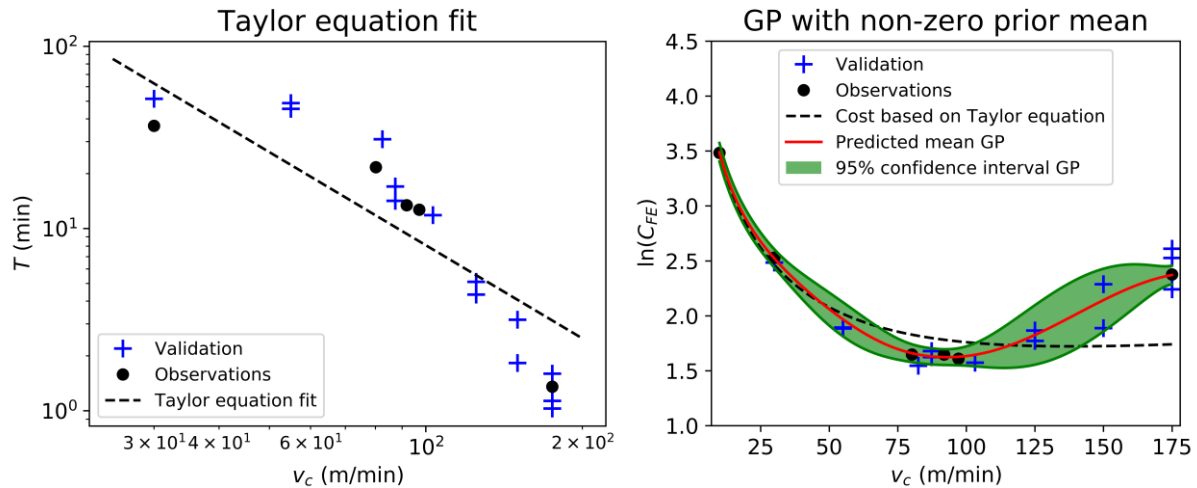


Figure 10.6: Taylor equation fit and Gaussian process regression with prior mean based on Taylor equation (Model 3) after 6 experiments

The last investigated approach is multi-task learning (Model 4), as shown in Figure 10.7. As before, the multi-task learning case is started with two initial experiments at 10 m/min and 30 m/min. In addition to these two starting points, the multi-task model incorporates the results of the previous measurements with the D10 and D60 coating. As a consequence, the algorithm requests points close to the optimum and reaches convergence after 4 experiments. After these 4 experiments the model is able to predict the data very well, especially close to the optimum. Only the variation at high cutting speed is again slightly underestimated due to the assumption of Gaussian noise that is modelled independently of the cutting speed. The model results for the D30 coating are very similar to the results of the D60 coating. This similarity is exploited by the multi-task learning approach, leading to a fast convergence.

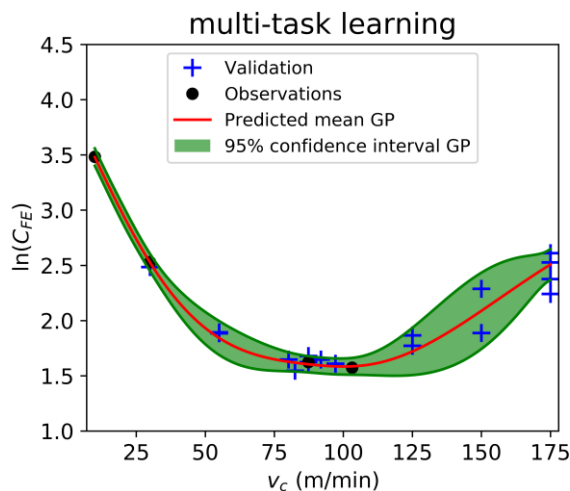


Figure 10.7: Results for multi-task learning (Model 4) after 4 experiments

Figure 10.8 shows a comparison of all tested models. It can be seen that the standard Gaussian process model without expert knowledge (Model 1) starts to sample close to the optimum only after 7 experiments and converges after 10 experiments. The performance of the Gaussian process model with fixed hyperparameters (Model 2) and the non-zero prior mean function (Model 3) behave very similarly. They start to sample parameters close to the optimum after 4 experiments and converge after 6 experiments. The best performance is achieved with the multi-task learning approach (Model 4), which first samples a parameter close to the optimum after 3 experiments and converges after 4 experiments. In summary, all tested methods which include expert knowledge or share knowledge between tasks are suited to improve significantly the sample efficiency compared to the standard Gaussian process model.

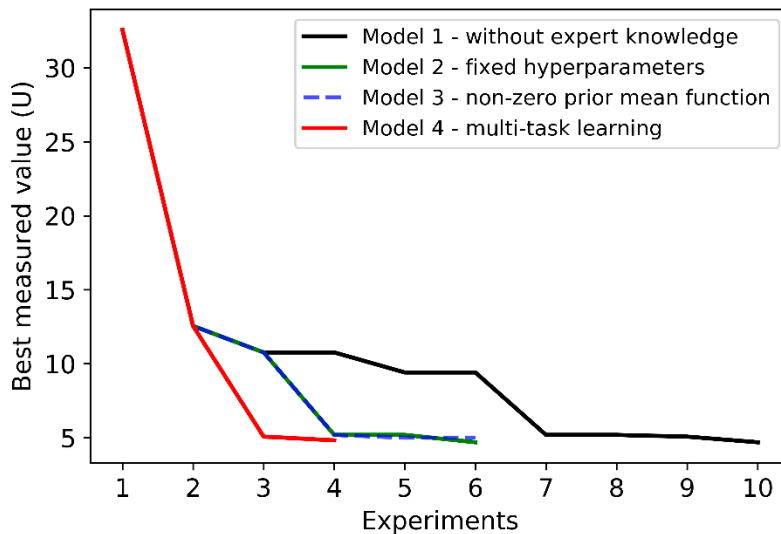


Figure 10.8: Performance comparison of different Gaussian process models

11 Conclusion and Outlook

Based on the identified research gap, data-driven optimization for knowledge acquisition of expert systems, quantification of process performance by a sensor setup, and use of prior knowledge and transfer of knowledge have been investigated exemplarily for grinding and turning.

Gaussian process models combined with Bayesian optimization for data-driven optimization have been demonstrated for grinding and turning. The tested approaches showed a high flexibility, produced physically plausible results, and can find optimal parameters within a few iterations. In this study up to two parameters have been used for optimization. In future it is recommended to extend the approach to additional parameters such as dressing wheel speed and oscillation frequency of the grinding wheel. Furthermore, the inclusion of constraints and a stopping criterion in the optimization have been demonstrated successfully. In this study, avoiding tool or machine damage by misspecification of machining parameters has been ensured by selecting an appropriate parameter optimization range and utilizing sensorial feedback. Future research is necessary to investigate whether this approach is sufficient. An alternative is to consider safety for the selection of test parameters as demonstrated in [11]. As shown in chapter 5, discontinuities or steps in the modelled function are not captured well by Gaussian process regression because predictions depend on correlations between nearby points. This topic is open to future research and a promising approach is to combine Bayesian methods with neural networks. For simplicity, the Gaussian process prior has been combined with a Gaussian likelihood for the regression case because in this way the modelling stays analytically traceable. Assuming a Gaussian likelihood is an approximation and does not always match reality precisely, as shown in chapter 10. A direction for future research is to use tailored likelihoods for the optimization task at hand, which typically requires the use of approximation or sampling methods.

Process performance in longitudinal turning has been determined using tool life and surface roughness measurements. For plunge face grinding of tungsten carbide cutting inserts, a wheel integrated optical sensor has been used for temperature detection, which allowed accurate detection of grinding burn. For plunge face grinding of PCBN cutting inserts, the wear of the grinding wheel has been measured by a fiber embedded inside the abrasive layer of the grinding

wheel, and an interferometer. Furthermore, the surface roughness and the grinding forces have been measured. Having all these measurements allowed optimization of longitudinal turning and plunge face grinding. However, several extensions are possible. The used optical wear measurement requires to stop the grinding wheel, connect the fibers, and afterwards conduct a measurement. For industrial application it is recommended to investigate approaches, which do not require manual work for the wear measurement. An option is to transmit the optical signal by a rotary joint from the rotating to the non-rotating part, as shown in [157], or to place the electronics on the grinding wheel and to transmit the signal wireless to the non-rotating part, similar to the temperature measurement as described in section 7.1.3. Furthermore, approaches to further improve the measurement uncertainty of the wear measurement such as using more sensors are desired. Overall, the needed sensors strongly depend on the requirements on the final part and specific machining operation. Therefore, in future it is recommended to include additional sensorial feedback to cover a broad range of applications and thereby improve industrial applicability. Interesting quantities for future research are geometry errors of the workpiece and cutting edge roughness of the workpiece after grinding.

Different methods to include expert knowledge and transfer of knowledge have been investigated. All methods utilizing expert knowledge or transfer of knowledge reduced the number of experiments by at least 40% compared to the standard approach without expert knowledge, showing the potential of the investigated methods. Due to the increased data-efficiency, it is recommended to use prior knowledge and transfer knowledge wherever possible.

To further improve the industrial applicability, it is recommended to combine the investigated methods with an expert system for data handling. Figure 11.1 shows a concept for such a system. The procedure is started with a manufacturing task from a high-level production planning and control system. Afterwards similar tasks or prior knowledge are searched in the knowledge base and transferred to the Bayesian optimization algorithm. As the knowledge base grows it might be necessary to pre-filter similar tasks because supplying too many data points to Bayesian optimization will ultimately significantly increase the computational effort. Besides available knowledge, cost parameters must be provided to the optimization. The cost parameters depend on purchasing prices of the tool and machine but also on the workload of the factory and must be supplied by a high-level production planning and control system. The cost parameters can be

provided to the parameter selection system based on fairly large time intervals such as once a day. Afterwards Bayesian optimization selects process parameters which are informative about the optimum. Performance measures and product quality data which results from operation with the selected process parameters is used to update the Bayesian optimization algorithm. Furthermore, the performance and quality data are stored in the knowledge base for later use for the optimization of similar cases. The Bayesian optimization algorithm selects process parameters until convergence is reached. Afterwards the manufacturing process is operated with the predicted best parameters.

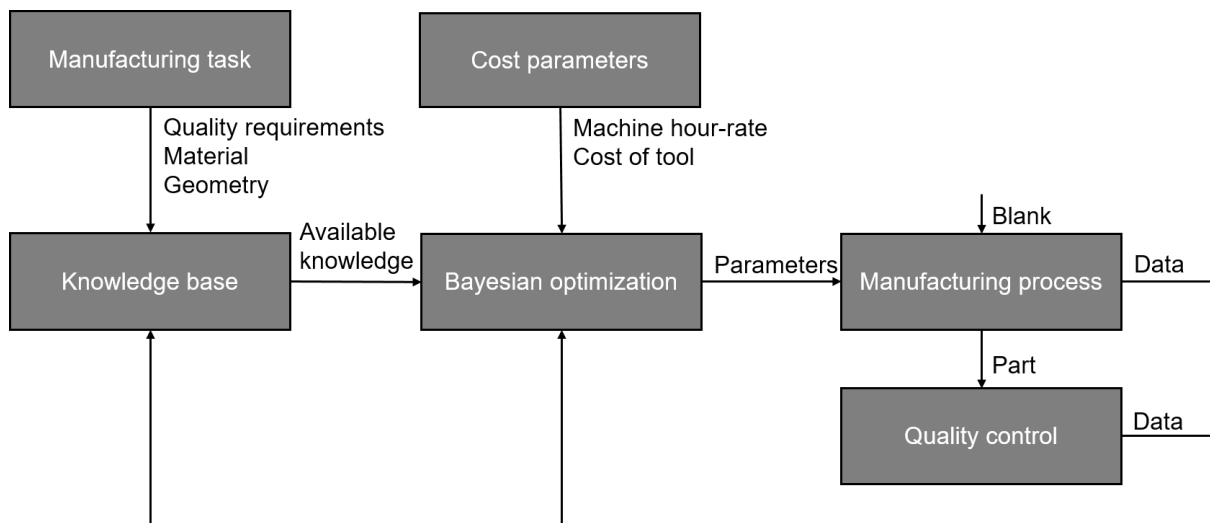


Figure 11.1: Concept for integration of Bayesian optimization in an expert system

Bibliography

1. A. T. Abbas, K. Hamza, M. F. Aly, E. A. Al-Bahkali (2016) *Multiobjective optimization of turning cutting parameters for J-steel material*, Advances in Materials Science and Engineering. 2016: ID 6429160.
2. H. Abdelrahman, F. Berkenkamp, J. Poland, A. Krause (2016) *Bayesian optimization for maximum power point tracking in photovoltaic power plants*, 2016 European Control Conference (ECC). p. 2078-2083.
3. A. Abdullah, A. Pak, M. Farahi, M. Barzegari (2007) *Profile wear of resin-bonded nickel-coated diamond wheel and roughness in creep-feed grinding of cemented tungsten carbide*, Journal of Materials Processing Technology. 183(2-3): p. 165-168.
4. M. A. Alvarez, L. Rosasco, N. D. Lawrence (2012) *Kernels for vector-valued functions: a review*, Foundations and Trends in Machine Learning. 4(3): p. 195-266.
5. M. Aramesh, B. Shi, A. O. Nassef, H. Attia, M. Balazinski, H. A. Kishawy (2013) *Meta-modeling optimization of the cutting process during turning titanium metal matrix composites (Ti-MMCs)*, Procedia CIRP. 8: p. 576-581.
6. N. Arunachalam, B. Ramamoorthy (2007) *Texture analysis for grinding wheel wear assessment using machine vision*, Proceedings of the Institution of Mechanical Engineers, Part B: Journal of Engineering Manufacture. 221(3): p. 419-430.
7. B. Azarhoushang, T. Stehle, H. Kitzig-Frank, H.-C. Möhring (2017) *Effects of grinding process parameters on the surface topography of PCBN cutting inserts*, International Journal of Abrasive Technology. 8(2): p. 121-132.
8. J. Badger (2009) *Factors affecting wheel collapse in grinding*, CIRP Annals. 58(1): p. 307-310.
9. J. Badger (2015) *Grinding of sub-micron-grade carbide: contact and wear mechanisms, loading, conditioning, scrubbing and resin-bond degradation*, CIRP Annals. 64(1): p. 341-344.
10. J. Bergstra, Y. Bengio (2012) *Random search for hyper-parameter optimization*, Journal of Machine Learning Research. 13(10): p. 281-305.

11. F. Berkenkamp, A. Krause, A. P. Schoellig (2021) *Bayesian optimization with safety constraints: safe and automatic parameter tuning in robotics*, Machine Learning.
12. C. Bobst, M. Maier, A. Rupenyan-Vasileva (2020) *Method for autonomous optimization of a grinding process*, EP3736648A1, European patent office.
13. C. Böhm (2001) *Entwicklung und Erprobung sensorintegrierter Schleifwerkzeuge*, (Diss.) Universität Bremen.
14. G. E. P. Box, W. G. Hunter, J. S. Hunter (1978) *Statistics for experimenters : an introduction to design, data analysis, and model building*. John Wiley & Sons, New York.
15. E. Brinksmeier, J. C. Aurich, E. Govekar, C. Heinzel, H.-W. Hoffmeister, F. Klocke, J. Peters, R. Rentsch, D. J. Stephenson, E. Uhlmann, K. Weinert, M. Wittmann (2006) *Advances in modeling and simulation of grinding processes*, CIRP Annals. 55(2): p. 667-696.
16. E. Brinksmeier, C. Heinzel, L. Meyer (2005) *Development and application of a wheel based process monitoring system in grinding*, CIRP Annals. 54(1): p. 301-304.
17. E. Brinksmeier, F. Werner (1992) *Monitoring of grinding wheel wear*, CIRP Annals. 41(1): p. 373-376.
18. A. O. K. Buttner, G. Bullen (1970) *The temperature of grinding wheel and workpiece*, Tooling. 24(12): p. 43-56.
19. M. Castejón, E. Alegre, J. Barreiro, L. K. Hernández (2007) *On-line tool wear monitoring using geometric descriptors from digital images*, International Journal of Machine Tools and Manufacture. 47(12-13): p. 1847-1853.
20. C. H. Che-Haron (2001) *Tool life and surface integrity in turning titanium alloy*, Journal of Materials Processing Technology. 118(1-3): p. 231-237.
21. N. Chen, Z. Qian, I. T. Nabney, X. Meng (2014) *Wind power forecasts using Gaussian processes and numerical weather prediction*, IEEE Transactions on Power Systems. 29(2): p. 656-665.

22. H.-Z. Choi (1986) *Beitrag zur Ursachenanalyse der Randzonenbeeinflussung beim Schleifen*. Fortschritt-Berichte VDI. Reihe 2, Fertigungstechnik Nr. 119. VDI-Verlag, Düsseldorf.
23. S. K. Choudhury, K. K. Kishore (2000) *Tool wear measurement in turning using force ratio*, International Journal of Machine Tools and Manufacture. 40(6): p. 899-909.
24. J. D. Cogdell (1991) *In-process workpiece temperature sensor*, Precision Engineering. 13(2): p. 135-138.
25. T. Cohn, L. Specia (2013) *Modelling annotator bias with multi-task Gaussian processes: An application to machine translation quality estimation*, Proceedings of the 51st Annual Meeting of the Association for Computational Linguistics (Volume 1: Long Papers). p. 32-42.
26. D. C. Cruz, V. L. Sordi, C. E. H. Ventura (2020) *Surface analysis of WC-5%Co cemented tungsten carbide cutting insert after plunge-face grinding*, The International Journal of Advanced Manufacturing Technology. 108(1): p. 323-330.
27. M. P. Deisenroth, D. Fox, C. E. Rasmussen (2015) *Gaussian processes for data-efficient learning in robotics and control*, IEEE Transactions on Pattern Analysis and Machine Intelligence. 37(2): p. 408-423.
28. B. Denkena, T. Grove, L. Behrens (2015) *Significant influence factors on the grinding tool wear and cutting mechanisms during grinding of PCBN inserts*, Production Engineering. 9(2): p. 187-193.
29. B. Denkena, T. Grove, L. Behrens (2016) *Wear mechanisms in grinding of PCBN*, Advanced Materials Research. 1136: p. 555-560.
30. B. Denkena, T. Grove, L. Behrens, D. Müller-Cramm (2020) *Wear mechanism model for grinding of PCBN cutting inserts*, Journal of Materials Processing Technology. 277: ID 116474.
31. B. Denkena, J. Köhler, C. E. H. Ventura (2014) *Grinding of PCBN cutting inserts*, International Journal of Refractory Metals and Hard Materials. 42: p. 91-96.
32. B. Denkena, J. Köhler, C. E. H. Ventura (2014) *Influence of grinding parameters on the quality of high content PCBN cutting inserts*, Journal of Materials Processing Technology. 214(2): p. 276-284.

33. Diametal AG (2017) *Precision turning tools catalog 5*. Biel/Bienne, Switzerland.
34. DIN 8580:2003-09 (2003) *Fertigungsverfahren - Begriffe, Einteilung*.
35. DIN 8589-1:2003-09 (2003) *Fertigungsverfahren Spanen - Teil 1: Drehen; Einordnung, Unterteilung, Begriffe*.
36. DIN 8589-11:2003-09 (2003) *Fertigungsverfahren Spanen - Teil 11: Schleifen mit rotierendem Werkzeug; Einordnung, Unterteilung, Begriffe*.
37. DIN ISO 513:2014-05 (2014) *Classification and application of hard cutting materials for metal removal with defined cutting edges - designation of the main groups and groups application*.
38. DIN ISO 525:2015-02 (2015) *Schleifkörper aus gebundenem Schleifmittel - Allgemeine Anforderungen*.
39. DIN ISO 1832:2017-06 (2017) *Indexable inserts for cutting tools - designation*.
40. A. E. Diniz, J. J. Liu, D. A. Dornfeld (1992) *Correlating tool life, tool wear and surface roughness by monitoring acoustic emission in finish turning*, Wear. 152(2): p. 395-407.
41. D. Dornfeld, H. G. Cai (1984) *An investigation of grinding and wheel loading using acoustic emission*, Journal of Engineering for Industry. 106(1): p. 28-33.
42. E. A. Feigenbaum, P. McCorduck (1983) *The fifth generation: artificial intelligence and Japan's computer challenge to the world*. Addison-Wesley, Reading, Massachusetts.
43. Z. Feng, X. Chen (2007) *Image processing of grinding wheel surface*, The International Journal of Advanced Manufacturing Technology. 32(5): p. 452-458.
44. G. Friedrich, M. Stumptner (1990) *Einführung*, in G. Gottlob, T. Frühwirth, W. Horn (Eds.), *Expertensysteme*, Springer-Verlag, Wien: p. 1-19.

45. T. Friemuth (1999) *Schleifen hartstoffverstärkter keramischer Werkzeuge*. Fortschritt-Berichte VDI. Reihe 2, Fertigungstechnik Nr. 510. VDI-Verlag, Düsseldorf.
46. A. Fritsch (1997) *Schleifen von Cermets*. Fortschritt-Berichte VDI. Reihe 2, Fertigungstechnik Nr. 429. VDI-Verlag, Düsseldorf.
47. Y. Gal, Z. Ghahramani (2016) *Dropout as a Bayesian approximation: representing model uncertainty in deep learning*, Proceedings of The 33rd International Conference on Machine Learning. p. 1050-1059.
48. J. R. Gardner, M. J. Kusner, Z. E. Xu, K. Q. Weinberger, J. P. Cunningham (2014) *Bayesian optimization with inequality constraints*, Proceedings of the 31st International Conference on Machine Learning. p. 937-945.
49. M. H. Gholami, M. R. Azizi (2014) *Constrained grinding optimization for time, cost, and surface roughness using NSGA-II*, The International Journal of Advanced Manufacturing Technology. 73(5): p. 981-988.
50. A. Gołąbczak, T. Koziarski (2005) *Assessment method of cutting ability of CBN grinding wheels*, International Journal of Machine Tools and Manufacture. 45(11): p. 1256-1260.
51. P. W. Goldberg, C. K. I. Williams, C. M. Bishop (1997) *Regression with input-dependent noise: a Gaussian process treatment*, Advances in Neural Information Processing Systems. 10: p. 493-499.
52. P. Goovaerts (1997) *Geostatistics for natural resources evaluation*. Oxford University Press, Oxford.
53. E. Govekar, A. Baus, J. Gradišek, F. Klocke, I. Grabec (2002) *A new method for chatter detection in grinding*, CIRP Annals. 51(1): p. 267-270.
54. GPy. (since 2012) *GPy: A Gaussian process framework in python*. [cited 04.08.2021]; Available from: <http://github.com/SheffieldML/GPy>.
55. A. Graves, A.-r. Mohamed, G. Hinton (2013) *Speech recognition with deep recurrent neural networks*, 2013 IEEE International Conference on Acoustics, Speech and Signal Processing. p. 6645-6649.
56. A. Graves, J. Schmidhuber (2008) *Offline handwriting recognition with multidimensional recurrent neural networks*, Advances in Neural Information Processing Systems. 21: p. 545-552.

57. C. Guestrin, A. Krause, A. P. Singh (2005) *Near-optimal sensor placements in gaussian processes*, Proceedings of the 22nd International Conference on Machine Learning. p. 265-272.
58. G. Hammann (1998) *Modellierung des Abtragsverhaltens elastischer, robotergeführter Schleifwerkzeuge*. ISW Forschung und Praxis, Berichte aus dem Institut für Steuerungstechnik der Werkzeugmaschinen und Fertigungseinrichtungen der Universität Stuttgart, Band 123. Springer, Berlin, Heidelberg.
59. K. Hashmi, I. D. Graham, B. Mills (2003) *Data selection for turning carbon steel using a fuzzy logic approach*, Journal of Materials Processing Technology. 135(1): p. 44-58.
60. H. Helbig (2006) *Knowledge representation and the semantics of natural language*. Springer, Berlin, Heidelberg.
61. H. Helbig (2008) *Wissensverarbeitung und die Semantik der natürlichen Sprache: Wissensrepräsentation mit MultiNet (2. Auflage)*. Springer, Berlin, Heidelberg.
62. J. M. Hernández-Lobato, M. A. Gelbart, M. W. Hoffman, R. P. Adams, Z. Ghahramani (2015) *Predictive entropy search for Bayesian optimization with unknown constraints*, Proceedings of the 32nd International Conference on Machine Learning. p. 1699-1707.
63. J. M. Hernández-Lobato, M. W. Hoffman, Z. Ghahramani (2014) *Predictive entropy search for efficient global optimization of black-box functions*, Advances in Neural Information Processing Systems.
64. H. W. Hoffmeister, S. Illenseer, T. Weber (2000) *Qualitätssicherungsmaßnahmen beim Schleifen, Sensorik und Simulation optimieren Fertigungsprozess*, VDI-Z integrierte Produktion : Organ der VDI-Gesellschaft Produktionstechnik (VDI-ADB). 142(3/4): p. 32-36.
65. R. M. Homami, A. F. Tehrani, H. Mirzadeh, B. Movahedi, F. Azimifar (2014) *Optimization of turning process using artificial intelligence technology*, The International Journal of Advanced Manufacturing Technology. 70(5-8): p. 1205-1217.
66. F. H. Hughes, B. Richards (1966) *Measurement of the stresses set up in a resin bonded diamond grinding wheel while grinding Harmet G6 tungsten carbide*, Journal of Engineering for Industry. 88(2): p. 157-163.

67. I. Inasaki (1991) *Monitoring and optimization of internal grinding process*, CIRP Annals. 40(1): p. 359-362.
68. I. Inasaki, H. R. Meyer, F. Klocke, J. Shibata, G. Spur, H. K. Tonshoff, H. G. Wobker (1999) *4 - Grinding*, in I. D. Marinescu, H. K. Tonshoff, I. Inasaki (Eds.), *Handbook of ceramic grinding & polishing*, William Andrew, Norwich, NY: p. 190-323.
69. D. Inaudi (2004) *SOFO sensors for static and dynamic measurements*, 1st FIG International Symposium on Engineering Surveys for Construction Works and Structural Engineering.
70. ISO 3685:1993(E) (1993) *Tool-life testing with single point turning tools*.
71. ISO 14104:2017(E) (2017) *Gears - surface temper etch inspection after grinding, chemical method*.
72. P. Jackson (1999) *Introduction to expert systems (3rd edition)*. Addison-Wesley, Harlow.
73. S. Jermolajev, E. Brinksmeier (2014) *A new approach for the prediction of surface and subsurface properties after grinding*, Advanced Materials Research. 1018: p. 189-196.
74. D. R. Jones, M. Schonlau, W. J. Welch (1998) *Efficient global optimization of expensive black-box functions*, Journal of Global Optimization. 13(4): p. 455-492.
75. A. G. Journel, C. J. Huijbregts (1978) *Mining geostatistics*. Academic Press, London.
76. B. Karpuschewski, O. Bleicher, M. Beutner (2011) *Surface integrity inspection on gears using Barkhausen noise analysis*, Procedia Engineering. 19: p. 162-171.
77. B. Karpuschewski, M. Wehmeier, I. Inasaki (2000) *Grinding monitoring system based on power and acoustic emission sensors*, CIRP Annals. 49(1): p. 235-240.
78. S. Khamel, N. Ouelaa, K. Bouacha (2012) *Analysis and prediction of tool wear, surface roughness and cutting forces in hard turning with CBN tool*, Journal of Mechanical Science and Technology. 26(11): p. 3605-3616.

79. O. Kienzle, H. Münnich (1957) *Feststellung der Spannungen, Dehnungen und Bruchdrehzahlen der unter Fliehkraft und Bearbeitungskraft beanspruchten Schleifkörper*. Forschungsberichte des Wirtschafts- und Verkehrsministeriums Nordrhein-Westfalen Nr. 232. Springer Fachmedien, Wiesbaden.
80. F. Klocke (2015) *Fertigungsverfahren 5: Gießen, Pulvermetallurgie, Additive Manufacturing* (4. Auflage). Springer, Berlin, Heidelberg, Germany.
81. F. Klocke (2011) *Manufacturing processes 1 : cutting*. Springer, Berlin, Heidelberg, Germany.
82. F. Klocke (2009) *Manufacturing processes 2 : grinding, honing, lapping*. Springer, Berlin, Heidelberg, Germany.
83. F. Klocke (2013) *Manufacturing processes 4: forming*. Springer, Berlin, Heidelberg, Germany.
84. F. Klocke, W. König (2007) *Fertigungsverfahren 3: Abtragen, Generieren Lasermaterialbearbeitung* (4. Auflage). Springer, Berlin, Heidelberg, Germany.
85. A. A. Klyukin, M. G. Postrigajlo (1991) *Device for measuring temperature when grinding*, SU1642269A1, USSR - Soviet Union Patent.
86. D. Kong, Y. Chen, N. Li (2018) *Gaussian process regression for tool wear prediction*, Mechanical Systems and Signal Processing. 104: p. 556-574.
87. Y. Koren (2010) *The global manufacturing revolution*. John Wiley & Sons, Hoboken, New Jersey.
88. A. K. Koziarski (1995) *Layer thermocouple: a new instrument for the assessment of the grinding wheel cutting ability*, European Journal of Mechanical Engineering. 40(2): p. 67-70.
89. P. Krajnik, J. Kopac, A. Sluga (2005) *Design of grinding factors based on response surface methodology*, Journal of Materials Processing Technology. 162-163: p. 629-636.
90. D. W. Kramer (1998) *ECD-Schleifen: Neue Möglichkeiten in der schleiftechnischen Bearbeitung von Wendeschneidplatten aus modernen*

Schneidwerkstoffen mit elektrochemisch in-Prozess geregeltem Schärfen,
(Diss.) ETH Zurich.

91. A. Krizhevsky, I. Sutskever, G. E. Hinton (2012) *ImageNet classification with deep convolutional neural networks*, Advances in Neural Information Processing Systems. p. 1097-1105.
92. P. Kurzweil, P. Scheipers (2010) *Chemie: Grundlagen, Aufbauwissen, Anwendungen und Experimente* (8. Auflage). Vieweg+Teubner, Wiesbaden.
93. H. J. Kushner (1964) *A new method of locating the maximum point of an arbitrary multipeak curve in the presence of noise*, Journal of Basic Engineering. 86(1): p. 97-106.
94. J.-S. Kwak (2005) *Application of Taguchi and response surface methodologies for geometric error in surface grinding process*, International Journal of Machine Tools and Manufacture. 45(3): p. 327-334.
95. S. Lachance, R. Bauer, A. Warkentin (2004) *Application of region growing method to evaluate the surface condition of grinding wheels*, International Journal of Machine Tools and Manufacture. 44(7): p. 823-829.
96. D. Lange, W. Scherer (2016) *Mess- und Überwachungssysteme beim Schleifen* Schweizer Schleif-Symposium, Schweizer Schleif-Symposium.
97. C. W. Lee, T. Choi, Y. C. Shin (2003) *Intelligent model-based optimization of the surface grinding process for heat-treated 4140 steel alloys with aluminum oxide grinding wheels*, Journal of Manufacturing Science and Engineering. 125(1): p. 65-76.
98. C. W. Lee, Y. C. Shin (2000) *Evolutionary modelling and optimization of grinding processes*, International Journal of Production Research. 38(12): p. 2787-2813.
99. T. W. Liao, L. J. Chen (1994) *A neural network approach for grinding processes: modelling and optimization*, International Journal of Machine Tools and Manufacture. 34(7): p. 919-937.
100. B. Likar, J. Kocijan (2007) *Predictive control of a gas–liquid separation plant based on a Gaussian process model*, Computers & Chemical Engineering. 31(3): p. 142-152.

101. Y.-J. Lin, Y.-Y. Hsieh, C.-Y. Huang (2019) *Ontology-based manufacturing control systems (MCS)*, Procedia Manufacturing. 39: p. 1906-1912.
102. H. Liu, Y.-S. Ong, J. Cai (2018) *A survey of adaptive sampling for global metamodeling in support of simulation-based complex engineering design*, Structural and Multidisciplinary Optimization. 57(1): p. 393-416.
103. D. Lizotte, T. Wang, M. Bowling, D. Schuurmans (2007) *Automatic gait optimization with Gaussian process regression*, Proceedings of the 20th International Joint Conference on Artificial Intelligence. p. 944-949.
104. M. Maier, T. Gittler, L. Weiss, C. Bobst, S. Scholze, K. Wegener (2019) *Sensors as an enabler for self-optimizing grinding machines*, MM Science Journal. 2019(04): p. 3192-3199.
105. M. Maier, H. Kunstmann, R. Zwicker, A. Rupenyan, K. Wegener (2022) *Autonomous and data-efficient optimization of turning processes using expert knowledge and transfer learning*, Journal of Materials Processing Technology (in press).
106. M. Maier, A. Rupenyan, M. Akbari, R. Zwicker, K. Wegener (2020) *Turning: Autonomous process set-up through Bayesian optimization and Gaussian process models*, Procedia CIRP. 88: p. 306-311.
107. M. Maier, A. Rupenyan, C. Bobst, K. Wegener (2020) *Self-optimizing grinding machines using Gaussian process models and constrained Bayesian optimization*, The International Journal of Advanced Manufacturing Technology. 108(1): p. 539-552.
108. M. Maier, A. Rupenyan, S. Scholze, K. Wegener (2020) *Einrichten von Schleifmaschinen auf der Basis der Bayesschen Optimierung*, in H. W. Hoffmeister, B. Denkena (Eds.), *Jahrbuch Schleifen, Honen, Läppen und Polieren*, Vulkan-Verlag, Essen: p. 140-149.
109. M. Maier, R. Zwicker, M. Akbari, A. Rupenyan, K. Wegener (2019) *Bayesian optimization for autonomous process set-up in turning*, CIRP Journal of Manufacturing Science and Technology. 26: p. 81-87.
110. S. Malkin, N. H. Cook (1971) *The wear of grinding wheels: Part 1—attritious wear*, Journal of Engineering for Industry. 93(4): p. 1120-1128.

111. G. Manimaran, M. P. Kumar (2013) *Multiresponse optimization of grinding AISI 316 stainless steel using grey relational analysis*, Materials and Manufacturing Processes. 28(4): p. 418-423.
112. I. D. Marinescu, W. B. Rowe, B. Dimitrov, H. Ohmori (2013) *Tribology of abrasive machining processes (second edition)*. William Andrew, Oxford.
113. M. D. Mckay, R. J. Beckman, W. J. Conover (2000) *A comparison of three methods for selecting values of input variables in the analysis of output from a computer code*, Technometrics. 42(1): p. 55-61.
114. P. S. Midha, C. B. Zhu, G. J. Trmal (1991) *Optimum selection of grinding parameters using process modelling and knowledge based system approach*, Journal of Materials Processing Technology. 28(1): p. 189-198.
115. T. P. Minka (2001) *Expectation propagation for approximate Bayesian inference*, Proceedings of the Seventeenth Conference on Uncertainty in Artificial Intelligence. p. 362-369.
116. T. Misaka, J. Herwan, O. Ryabov, S. Kano, H. Sawada, N. Kasashima, Y. Furukawa (2020) *Prediction of surface roughness in CNC turning by model-assisted response surface method*, Precision Engineering. 62: p. 196-203.
117. J. Mockus, V. Tesis, A. Zilinskas (1978) *The application of Bayesian methods for seeking the extremum*, in L. C. W. Dixon, G. P. Szegö (Eds.), *Towards Global Optimisation 2*, North-Holland, Amsterdam: p. 117–129.
118. R. Mookherjee, B. Bhattacharyya (2001) *Development of an expert system for turning and rotating tool selection in a dynamic environment*, Journal of Materials Processing Technology. 113(1-3): p. 306-311.
119. G. E. Moore (1965) *Cramming more components onto integrated circuits*, Electronics. 38(8).
120. M. N. Morgan, R. Cai, A. Guidotti, D. R. Allanson, J. L. Moruzzi, W. B. Rowe (2007) *Design and implementation of an intelligent grinding assistant system*, International Journal of Abrasive Technology. 1(1): p. 106-135.
121. L. Muñoz-González, M. Lázaro-Gredilla, A. R. Figueiras-Vidal (2011) *Heteroscedastic Gaussian process regression using expectation*

propagation, 2011 IEEE International Workshop on Machine Learning for Signal Processing. p. 1-6.

122. R. M. Neal (1999) *Regression and classification using Gaussian process priors*, in J. M. Bernardo, J. O. Berger, A. P. Dawid, A. F. M. Smith (Eds.), *Bayesian Statistics 6: Proceedings of the Sixth Valencia International Meeting*, Oxford University Press, New York: p. 475-501.
123. C. Y. Nian, W. H. Yang, Y. S. Tarng (1999) *Optimization of turning operations with multiple performance characteristics*, Journal of Materials Processing Technology. 95(1-3): p. 90-96.
124. J. Nocedal, S. J. Wright (2006) *Numerical optimization (2nd edition)*. Springer, New York, NY.
125. R. Oesterle (1975) *Verfahren zur Messung der Arbeitstemperatur von Schleifkörpern während des Schleifprozesses*, 112377, Deutsche Demokratische Republik Amt für Erfindungs- und Patentwesen.
126. H. Opitz, J. Peklenik, K. Brückner (1964) *Untersuchung der Eigenschaften von Schleifkörpern und ihr Verhalten im Schleifvorgang*. Forschungsberichte des Landes Nordrhein-Westfalen Nr. 1292. Westdeutscher Verlag, Köln, Opladen.
127. K. Orgawa, A. Nagata, K. Inoue (1991) *Grinding wheel having grinding monitoring and automatic wheel balance control functions*, EP0460282A1, European patent office.
128. P. J. Pawar, R. V. Rao, J. P. Davim (2010) *Multiobjective optimization of grinding process parameters using particle swarm optimization algorithm*, Materials and Manufacturing Processes. 25(6): p. 424-431.
129. F. Pedregosa, G. Varoquaux, A. Gramfort, V. Michel, B. Thirion, O. Grisel, M. Blondel, P. Prettenhofer, R. Weiss, V. Dubourg, J. Vanderplas, A. Passos, D. Cournapeau (2011) *Scikit-learn: machine learning in Python*, Journal of Machine Learning Research. 12(85): p. 2825-2830.
130. W. Pickert (1992) *Verfahren und Vorrichtung zum Vermeiden von thermischen Überbeanspruchungen von Werkstücken beim Schleifen (Schleifbrand)* EP0472844A2, European patent office.
131. R. V. Rao (2011) *Advanced modeling and optimization of manufacturing processes: International research and development*. Springer, London.

132. R. V. Rao, P. J. Pawar (2010) *Grinding process parameter optimization using non-traditional optimization algorithms*, Proceedings of the Institution of Mechanical Engineers, Part B: Journal of Engineering Manufacture. 224(6): p. 887-898.
133. C. E. Rasmussen, H. Nickisch (2010) *Gaussian processes for machine learning (GPML) toolbox*, Journal of Machine Learning Research. 11(100): p. 3011-3015.
134. C. E. Rasmussen, C. K. I. Williams (2006) *Gaussian processes for machine learning*. MIT Press, Cambridge, Massachusetts.
135. A. C. Rencher, W. F. Christensen (2012) *Methods of multivariate analysis (3rd edition)*. John Wiley & Sons, Hoboken, New Jersey.
136. T. J. Ross (2010) *Fuzzy logic with engineering applications (3rd edition)*. John Wiley & Sons, Chichester, West Sussex, United Kingdom.
137. W. B. Rowe (2014) *Principles of modern grinding technology (2nd edition)*. William Andrew, Waltham, Massachusetts.
138. W. B. Rowe, S. C. E. Black, B. Mills, H. S. Qi, M. N. Morgan (1995) *Experimental investigation of heat transfer in grinding*, CIRP Annals. 44(1): p. 329-332.
139. W. B. Rowe, L. Yan, I. Inasaki, S. Malkin (1994) *Applications of artificial intelligence in grinding*, CIRP Annals. 43(2): p. 521-531.
140. R. Rudrapati, P. K. Pal, A. Bandyopadhyay (2016) *Modeling and optimization of machining parameters in cylindrical grinding process*, The International Journal of Advanced Manufacturing Technology. 82(9): p. 2167-2182.
141. T. P. Ryan (2007) *Modern experimental design*. John Wiley & Sons, Hoboken, New Jersey.
142. A. Sadek, M. Aly, K. Hamza, M. Meshreki, A. O. Nassef, H. Attia (2015) *Optimization of cutting conditions in vibration assisted drilling of composites via a multi-objective EGO implementation*, Proceedings of the ASME 2015 International Design Engineering Technical Conferences and Computers and Information in Engineering Conference.

143. M. Sakakura, I. Inasaki (1993) *Intelligent data base for grinding operations*, CIRP Annals. 42(1): p. 379-382.
144. M. Sakakura, S. Tsukamoto, T. Fujiwara, I. Inasaki (2006) *A skill-formation model for grinding operations*, Machining Science and Technology. 10(4): p. 457-470.
145. E. Saljé, U. Harbs (1990) *Wirkungsweisen und Anwendungen von Konditionierverfahren*, CIRP Annals. 39(1): p. 337-340.
146. T. J. Santner, B. J. Williams, W. I. Notz (2018) *The design and analysis of computer experiments (2nd edition)*. Springer, New York, NY.
147. G. Sathyanarayanan, I. Joseph Lin, M.-K. Chen (1992) *Neural network modelling and multiobjective optimization of creep feed grinding of superalloys*, International Journal of Production Research. 30(10): p. 2421-2438.
148. E. Sauter, E. Sarikaya, M. Winter, K. Wegener (2021) *In-process detection of grinding burn using machine learning*, The International Journal of Advanced Manufacturing Technology. 115(7): p. 2281-2297.
149. S. Scholze, M. Maier, L. Weiss (2020) *Tool device and method for measuring a condition of a machining tool*, EP3666457A1, European patent office.
150. B. Shahriari, K. Swersky, Z. Wang, R. P. Adams, N. d. Freitas (2016) *Taking the human out of the loop: A review of Bayesian optimization*, Proceedings of the IEEE. 104(1): p. 148-175.
151. A. Shapiro, D. Dentcheva, A. Ruszczyński (2009) *Lectures on stochastic programming: modeling and theory (2nd edition)*. Society for Industrial and Applied Mathematics, Philadelphia.
152. A. N. Siddiquee, Z. A. Khan, Z. Mallick (2010) *Grey relational analysis coupled with principal component analysis for optimisation design of the process parameters in in-feed centreless cylindrical grinding*, The International Journal of Advanced Manufacturing Technology. 46(9): p. 983-992.
153. S. S. Silin (1975) *Novel method of measuring temperature in the grinding zone with a semi-synthetic thermocouple*, Machines & Tooling : selective translation from the Russian. 46(3): p. 53-54.

154. D. Singh, P. V. Rao (2007) *A surface roughness prediction model for hard turning process*, The International Journal of Advanced Manufacturing Technology. 32(11): p. 1115-1124.
155. M. K. Sinha, D. Setti, S. Ghosh, P. Venkateswara Rao (2016) *An investigation on surface burn during grinding of Inconel 718*, Journal of Manufacturing Processes. 21: p. 124-133.
156. J. Snoek, H. Larochelle, R. P. Adams (2012) *Practical Bayesian optimization of machine learning algorithms*, Advances in Neural Information Processing Systems. p. 2951-2959.
157. J. W. Snow (1998) *An overview of fibre optic rotary joint technology and recent advances*, IFAC Proceedings Volumes. 31(33): p. 77-81.
158. I. M. Sobol (1967) *On the distribution of points in a cube and the approximate evaluation of integrals*, USSR Computational Mathematics and Mathematical Physics. 7(4): p. 86-112.
159. N. Srinivas, A. Krause, S. Kakade, M. Seeger (2010) *Gaussian process optimization in the bandit setting: no regret and experimental design*, Proceedings of the 27th International Conference on Machine Learning. p. 1015-1022.
160. D. H. Stamatatis (2002) *Six sigma and beyond: Design of experiments*. Vol. 5, CRC Press, Boca Raton, Florida.
161. K. Swersky, J. Snoek, R. P. Adams (2013) *Multi-task Bayesian optimization*, Advances in Neural Information Processing Systems. p. 2004-2012.
162. G. Taguchi (1993) *Taguchi on robust technology development: Bringing quality engineering upstream*. ASME Press, New York.
163. K. Tanaka, P. Koshy (2019) *A pneumatic sensor for grinding wheel condition monitoring*, Precision Engineering. 56: p. 62-68.
164. J. Tang, J. Du, Y. Chen (2009) *Modeling and experimental study of grinding forces in surface grinding*, Journal of Materials Processing Technology. 209(6): p. 2847-2854.

165. P. H. O. Teixeira, R. R. Rego, F. W. Pinto, J. de Oliveira Gomes, C. Löpenhaus (2019) *Application of Hall effect for assessing grinding thermal damage*, Journal of Materials Processing Technology. 270: p. 356-364.
166. V. T. Thang, N. A. Tuan, N. V. Tiep (2017) *Application of pneumatic measuring probe to determine appropriate time for dressing grinding wheel in profile grinding for the inner ring groove of ball bearing*, Journal of Engineering and Science Research. 1(2): p. 222-227.
167. H. K. Tönshoff (2014) *Cutting, fundamentals*, in The International Academy for Production, L. Laperriüre, G. Reinhart (Eds.), *CIRP Encyclopedia of Production Engineering*, Springer, Berlin, Heidelberg: p. 345-357.
168. H. K. Tönshoff (2010) *Massivumformteile wirtschaftlich spanen*. Industrieverband Massivumformung, Hagen, Germany.
169. H. K. Tönshoff (1995) *Werkzeugmaschinen: Grundlagen*. Springer, Berlin, Heidelberg.
170. H. K. Tönshoff, T. Friemuth, J. C. Becker (2002) *Process monitoring in grinding*, CIRP Annals. 51(2): p. 551-571.
171. H. K. Tönshoff, M. Zinngrebe, M. Kemmerling (1986) *Optimization of internal grinding by microcomputer-based force control*, CIRP Annals. 35(1): p. 293-296.
172. Tyrolit (2020) *Precision grinding product catalogue*. Schwarz, Austria.
173. T. Ueda, H. Tanaka, A. Torii, T. Matsuo (1993) *Measurement of grinding temperature of active grains using infrared radiation pyrometer with optical fiber*, CIRP Annals. 42(1): p. 405-408.
174. B. Varghese, S. Pathare, R. Gao, C. Guo, S. Malkin (2000) *Development of a sensor-integrated “intelligent” grinding wheel for in-process monitoring*, CIRP Annals. 49(1): p. 231-234.
175. J. Villemonteix, E. Vazquez, E. Walter (2009) *Bayesian optimization for parameter identification on a small simulation budget*, IFAC Proceedings Volumes. 42(10): p. 1603-1608.

176. S. Wang, Y. Tian, C. J. Tay, C. Quan (2003) *Development of a laser-scattering-based probe for on-line measurement of surface roughness*, Applied Optics. 42(7): p. 1318-1324.
177. D. A. Waterman (1986) *A guide to expert systems*. Addison-Wesley, Reading, Massachusetts.
178. K. Wegener, H.-W. Hoffmeister, B. Karpuschewski, F. Kuster, W.-C. Hahmann, M. Rabiey (2011) *Conditioning and monitoring of grinding wheels*, CIRP Annals. 60(2): p. 757-777.
179. X. M. Wen, A. A. O. Tay, A. Y. C. Nee (1992) *Micro-computer-based optimization of the surface grinding process*, Journal of Materials Processing Technology. 29(1-3): p. 75-90.
180. F. Werner (1991) *Sensortechnik und Kenngrößen zur Beurteilung des Einsatzverhaltens von Schleifscheiben*, Sensor 91 : 5. Intern. Ausstellung mit Kongress für Sensorik & Systemtechnik. p. 113-128.
181. E. Westkämper (1994) *Automatic supervision of surface grinding*, in M. Szafarczyk (Ed.), *Automatic supervision in manufacturing*, Springer, London: p. 67-81.
182. C. Wirtz, A. Dehmer, D. Trauth, P. Mattfeld, F. Klocke (2018) *Analysis of the grinding wheel wear in dependency of the cemented carbide specification*, The International Journal of Advanced Manufacturing Technology. 99(1): p. 747-754.
183. H.-G. Wobker (1992) *Schleifen keramischer Schneidstoffe*. Fortschritts-Berichte VDI. Reihe 2, Fertigungstechnik Nr. 237. VDI-Verlag, Düsseldorf.
184. C. J. Wohlmuth (1984) *Surface temperature control apparatus*, US4438598A, United states patent and trademark office.
185. A. V. Yakimov, Y. A. Kazimirchik (1964) *Investigation of temperatures in the grinding zone*, Russian Engineering Journal : selective translation from the Russian. 44(8): p. 51-53.
186. W. H. Yang, Y. S. Tarn (1998) *Design optimization of cutting parameters for turning operations based on the Taguchi method*, Journal of Materials Processing Technology. 84(1-3): p. 122-129.

187. Z. Yang, Z. Yu (2012) *Grinding wheel wear monitoring based on wavelet analysis and support vector machine*, The International Journal of Advanced Manufacturing Technology. 62(1): p. 107-121.
188. Z. Yang, Z. Yu, C. Xie, Y. Huang (2014) *Application of Hilbert–Huang transform to acoustic emission signal for burn feature extraction in surface grinding process*, Measurement. 47: p. 14-21.
189. H. Yoshikawa, T. Sata (1963) *Study on Wear of Grinding Wheels: I—Bond Fracture in Grinding Wheels*, Journal of Engineering for Industry. 85(1): p. 39-42.
190. L. Zadeh (1963) *Optimality and non-scalar-valued performance criteria*, IEEE Transactions on Automatic Control. 8(1): p. 59-60.
191. L. Zhang, C. Ren, C. Ji, Z. Wang, G. Chen (2016) *Effect of fiber orientations on surface grinding process of unidirectional C/SiC composites*, Applied Surface Science. 366: p. 424-431.

Appendix A Equations for multi-task learning

In this section the calculation of $\underline{\underline{K}}(\underline{\underline{X}}, \underline{\underline{X}})$ and $\underline{\underline{K}}_{x_*}$ is shown based on [4]. The equation (4.10) can be written componentwise as follows,

$$(\underline{K}(\underline{x}, \underline{x}'))_{d,d'} = \sum_{q=1}^Q b_{d,d'}^q k_q(\underline{x}, \underline{x}') \quad (\text{A.1})$$

where $b_{d,d'}^q$ are the coefficients of the coregionalization matrix $\underline{\underline{B}}$ modelling the covariance between the different outputs and $k_q(\underline{x}, \underline{x}')$ are the kernels modelling the covariance between different process parameters. The matrix $\underline{\underline{K}}(\underline{\underline{X}}, \underline{\underline{X}})$ with dimensions $ND \times ND$, for N data points per output and D number of outputs can be calculated as follows,

$$\underline{\underline{K}}(\underline{\underline{X}}, \underline{\underline{X}}) = \begin{pmatrix} (\underline{\underline{K}}(\underline{\underline{X}}_1, \underline{\underline{X}}_1))_{1,1} & \dots & (\underline{\underline{K}}(\underline{\underline{X}}_1, \underline{\underline{X}}_D))_{1,D} \\ \vdots & \ddots & \vdots \\ (\underline{\underline{K}}(\underline{\underline{X}}_D, \underline{\underline{X}}_1))_{D,1} & \dots & (\underline{\underline{K}}(\underline{\underline{X}}_D, \underline{\underline{X}}_D))_{D,D} \end{pmatrix} \quad (\text{A.2})$$

where $\underline{\underline{X}}_d$ is the input training data for output d . The blocks $(\underline{\underline{K}}(\underline{\underline{X}}_d, \underline{\underline{X}}_{d'}))_{d,d'}$ of the matrix $\underline{\underline{K}}(\underline{\underline{X}}, \underline{\underline{X}})$ can be calculated as follows by using equation (A.1).

$$(\underline{\underline{K}}(\underline{\underline{X}}_d, \underline{\underline{X}}_{d'}))_{d,d'} = \begin{pmatrix} (K(\underline{x}_1, \underline{x}_1))_{d,d'} & \dots & (K(\underline{x}_1, \underline{x}_N))_{d,d'} \\ \vdots & \ddots & \vdots \\ (K(\underline{x}_N, \underline{x}_1))_{d,d'} & \dots & (K(\underline{x}_N, \underline{x}_N))_{d,d'} \end{pmatrix} \quad (\text{A.3})$$

The matrix $\underline{\underline{K}}_{x_*}$ with dimensions $D \times ND$ and entries $(\underline{K}(\underline{x}_*, \underline{x}_j))_{d,d'}$ can be calculated as follows.

$$\underline{\underline{K}}_{x_*} = \begin{pmatrix} (\underline{K}(\underline{x}_*, \underline{x}_j))_{1,1} & \dots & (\underline{K}(\underline{x}_*, \underline{x}_j))_{1,D} \\ \vdots & \ddots & \vdots \\ (\underline{K}(\underline{x}_*, \underline{x}_j))_{D,1} & \dots & (\underline{K}(\underline{x}_*, \underline{x}_j))_{D,D} \end{pmatrix} \quad (\text{A.4})$$

$$(\underline{K}(\underline{x}_*, \underline{x}_j))_{d,d'} = ((K(\underline{x}_*, \underline{x}_1))_{d,d'} \ \dots \ (K(\underline{x}_*, \underline{x}_N))_{d,d'}) \quad (\text{A.5})$$

Appendix B Expectation propagation algorithm

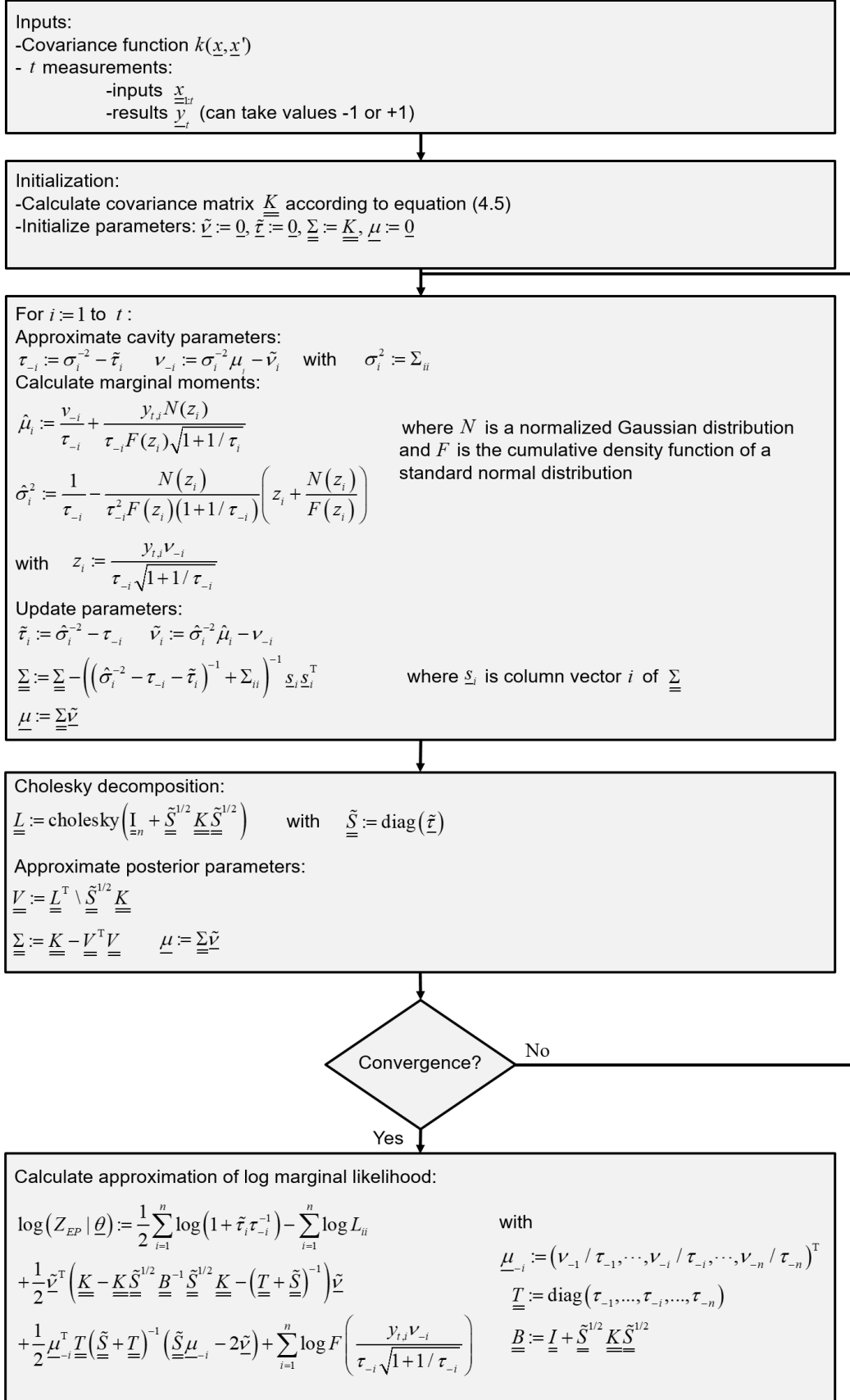


Figure B.1: Calculation of log marginal likelihood with expectation propagation algorithm according to [134]

Inputs:

-Covariance function $k(\underline{x}, \underline{x}')$

- t measurements:

-inputs $\underline{\underline{x}}_t$

-results $\underline{\underline{y}}_t$ (can take values -1 or +1)

-Parameters $\tilde{\nu}, \tilde{\tau}$

-test input \underline{x}_*

Predict probability for $y=+1$:

$$\underline{\underline{L}} := \text{cholesky}\left(\underline{\underline{I}}_n + \tilde{\underline{\underline{S}}}^{1/2} \underline{\underline{K}} \tilde{\underline{\underline{S}}}^{1/2}\right)$$

with $\tilde{\underline{\underline{S}}} := \text{diag}(\tilde{\tau})$
with covariance matrix $\underline{\underline{K}}$ according to equation (4.5)

$$\underline{\underline{z}} := \tilde{\underline{\underline{S}}}^{1/2} \underline{\underline{L}}^T \setminus \left(\underline{\underline{L}} \setminus \left(\tilde{\underline{\underline{S}}}^{1/2} \underline{\underline{K}} \tilde{\nu} \right) \right)$$

$$\bar{f}_* := \underline{k}(\underline{x}_*)^T (\tilde{\nu} - \underline{\underline{z}})$$

$$\underline{v} := \underline{\underline{L}} \setminus \left(\tilde{\underline{\underline{S}}}^{1/2} \underline{k}(\underline{x}_*) \right)$$

$$V[f_*] := k(\underline{x}_*, \underline{x}_*) - \underline{v}^T \underline{v}$$

$$p(\underline{x}_*) := F\left(\bar{f}_* / \sqrt{1+V[f_*]}\right)$$

Figure B.2: Calculation of prediction with expectation propagation algorithm according to [134]

List of publications relevant to thesis

This thesis is largely based on the publications listed below. The chapters 2 Fundamentals of manufacturing processes and 3 State of the art in parameter selection of manufacturing processes are based on all publications. For the other chapters the relevant publications are introduced in the beginning of each chapter.

Conference:

M. Maier, A. Rupenyan, M. Akbari, R. Zwicker, K. Wegener (2020) *Turning: Autonomous process set-up through Bayesian optimization and Gaussian process models*, Procedia CIRP. 88: p. 306-311.

Journals:

M. Maier, R. Zwicker, M. Akbari, A. Rupenyan, K. Wegener (2019) *Bayesian optimization for autonomous process set-up in turning*, CIRP Journal of Manufacturing Science and Technology. 26: p. 81-87.

M. Maier, A. Rupenyan, C. Bobst, K. Wegener (2020) *Self-optimizing grinding machines using Gaussian process models and constrained Bayesian optimization*, The International Journal of Advanced Manufacturing Technology. 108(1): p. 539-552.

M. Maier, T. Gittler, L. Weiss, C. Bobst, S. Scholze, K. Wegener (2019) *Sensors as an enabler for self-optimizing grinding machines*, MM Science Journal. 2019(04): p. 3192- 3199.

M. Maier, H. Kunstmann, R. Zwicker, A. Rupenyan, K. Wegener (2022) *Autonomous and data-efficient optimization of turning processes using expert knowledge and transfer learning*, Journal of Materials Processing Technology (in press).

K. Wegener, S. Weikert, J. Mayr, M. Maier, V.O. Ali Akbari, M. Postel (2021), *Operator integrated – concept for manufacturing intelligence*, Journal of Machine Engineering. 21(4): p. 5 -28.

Book section:

M. Maier, A. Rupenyan, S. Scholze, K. Wegener (2020) *Einrichten von Schleifmaschinen auf der Basis der Bayesschen Optimierung*, in H. W. Hoffmeister, B. Denkena (Eds.), *Jahrbuch Schleifen, Honen, Läppen und Polieren*, Vulkan-Verlag, Essen: p. 140-149.

Patent applications:

S. Scholze, M. Maier, L. Weiss (2020) *Tool device and method for measuring a condition of a machining tool*, EP3666457A1, European Patent Office.

C. Bobst, M. Maier, A. Rupenyan-Vasileva (2020) *Method for autonomous optimization of a grinding process*, EP3736648A1, European Patent Office.